INFORMATION TO USERS

This manuscript has been reproduced from the microfilm master. UMI films the text directly from the original or copy submitted. Thus, some thesis and dissertation copies are in typewriter face, while others may be from any type of computer printer.

The quality of this reproduction is dependent upon the quality of the copy submitted. Broken or indistinct print, colored or poor quality illustrations and photographs, print bleedthrough, substandard margins, and improper alignment can adversely affect reproduction.

In the unlikely event that the author did not send UMI a complete manuscript and there are missing pages, these will be noted. Also, if unauthorized copyright material had to be removed, a note will indicate the deletion.

Oversize materials (e.g., maps, drawings, charts) are reproduced by sectioning the original, beginning at the upper left-hand corner and continuing from left to right in equal sections with small overlaps. Each original is also photographed in one exposure and is included in reduced form at the back of the book.

Photographs included in the original manuscript have been reproduced xerographically in this copy. Higher quality 6" x 9" black and white photographic prints are available for any photographs or illustrations appearing in this copy for an additional charge. Contact UMI directly to order.

UMI®

Bell & Howell Information and Learning
300 North Zeeb Road, Ann Arbor, MI 48106-1346 USA
800-521-0600

RELATIONSHIP BETWEEN THE AEROSOL NUMBER DISTRIBUTION AND THE CLOUD CONDENSATION NUCLEI SUPERSATURATION SPECTRUM

A

THESIS

Presented to the Faculty

of the University of Alaska Fairbanks

in Partial Fulfillment of the Requirements

for the Degree of

DOCTOR OF PHILOSOPHY

By

Will Hart Cantrell II, B.A

Fairbanks, Alaska

May 1999

RELATIONSHIP BETWEEN THE AEROSOL NUMBER DISTRIBUTION AND THE CLOUD CONDENSATION NUCLEI SUPERSATURATION SPECTRUM

By

Will Hart Cantrell II

RECOMMENDED:

Advisory Committee Chair

Department Head

APPROVED:

Dean, College Science, Engineering and Mathematics

Dean of the Graduate School

4-9-99

Date

Abstract

Though Cloud Condensation Nuclei (CCN) are a subset of atmospheric aerosol, relatively little is known of what links the two. A recently developed instrument called the CCN Remover, which directly relates the CCN supersaturation spectrum to the aerosol number distribution, is described. Instrumental errors are quantified and laboratory tests used to verify the instrument's accuracy are also presented.

We made measurements with the CCN Remover in the Aerosol Characterization Experiment 2 (ACE 2) and the INdian Ocean EXperiment (INDOEX). These two multinational field campaigns shared the objective of investigating aerosol particles' ability to modulate cloud albedo by activating as CCN. In both instances, we found that aerosol particles were not activating with the characteristics of pure ammonium sulfate, which is generally regarded as the major component of the majority of aerosol particles which act as CCN. Either a substantial fraction of the aerosol was not participating in the activation process or the presence of a hydrophobic surface film inhibited water vapor transport. Measurements of the aerosol's chemical composition and hygroscopic growth factors are used to examine these possibilities.

Anthropogenic activity is modifying the properties of natural aerosol particles in a way which could affect their ability to act as CCN. We discuss evidence for aerosol particles coated with sulfuric acid in an Arctic air mass in support of this claim.

In some instances, the connection between aerosol and CCN can be inferred directly from the aerosol number distribution. Clouds segregate aerosol into two populations - those that act as CCN and those that do not, and when the cloud evaporates, the aerosol number distribution bears the signature of the cloud through which it has cycled - a minimum in the aerosol number distribution. The diameter at which this minimum occurs can be related to the maximum supersaturation in the cloud, and the number of particles larger than the minimum is the population of particles that

acted as CCN. Over 1,000 bimodal aerosol number distributions from five widely separated locations have been analyzed for maximum supersaturation and cloud droplet (or CCN) concentrations.

Table of Contents

List of Figures

List of Tables

Acknowledgments

"If I have seen further it is by standing upon the shoulders of Giants."

-Sir Isaac Newton

If the above quote is true for Isaac Newton, it is even more so for me, whose scientific eyesight is much less keen. There are many people who have helped me to climb up the mountain of scientific knowledge to the vantage point I now have.

I would like to especially thank my advisor, Dr. Glenn Shaw. Of the myriad things which he taught me the three most valuable were by example. The first is that you should never become so bogged down in the details that you lose sight of the big picture. The second is that research should be driven by your own curiosity. The third is that scientific writing does not have to be excruciatingly dull, boring, and impersonal. Glenn urged me to read the papers of John Aitken, and set a similar example in his own writing.

I also want to extend a special thanks to Dr. Richard Benner, who taught me that the Devil and, quite frequently, significant science is in the details. His advice was the perfect counterbalance to Glenn's frequent admonition to step back and look at the big picture. I will also say that having Rich as a coathor on a paper can be an excruciating experience, but the finished product was always better as a result of his reading.

Thanks to my committee members, Dr. Sue Ann Bowling, Dr. Channon Price, and Dr. Gerd Wendler, who were always willing to lend their experience and expertise when asked.

Thank you to my fellow graduate students. You were always willing to listen to my crazy ideas and point out any flaws. Thanks especially to David Veazey for teaching me not to be afraid to take the equipment apart. More often than not, you can get it

back together again. Thanks also to Dennis Nicks, Dorte Dissing, Eric Breitenberger, Peter Delamere, Jen Simmons, Jen Kimball, Clara Jodwalis, Qiang Ji, Matt Heavner, Jen Danielson, Barbara Trost, Lee Ann Smith, Ryan Woodard, and Sasha Mahura.

I would like to thank Glenn and Rich again for sending me to Homer in the summer of 1996. I met my wife, Cindi Cooper, there. Thank you Cindi, for putting up with my complaints when I had them, for sharing my joy, and for waiting through two long winters for me to come back from the tropics.

Like most science today, much of the work in this thesis has been collaborative. Dr. Qiang Ji and Dr. Glenn Shaw were the original inventors of the Cloud Condensation Remover described in Chapter 2. Though I modified their original design, without that as a template, I would never have been able to do most of the work described in Chapters 3 and 4.

The second Aerosol Characterization Experiment (ACE 2) was a large, multinational experiment; our measurements there were only a small part of the whole. The hygroscopic growth factor measurements described in Chapter 3 were done by Dr. Covert at the University of Washington. The aerosol chemical data were provided by Christian Neβess and Dr. Jost Heintzenberg of the Institute for Tropospheric Research in Leipzig, Germany. Dr. Alfred Wiedensohler and Diana Weiss, also at IfT in Germany provided aerosol number distributions which I used in the quality control of my own data. Use of this data is gratefully acknowledged.

The INDian Ocean EXperiment was another large, multinational field campaign. The measurements of carbonaceous aerosol mass were done by Dr. Helene Cachier of LSCA/CFR laboratoire mixte CEA-CNRS in France and the mass of the ionic aerosol species was done by Dr. Lennart Granat at Stockholm University in Sweden. These measurements are used in Chapter 4, and are gratefully acknowledged. I would also like to thank the captain and crew of the R/V Sagar Kanya.

The measurements described in Chapter 5 were a collaborative effort between

myself, Dr. Glenn Shaw, Dr. Richard Benner, and David Veazey.

The work described in Chapter 6 is a collaborative effort between myself, Dr. Glenn Shaw and Dr. Richard Benner. I would like to thank Dr. David Covert and Dr. Tad Anderson for their assistance at Cheeka Peak Observatory. The data collection at Poker Flat was principally done by David Veazey with some assistance from me. The data collection in Hawaii was done by David Veazey and Dr. Qiang Ji. The data collection at Wallops Island was done by myself and Dr. Qiang Ji. The data collection in Homer was done by myself and David Veazey. Dennis Nicks and Dr. Clara Jodwalis assisted in the general setup at the site. Dr. Joyce Harris at NOAA / CMDL supplied the back trajectories for Homer, and Dr. Alexander Smirnov at NASA / Goddard supplied the back trajectories for Wallops Island.

Funding for the work described in this thesis was provided by the National Aeronautical and Space Administration; the National Science Foundation / Atmospheric Chemistry Division; the INDOEX project, which is administered by the Center for Clouds, Chemistry and Climate at the University of California San Diego; the Geophysical Institute; the University of Alaska Fairbanks Graduate School through a Thesis Completion Fellowship; and the Center for Global Change and Arctic System Science.

Chapter 1

Introduction

"Nature will laugh at you." -S. Manabe

Why study Cloud Condensation Nuclei?

The driving force behind much of the research in the atmospheric sciences today is the recognition that anthropogenic activity may be altering Earth's climate. Jones *et al.* [1995] show that there has been an increase in the globally averaged, near-surface temperature of approximately 0.5 °C over the past 100 years (see Pielke *et al.*, 1998 for a dissenting view). This increase in surface temperature is coincident with an increase in atmospheric concentrations of carbon dioxide, one of the principal greenhouse gases. Since this increase in carbon dioxide can be attributed to anthropogenic activity, some suggest that the increase in near-surface temperatures arises from human activities.

However, the temperature increase has not been uniform in space or time [*Jones et al.*, 1995]. The many factors that determine near-surface temperature, or more generally climate, interact in complex and nonlinear ways. Even though greenhouse radiative forcing may be relatively uniform over the planet, the temperature response can vary substantially from region to region. Detecting a greenhouse warming signal amid the cacophony of noise introduced by the nonlinearities of the feedback mechanisms inherent in the climate system can be very difficult. Determining how the climate system will continue responding to changes in one or more of its forcing terms is even harder. In fact, solving the climate change problem in "closed form" is impossible.

The only way to investigate simultaneously how the physical processes that constitute the climate system may change is to model them. General circulation models (GCMs) describe the redistribution of heat, momentum, and water vapor based on

physical principles. The nonlinear nature of the equations which characterize these processes is what makes a solution in "closed form" impossible. Including every process in the model of a system which encompasses 16 orders of magnitude on spatial scales (molecules to large circulation patterns) and at least nine orders of magnitude on a temporal scale (cloud formation to ocean response) is impossible. Many processes must be highly simplified, or parameterized.

Parameterization is a necessary evil. Modeling the detailed growth of a single ice crystal can take hours on a supercomputer. Using this level of detail in simulations of climate which span centuries to thousands of years is unrealistic. It would be much faster to simply wait and see what happens as anthropogenic activities perturb the climate system. Processes like this must be simplified, yet there are inherent dangers in doing so. Parameterizations of complex processes are usually valid only over a narrow range of conditions. If the conditions stray outside that range, the parameterization may break down. Inadequate parameterizations of crucial processes are one reason that many GCMs fail to capture certain elements of the climate system. Clouds are one element that have been identified as being poorly parameterized in GCMs [*Boucher and Lohmann*, 1995]. To improve the predictive power of GCMs, especially on the regional scale, cloud parameterizations must be improved.

Clouds affect climate through their impact on the Earth's radiation balance and its hydrologic cycle. A cloud's horizontal extent, depth, lifetime, and geographic location all affect Earth's energy balance. These parameters are determined through the interaction of dynamics and microphysics; it is these processes and their interactions which must be correctly parameterized.

GCMs have a particularly hard time dealing with cloud microphysics for several reasons. The microphysical processes occur on scales of nanometers to centimeters while the resolution of most GCMs used for climate studies is hundreds of kilometers. More importantly, many important cloud microphysical processes are not well understood.

Poorly understood processes make even more poorly parameterized processes. Cloud formation or activation, which lasts for a few seconds to minutes, has a significant influence on many cloud properties that persist throughout the lifetime of the cloud. It is one process that is incompletely understood, and which needs to be improved in GCMs [*Ghan et al.*, 1997].

Every cloud in Earth's atmosphere forms because of the confluence of two quantities - air which is supersaturated with respect to water vapor and small particles suspended in the air mass. Water vapor supersaturation is a necessary but not sufficient condition for cloud formation in the atmosphere. If the degree of supersaturation is very slight, embryonic water droplets might form, but they almost instantly evaporate because the Kelvin effect is so large for particles with such small radii. Supersaturations of approximately 400% are necessary for the homogeneous formation of water droplets. However, water droplets can and do form at slight supersaturations if there are nucleation sites present.

These nucleation sites, called cloud condensation nuclei (CCN), determine the cloud's initial cloud droplet concentration, which influences the optical depth, cloud lifetime, and the probability that the cloud will produce precipitation. If a large number of CCN are activated (*i.e.* there is a large initial concentration of droplets), the resulting cloud will be brighter, with a larger optical depth than if fewer CCN had activated [*Twomey*, 1991]. Activating more CCN also means that the available water vapor will be shared between more cloud droplets, which will be smaller as a result. A large number of small cloud droplets can lead to "fluvial constipation" [*Hudson*, 1993]; the cloud has a lower chance of precipitating. This decreased probability of precipitation may enhance the cloud's lifetime [*Albrecht*, 1989].

If the effects of CCN on clouds are not properly represented in GCMs, there are apt to be deficiencies in the model's treatment of Earth's radiation balance and hydrologic cycle. These deficiencies will feed back into model's treatment of dynamics

and temperature fields, among other variables.

Why I study CCN. I stated that the driving force behind most of the research being done in atmospheric science today is the possibility of anthropogenic perturbation of Earth's climate. While it is true that most of the funding which drives research in atmospheric science is driven by the spectre of human-induced climate change, scientists today probe the secrets of the sky for the same reason that the pioneers of atmospheric science did. They are fascinated by the topic that they are investigating.

Why is the study of CCN being funded? Humans could be affecting the climate by perturbing concentrations of CCN. Why do I study CCN? I find the subject intrinsically interesting.

Measurement of aerosol particles and CCN

The total collection of particulate matter suspended in the atmosphere is the atmospheric aerosol, but not every particle suspended in the atmosphere will act as a CCN at the slight supersaturations most clouds reach. Only a subset will act as CCN. Finding this subset of the aerosol can be done either experimentally or theoretically.

If a particle's chemical composition and morphology are known, its ability to act as a CCN can be calculated using a framework laid down by Hilding Köhler in his 1936 paper, "The nucleus in and the growth of hygroscopic droplets." Köhler combined the Kelvin effect, which describes the increase in the equilibrium water vapor pressure over a curved surface, and the Raoult effect, which describes the decrease in the water vapor pressure over solutions, to form the theoretical framework of cloud droplet formation that bears his name. Subsequent research has extended the theory, which accounted for simple electrolytes in solution, to slightly soluble substances [*Laaksonen et al.*, 1998], organic species [*Cruz and Pandis*, 1998; *Li et al.*, 1998; *Shulman et al.*, 1996], and particle morphology [*Cruz and Pandis*, 1998].

However, determining a particle's complete chemical composition and

morphology in the atmosphere is a daunting, if not impossible, task. Transforming information solely about aerosol particles into information on CCN is usually not practical. To make the determination that an aerosol particle is or is not a CCN, it must be subjected to a supersaturated environment. If it becomes a cloud droplet, it is a CCN, otherwise it is not.

The earliest measurements of aerosol number concentration took advantage of the fact that every aerosol particle will activate, or become a CCN, if the applied supersaturation is high enough. In the last two decades of the nineteenth century, John Aitken investigated the number concentration of atmospheric aerosol in a variety of conditions using an expansion chamber which produced a very high supersaturation (over 10%). Practically all of the aerosol particles in the chamber activated and formed a cloud, which could be observed with the naked eye. Using this type of chamber, he determined the number concentration by counting droplets with the aid of a microscope, and later by measuring the attenuation of light through the chamber. Aitken was able to prove that the clouds formed on aerosol particles by filtering the sample and observing that no cloud formed when a supersaturation was applied [*Aitken*, 1880].

Particles as small as 100 nanometers in diameter can be detected by passing them through a collimated beam of light, since they will scatter an appreciable amount of the light. The size of the particle can also be inferred since the intensity of the scattered light is proportional to the particle's diameter. However, the scattering also depends on the particle's refractive index, which is usually not known. Particles smaller than about 100 nanometers in diameter do not interact strongly enough with the light to be detected. Particles smaller than this can be detected by passing the sample stream across a reservoir of a fluid with a low vapor pressure (usually butanol). The reservoir is heated so that the air space immediately above it is saturated with respect to the gas phase of the fluid. As particles pass through this region into a cooler condenser tube, the butanol vapor condenses onto them, increasing their size. The larger particles can then be

detected by light scattering. With this instrument, known as a Condensation Particle Counter (CPC) or Condensation Nucleus Counter (CNC), particles as small as 10 nanometers in diameter can be counted. However, the information on size is lost since the particles grow to a near monodisperse distribution through the condensation of the butanol.

The information on the size of the aerosol particles can be regained by charging the aerosol particles, and passing them through an electric field. The balance between the electric and the drag force, which is quickly established for small particles, is given by :

$$neE = \frac{3\pi\eta V D_p}{C_c} \qquad (1)$$

where, n is the number of charges, e is the elementary charge, E is the electric field strength, η is the kinematic viscosity of the gas, V is the terminal velocity of the particle, D_p is the diameter of the particle, and C_c is the Cunningham slip coefficient.

The particle's terminal velocity in the applied electric field is directly proportional to the number of charges it carries and indirectly proportional to its diameter. Through an appropriate arrangement of charging apparatus, air flow, and electric field configuration, particles of a known mobility (B = V/applied force) can be separated from the aerosol distribution as a whole, then counted with a CNC. By varying the strength of the electric field, the entire range of mobilities can be sampled. If the distribution of charges on the aerosol is known or can be calculated, then the number distribution of aerosol can be obtained. (For a more complete discussion of the electrostatic classifier, see *Fuchs*, 1964 or *Hinds*, 1982.)

Measurement of the aerosol number concentration and distribution gives some insight into the nature of the CCN spectrum, which is the cumulative number of CCN

active at a specified supersaturation. The aerosol number distribution sets an upper limit to the CCN spectra, and can also provide some indication of the shape the CCN spectrum will take. However, the CCN spectra can only be measured by putting the aerosol particles into a supersaturated environment.

The supersaturated environment can be created by 1) an expansion chamber, 2) an isothermal haze chamber, or 3) a thermal gradient diffusion chamber. These are not the only methods which can be used to create a supersaturated environment, but they have been the three most commonly employed.

Expansion chamber. As mentioned above, the earliest aerosol particle counters were actually CCN counters that utilized a very high supersaturation (>17%), activating practically all aerosol particles. Because the degree of expansion can be difficult to control and the supersaturations produced are generally higher than those found in natural clouds, the expansion chamber is rarely used now for measurement of atmospheric CCN.

Isothermal haze chamber. The isothermal haze chamber, first designed by Laktionov [1972], covers the supersaturation range from about 0.01% to 0.2%. Its principle of operation comes from the nearly unique relationship between a particle's critical supersaturation (*i.e.* the supersaturation at which it becomes a CCN or activates) and its size at 100% relative humidity. The relationship may be written [*Fitzgerald et al.*, 1981] :

$$S_c = 77\left(\frac{2\sigma_w}{\rho_w R_v T}\right) D_{100}^{-1} \qquad (2)$$

where S_c is the critical supersaturation in per cent, σ_w is the surface tension of water, ρ_w is the density of pure water, R_v is the gas constant for water vapor, T is the temperature, and D_{100} is the diameter of the aerosol particle at 100% relative humidity.

The chamber is usually a long tube lined with a wet material. The residence time

in the tube is usually 100 seconds or more to give the large particles time enough to equilibrate with the water vapor. Particles are counted and sized when they exit the tube. With this information, a CCN supersaturation spectrum can be derived.

Thermal gradient diffusion chamber. A supersaturation can be created between two wet surfaces if the surfaces are at different temperatures. The temperature and vapor pressure profile between the two surfaces, which is set up by diffusion, is linear. The saturation vapor pressure profile, which is a function of temperature only, is nonlinear and is less than the ambient vapor pressure at every point between the two surfaces. Therefore, every point between the surfaces is supersaturated, with the maximum supersaturation occurring near the center point between the two surfaces. The degree of supersaturation is proportional to the temperature difference between the plates (see Chapter 2 for a more complete discussion).

This type of cloud chamber, as this device has been called, was originally developed by Langsdorf [1936] for cosmic ray studies. Wieland [1956] converted it for use in the study of CCN.

Aerosol particles are injected into the cloud chamber, where some activate and begin to grow. They rapidly (10s of seconds) become visible to the naked eye. Early investigators photographed the droplets and counted them manually. Modern versions incorporate digital imagery and processing software. Other thermal gradient diffusion chambers use a flow-through design, which minimize particle loss by sedimentation. Droplets are counted and sized after passing through the chamber [*Hudson*, 1989]. The size of droplets after they exit the supersaturated environment of the chamber can be related to the supersaturation at which the aerosol particles activated.

Relationship between the aerosol number distribution and the CCN supersaturation spectrum

The relationship between the cloud condensation nuclei supersaturation spectrum and the aerosol number distribution is readily derived from Köhler theory in laboratory settings. However, in the atmosphere where aerosol composition and morphology are rarely known explicitly, the relationship between aerosol particles and CCN can be quite complex. If these two quantities could be linked, insight into both could be gained. Most CCN start as aerosol particles too small to activate at most atmospheric supersaturations; they are transformed through coagulation, gas-to-particle conversion, and heterogenous chemistry into larger particles which will activate at supersaturations on the order of a tenth of a percent. The dominant sink for aerosol is washout [*Pruppacher and Jaenicke*, 1995]; a particle which activates is much more likely to be removed from the atmosphere than one which does not activate.

Relating CCN to the aerosol number distribution would also benefit modeling efforts. GCMs are incorporating ever more sophisticated schemes to calculate CCN concentrations, but most of these schemes involve a parameterization based on the either the aerosol mass or number distribution [*Boucher and Lohman*, 1995; *Ghan et al.*, 1997]. With data which validates these representations, the models can continue to refine and improve their treatment of the indirect effect. Satellite remote sensing would also be improved. Though CCN cannot be detected directly by satellite, aerosol particles can. In some cases, a number distribution can be inferred. With a link between the aerosol number distribution and the CCN spectrum, satellite data can be used to build a truly global database of CCN. This could be compared with global estimates of cloud albedo and effective cloud droplet radius to test aerosol particles' effect on clouds on a global scale.

Systematic attempts to define the link between aerosol particles and CCN outside of the laboratory have been scarce. Most measurements have concentrated on either

aerosol particles or CCN, but not both. A theoretical approach was put forward by Junge and McLaren [1971]. They calculated CCN spectra based on assumed aerosol size distributions and soluble salt contents and concluded that the size distribution was the most important factor in determining the shape. Compositional variations were secondary as long as at least 10% of the aerosol mass was soluble. Fitzgerald [1973] agreed that the shape of the spectrum is largely set by the aerosol number distribution, but determined that the concentration of CCN depends critically on the aerosol composition. Fitzgerald found that in a small metropolitan area (Fort Collins, CO), the measured CCN spectra and the CCN spectra calculated from the aerosol number distribution assuming a composition of ammonium sulfate, did not agree. He concluded that only 15 to 35% of the aerosol particles were composed of soluble material.

In cruises over the Atlantic and Mediterranean, Hoppel [1979] found that the measured and calculated CCN spectra agreed fairly well if a measured value of the soluble fraction and chemical composition was used to convert the aerosol number distribution to CCN spectrum. Liu *et al.* [1996] and Covert *et al.* [1998] came to similar conclusions.

In some situations, the aerosol number distribution is a direct indicator of the number concentration of CCN at a specific supersaturation. In the process of cloud formation, aerosol particles are segregated into those that serve as CCN and those that do not. Hoppel *et al.*[1986, 1994b] have shown that sulfate aerosol mass can be substantially increased through aqueous phase reactions. If the cloud then evaporates, those aerosol particles which were incorporated into cloud droplets are larger because of the additional mass. This produces a gap between aerosol particles which served as CCN and those that did not. The aerosol distribution assumes a bimodal character. The minimum between the two modes can be used as a proxy for the maximum supersaturation the cloud achieved, and the number concentration of particles with diameters greater than the minimum is the number concentration of cloud droplets in the

non-precipitating cloud cycle that produced the bimodal aerosol distribution [Hoppel *et al.*, 1996, Cantrell *et al.*, submitted].

Structure of the thesis

In Chapter 2 I discuss a new instrument and the technique used to establish a link between the aerosol number distribution and the CCN spectrum. Error analysis and laboratory tests show that the instrument is reliable for supersaturations above 0.13%.

Chapters 3 and 4 are a discussion of results from two large field campaigns. In the Aerosol Characterization Experiment 2 (ACE 2), we compare measurements of the CCN spectrum with CCN spectra calculated from aerosol number distributions, size-resolved aerosol chemical information, and aerosol hygroscopic growth data. Comparisons between the CCN spectrum and the aerosol number distribution reveal that a significant portion of the aerosol particles are not activating as efficiently as ammonium bisulfate or sulfate would have. However, when the hygroscopic growth data are incorporated into the calculation, the two curves agree to within 20% in most cases. In the first field phase of the INdian Ocean EXperiment, we show CCN and aerosol data from a south/north transect of the Indian Ocean. Increases of an order of magnitude in CCN active at 0.5% and in aerosol mass correlated with the position of the InterTropical Convergence Zone (ITCZ). Soluble species were depleted in the Northern Hemisphere air mass; inferred aerosol soluble fractions, ϵ, were as low as 0.05.

Measurement of CCN is not the only way to obtain information on cloud-aerosol interactions. In some cases, clouds leave a record of some of their properties on the aerosol number distributions that cycle through them. Chapter 5 presents a large database of bimodal aerosol number distributions, which are used to infer cloud droplet concentrations, maximum supersaturation in cloud, and geometric mean diameter of the cloud-processed mode. These properties were remarkably constant across five widely separated sites at which measurements were performed. Some notable differences are

also discussed.

Aerosol properties affect their ability to act as CCN. In Chapter 6, I present an episode indicating that some aerosol particles may be coated with sulfuric acid. This is contrasted with the possibility of a coating of an organic substance, which might inhibit aerosol particle's activation as CCN.

Chapter 7 is a summary of the results from Chapters 2 through 6. I also indicate some possible directions for further research.

Chapter 2

The Cloud Condensation Nuclei Remover

"One test is worth a thousand expert opinions." -Bill Nye, The Science Guy

Introduction

Cloud condensation nuclei are the subset of atmospheric aerosol which will activate or become cloud droplets at the slight supersaturations (usually < 1%) which occur during cloud activation. To determine which aerosol are CCN, the aerosol particles must be exposed to a supersaturated environment. If the particle grows to the size of a cloud droplet, then it is a CCN.

There are a number of methods by which a supersaturated environment can be created, but the most widely used is the thermal gradient diffusion chamber. The device, which was initially developed for cosmic ray studies [*Langsdorf*, 1936], was adapted by Wieland [1956] for use as a CCN counter. In this type of instrument, the air samples are processed as batches. One sample is drawn into the chamber, aerosol particles which activate and form droplets are counted, the chamber is flushed, and a new sample is introduced. The thermal gradient diffusion chamber can also be used as a flow-through device, in which the sample is drawn continuously through the chamber and droplets are counted as they exit [e.g. *Hudson and Squires*, 1973; *Fukuta and Saxena*, 1979; *Hudson*, 1989].

Detection of the activated CCN has been accomplished by photographing the chamber and counting the drops manually [*Twomey*, 1963; *Fitzgerald*, 1972], processing a digital image of the activated droplets with specifically designed software [Cloud

Condensation Nucleus Counter, Model DH-1 technical manual], and counting individual particles exiting the chamber with an optical particle counter [*Hudson and Alofs*, 1981]. All of these methods have inherent limitations. Counting the drops manually from photographs of the chamber is labor intensive. The drawback of digital processing is the small sample volume, which is defined by the intersection between the illuminating beam and the video camera's field of view. Because of this small sample volume, a reliable measurement at a single supersaturation takes 20 to 30 minutes. Counting activated CCN with an optical particle counter is usually straightforward. However, many devices derive the supersaturation at which a CCN activated from its size as it exits the chamber [*Hudson*, 1989]. This creates problems because many optical counters have a multi-valued response to particle size [*Fitzgerald et al.*, 1981].

We have developed a device which bypasses some of the problems inherent in counting and/or sizing activated droplets. We measure and compare the entire size distribution of aerosol after it has passed through a thermal gradient diffusion. The residence time in the chamber is long enough so that only aerosol which do not activate survive the passage through the chamber and are subsequently sized and counted. CCN become cloud droplets and settle to the bottom of the chamber, which is why we call the device the CCN Remover. By comparing aerosol size distributions which have been exposed to some known supersaturation to distributions which have not been exposed to a supersaturated environment, we can construct a CCN supersaturation spectrum.

The entire size distribution is measured as a function of supersaturation, so we can infer not only the number concentration of CCN, but can also see which aerosol **did not** become CCN at a specified supersaturation. This allows us to define a relationship between the aerosol number distribution and the CCN supersaturation spectrum. This information can be used to infer aerosol properties such as the soluble fraction of the particles.

Any instrument has errors associated with it, and these errors must be either

eliminated or quantified if the instrument is to have any utility. The biggest challenge for the CCN Remover is to quantify the errors in the imposed supersaturation. Because the supersaturation is forced by a temperature difference between the top and bottom plate of the Remover, the error in supersaturation can be derived by propagating errors in the measured temperatures at the top and bottom plate through to the resulting supersaturation. The supersaturation is a fairly sensitive function of temperature, but the desired precision can be obtained with commercially available temperature probes.

The CCN Remover

Figure 2.1 is an engineering drawing of the CCN Remover. Stripped to its essentials, it is two wetted, parallel plates with a specially designed inlet to insure that the sample air is sandwiched between a layer of particle-free, humidified air on the top and bottom. The inlet introduces the sample air flow to the center of the of the chamber, where the supersaturation is at its maximum. The particle-free sheath air constrains the sample flow to the center of the chamber. At the chamber's exit, approximately one liter per minute is drawn to the Scanning Mobility Particle Sizer (SMPS), where the aerosol particles which did not become CCN are sized and counted. The remainder of the flow is siphoned off as excess. Figure 2.2 is a diagram of the CCNR, SMPS, cooling, and temperature measurement system.

The temperature gradient, which forces the supersaturation in the chamber, is created by pumping cold water through the coolant channels in the bottom plate. The temperatures at the surface of the top and bottom plates are measured with thin-film resistance thermal devices (rtds).

The first step in measuring a CCN spectrum with the CCN Remover is to define a reference aerosol number distribution. To do this, we measure several distributions drawn through the Remover with no applied supersaturation. The average of these distributions is designated R. Then, distributions are sampled after having been

subjected to some supersaturation, S, in the Remover. Aerosol which act as CCN will form droplets and fall to the bottom of the chamber; they are removed from the air stream. These distributions are D(S).

The CCN spectrum is then given by :

$$CCN(S) = R - D(S) \qquad (1)$$

Elements of the Remover

The CCN Remover is simple in concept, but nowhere is the saying "The Devil is in the detail" more true than in instrument design and implementation.

Supersaturation field. Air in the chamber is supersaturated because the top and bottom plates are wet, and there is a temperature difference between them. A linear gradient in temperature and vapor pressure is set up by diffusion. These phenomena are described by :

$$\frac{\partial X}{\partial t} = M \nabla^2 X \qquad (2)$$

where in the case of temperature X = T (temperature) and M = κ (coefficient of thermal conductivity), and in the case of vapor diffusion X = e (vapor pressure) and M = D (coefficient of water vapor diffusion in air). In the steady state case, the equation becomes :

$$\frac{d^2X}{dz^2} = 0 \qquad (3)$$

The boundary conditions are $T = T_{z=h}$ at the surface of the upper plate and $T = T_{z=0}$ at the

surface of the lower plate. Similarly, $e = e_s(T_{z=h})$ at the upper plate and $e = e_s(T_{z=0})$ at the lower plate. The solutions are :

$$T(z) = (T_{z=h} - T_{z=0})\left(\frac{z}{h}\right) + T_{z=0} \qquad (4)$$

$$e(z) = (e_s(T_{z=h}) - e_s(T_{z=0}))\left(\frac{z}{h}\right) + e_s(T_{z=0}) \qquad (5)$$

The saturation vapor pressure, which is a function of temperature only, can be calculated from the Clausius-Clapeyron relationship :

$$e_s(T(z)) = e_0 \exp\left(\frac{L}{R_v}\left(\frac{T-T_0}{TT_0}\right)\right) \qquad (6)$$

where e_0 is a reference saturation vapor pressure at the temperature T_0, L is the latent heat of condensation, and R_v is the gas constant for water vapor.

Using Equations 4 - 6, the supersaturation can be calculated from :

$$S(z) = \frac{e(z)}{e_s(T(z))} - 1 \; . \qquad (7)$$

Figure 2.3 is a plot of the supersaturation profile in the chamber, calculated using Equation 7. The supersaturation is zero at both the top and bottom surfaces of the

chamber, where the vapor pressure equals the saturation vapor pressure. At all other points, the chamber is supersaturated with a maximum slightly above the center line of the chamber.

Sheath flow. There is a supersaturation profile in the chamber of the CCNR (an example is shown in Figure 2.3). To confine the sample stream to the region of maximum supersaturation, it is sandwiched between a layer of sheath air on top and bottom. The Remover's inlet was designed to insure that the flow within the chamber is laminar to prevent sample air from mixing out of the region of maximum supersaturation. The Reynold's number for a flow rate of 2.7 liters per minute is approximately 20. Flow between parallel plates is laminar for Reynold's numbers less than 2,300 [*Yuan*, 1967]. Tests with smoke have also demonstrated that the flow in the chamber is laminar. The flow is also stably stratified; the bottom plate is cooled, while the top plate remains at the ambient temperature. Mixing by convection in the chamber is negligible since the lapse rate can be as high as 2.5 K cm^{-1}.

Measuring from the sample flow and only the sample flow at the exit of the chamber is impractical. Some portion of the sheath flow could easily mix into the sample flow as it was taken from the chamber, introducing a systematic error. To avoid this difficulty, the air exiting the chamber is mixed and sampled. One liter per minute is drawn through the SMPS, where aerosol particles leaving the chamber are counted and sized. The remaining flow out of the chamber is siphoned off as excess. Since both sample and excess flow are measured, there is a dilution,

$$F = \frac{Q+A}{A} \qquad (8)$$

where F is the dilution factor, A is the aerosol flow, and Q is the sheath flow.

Residence time. The premise of the technique is that aerosol which act as

CCN will fall out of the sample stream. The residence time of aerosol particles in the chamber must be such that activated particles will fall out of the sample stream in approximately one minute. Ji *et al.* [1998] calculated the time required to remove an ammonium sulfate particle of the critical size (*i.e.* the smallest particle that will activate at the maximum supersaturation in the chamber). They used an artificial profile for the supersaturation in the chamber, and did not consider the full expression for the growth of a solution droplet. However, by making those two simplifications, they were able to acquire a closed-form expression for a CCN's residence time in the chamber.

I modeled the time for a CCN to fall out of the chamber using the calculated supersaturation profile, and a more comprehensive expression for the growth of a solution drop. The supersaturation profile is given by Equation 7. For the growth of a solution drop, I used a slightly modified form of the equation describing the growth of a droplet by diffusion developed by Fukuta and Walter [1970] :

$$\frac{dr}{dt} = \frac{1}{r} \frac{1+.01S-\exp\left(\frac{2\sigma}{\rho_L R_v T r}\right)\left[\frac{n}{n+i\,n_s}\right]}{\frac{L^2}{KR_vT^2}+\frac{R_vT(r+\lambda)}{De_s r}} \qquad (9)$$

where r is the particle radius, S is the supersaturation (in %), σ is the surface tension of the solution droplet, ρ_L is the density of the solution, n is the number of moles of water present in the droplet, i is the van't Hoff factor, n_s is the number of moles of solute present in the droplet, K is the thermal conductivity of air, λ is the condensation length, and D is the diffusivity of water vapor in air.

The exponential term in the numerator on the right hand side of Equation 9 is due to the Kelvin effect, which increases the saturation vapor pressure over a curved surface. Note that this term approaches one as the droplet grows. The term in square brackets on

the right hand side is an expression for the Raoult effect, which describes the depression of the saturation vapor pressure over solutions. Note that this term also approaches one as the droplet grows. The two terms in the denominator of Equation 9 account for the fact that latent heat is released as vapor condenses onto the drop, changing the growing droplet's temperature.

The velocity of the falling drop is determined by the balance between the gravitational and drag force. The Stokes' fall speed is :

$$V = \frac{2r^2\rho_d g}{9\eta} \qquad (10)$$

where v is the settling velocity (equilibrium speed), ρ_d is the density of the particle, g is the gravitational acceleration, and η is the kinematic viscosity of air.

Figure 2.4 shows the calculated and modeled times for a CCN of the critical size to fall out of the chamber. The calculated residence time in the chamber is higher than the modeled time for all critical supersaturations greater than 0.03%. At the highest supersaturations, the discrepancy between the two curves is much less than the residence time of sample air in the chamber. (Times greater than the residence time, which is approximately 75 seconds, are cross hatched on the plot.) The discrepancy is most extreme for $0.13\% > S_{crit} > .035\%$ ($110 < D_{CCN} < 260$ nm).

The approximate expression for a droplet's growth rate used by Ji *et al.* [1998] is :

$$r\frac{dr}{dt} = GS \qquad (11)$$

where G is a constant (100 $\mu m^2 s^{-1}$), and S is the applied supersaturation. It does not account for latent heat release or allow the droplets to shrink as long as the

supersaturation in the chamber is above zero. Equation 9 does incorporate latent heat, and allows droplets to grow or shrink in response to the supersaturation above the surface of the drop. Since the Kelvin and Raoult effect modify the supersaturation above the surface of the droplet, a droplet can shrink even in a supersaturated environment.

For small droplets, Equation 11 overestimates the droplets' diameter after about a second of elapsed time. Figure 2.5 illustrates the growth curves predicted by Equations 9 and 11 respectively for 50 nm droplets subjected to a maximum supersaturation of 0.42%, which is the critical supersaturation for that size ammonium sulfate particle. Equation 11 overestimates the particle's diameter by approximately 20% after 15 seconds of growth.

For particles with critical supersaturations between 0.13% and 0.035%, Equation 11 not only overestimates the droplets' size, but predicts growth when the droplets actually shrink. This case is also shown in Figure 2.5 for 100 nm particles. Aerosol particles begin to grow when they first enter the supersaturated environment of the Remover, but for these large particles, the growth is comparatively slow. The rate of growth is not rapid enough to keep up with the rate of fall through the decreasing supersaturation in the CCNR. The droplets fall into a region of the chamber in which they are subsaturated. The droplets shrink, which decreases the speed at which they fall. This effect allows some droplets to traverse the chamber (*i.e.* not fall out), even though they have been subjected to the critical supersaturation necessary for activation.

The time required to remove successively larger particles goes through a maximum and begins to decrease (see Figure 2.4). Larger particles are removed because even as haze droplets, they are large enough to fall out of the chamber within a minute.

Removal of large CCN and transmission of CCN in the size range $260 < D_p < 110$ nm limits the Remover's effective supersaturation range. Ji *et al.* [1998] calculated 0.064% as a theoretical lower limit for the supersaturation which can be used in the Remover, but they go on to recommend that 0.1% is the lowest practical supersaturation

which should be used. The modeled times for an aerosol particle to fall out of the chamber support this assertion. These particles do fall out of the chamber when exposed to higher supersaturations, so data for supersaturations in the chamber greater than 0.13% are considered to be valid.

Error Analysis

Every instrument has errors associated with it. If the instrument is to be used and "trusted", these errors must either be eliminated or quantified.

Supersaturation. The supersaturation is calculated from measurements of the temperature at the surface of the top and bottom of the chamber. The rtds (Omega Engineering Inc., Stamford CT) agreed with each other to within 5% as shipped. I performed a one-point calibration with boiling water, and verified that the variation between rtds was minimal (approximately 1%) by recording the temperature of the bottom plate, which is a near-solid slab of aluminum, overnight.

Equation 7 can be used to calculate the supersaturation at the midplane of the chamber, provided that the vapor pressure and saturation vapor pressure are known there. These two quantities can be calculated from Equations 4 - 6. The error in the supersaturation due to an error in the measured temperature difference is then :

$$\frac{dS}{dT} = \frac{1}{e_s}\frac{de}{dT} - \frac{e}{e_s^2}\frac{de_s}{dT} \qquad (12)$$

where S is the supersaturation, T is the temperature, e is the vapor pressure, and e_s is the saturation vapor pressure.

The error in the vapor pressure is :

$$\frac{de}{dT} = \frac{z}{h}\left[\frac{de_s(T_{z=h})}{dT} - \frac{de_s(T_{z=0})}{dT}\right] + \frac{de_s(T_{z=0})}{dT} \qquad (13)$$

where $T_{z=h}$ and $T_{z=0}$ are the temperatures at the top and bottom plate respectively. For z = h/2, this expression reduces to the average error in the saturation vapor pressure in the chamber. So

$$\frac{de}{dT} = \left[\frac{de_s}{dT}\right]_{average}. \qquad (14)$$

The error in the saturation vapor pressure is :

$$\frac{de_s}{dT} = \frac{-e_s L}{RT^2} \qquad (15)$$

where L is the latent heat of condensation, and R is the gas constant. I have neglected the variation of the latent heat with temperature here, which introduces negligible error since the temperature range is less than 10 K.

Since $de_s/dT \approx [de_s/dT]_{average}$ (the difference between the two is 20 to 30%), Equation 12 simplifies to :

$$\frac{dS}{dT} \cong \frac{de_s}{dT}\left[\frac{e_s - e}{e_s^2}\right] \qquad (16)$$

A little more algebra and the use of Equation 15 and the definition of S gives an expression for the error in the supersaturation.

$$dS \cong \frac{SL}{RT^2} dT \qquad (17)$$

Figure 2.6 is a plot of Equation 17. The error in supersaturation introduced by a 0.5

degree error in the temperature measurement in the chamber is less than 0.03%.

However, the supersaturation in the chamber is a function of time as well as temperature gradient because the supersaturation is scanned between zero and one percent. Aerosol distributions passing through the CCNR are not exposed to a constant supersaturation, which introduces an error into the supersaturation assigned to the data points in the CCN spectrum.

Cold water is pumped through the bottom plate of the Remover to create the temperature gradient which induces the supersaturation in the chamber. The maximum temperature difference is established in less than five minutes. Aerosol number distributions sampled during this time are exposed to supersaturations ranging from less than 0.1% to greater than 1%. CCN data points derived from these distributions have very large errors in supersaturation associated with them.

Once the maximum supersaturation is established, the cold water flow is shut off, and the temperature of the bottom plate is allowed to come into equilibrium with the room temperature. This takes roughly one hour. Figure 2.7 is an example of how the supersaturation in the chamber changes during the acquisition of a CCN spectrum. The supersaturation decays exponentially, with a decay constant of 1.7×10^{-3} s^{-1}. Each aerosol distribution, which corresponds to a point on the CCN spectrum, takes three minutes. For supersaturations less than 0.5%, the rate of change is approximately 0.07% per data point on the CCN spectrum.

A water vapor deficit is another potential source of error in the supersaturation. The sheath air is humidified before it enters the chamber, so only the sample air, which enters the chamber at ambient humidity, must be "wetted". The characteristic time for water vapor to diffuse through the sample stream can be written as :

$$\tau = \frac{x^2}{2D} \qquad (18)$$

Using 0.3 cm for x, the thickness of the sample stream, and $D = 0.239\ cm^2\ s^{-1}$, $\tau \approx 0.2$ s, which is much less than the residence time of the sample in the chamber.

However, the growing CCN are constantly removing water vapor from the chamber. If the rate of vapor transport from the wet surfaces of the chamber is less than the rate of condensation of vapor onto the growing CCN, the vapor pressure will be less than that calculated using Equations 4 and 5.

A particle with a diameter of one micron will fall one centimeter in a minute and be removed from the chamber. If a CCN grows to this diameter immediately upon entering the Remover, it will fall out of the air stream. I assume an initial concentration of 1,000 CCN cm^{-3} of air, which corresponds to a moderately polluted air mass. In this case, $3x10^{-11}$ moles of water vapor must be removed from the chamber for the CCN to grow to 1 μm diameter. Knowing the approximate value of the vapor pressure in the chamber and using the ideal gas law, I can calculate the volume occupied by the water vapor. At a temperature of 293 K, and a water vapor pressure of 2330 Pa, the volume is $3x10^{-11}\ m^3$. This volume corresponds to a sphere with a radius of $3x10^{-4}$ m. Using Equation 18 again, I calculate a characteristic time of 4 ms for water vapor to "fill in" the deficit introduced by the growing droplets.

Equation 11, which **overestimates** the growth of droplets, predicts that a growing CCN reaches the diameter of 1 μm in approximately 1 sec. $\tau_{diffusion} << \tau_{droplet\ growth}$, so vapor depletion introduces no error into the calculated values of the supersaturation. Only at concentrations greater than $10^6\ cm^{-3}$ does vapor depletion begin to affect the vapor pressure field in the chamber.

Concentration of CCN. The concentration of CCN is inferred by comparing aerosol number distributions which are exposed to no supersaturation in the Remover and those that are exposed to some known supersaturation.

Accounting for the dilution of the sample by the sheath flow, the CCN concentration is inferred from :

$$CCN(S) = (R - D(S))F \qquad (19)$$

where CCN refers to the concentration, F is the dilution factor (see Equation 8), R is the reference distribution, and D is the distribution which has been exposed to some specific supersaturation S. So the error in the CCN concentration is :

$$dCCN = \frac{CCN}{F}dF + FdR - F(dD(S)) \qquad (20)$$

The error in the dilution factor can be written as :

$$dF = \frac{0.1Q}{A} \qquad (21)$$

The sheath and aerosol flow rates are checked with a volumetric flow meter, and are accurate to within 5%. For errors of this magnitude in the sheath and aerosol flow rate, the relative error, dF/F, is approximately 7%.

The reference value, R, in Equation 19 is an average of aerosol number distributions taken at S=0%. These distributions are taken before the supersaturation in the chamber is elevated and again after it has decayed back to zero. R is an average of distributions taken in both of these time frames. The error, dR, is the standard deviation of this average.

The error associated with the individual distributions is a consequence of the low concentration of particles with diameters greater than about 150 nm, and losses in the DMA for smaller particles. The cumulative effect is about 5%.

Another possible source of error in CCN concentration is removal mechanisms in

the CCNR other than fallout. Loss of small particles to the walls of the Remover by diffusion is negligible. The characteristic time for a 10 nm particle to diffuse 1 cm is eight minutes. Larger particles take much longer to diffuse to the walls.

Loss of small particles by diffusion to other particles is also small for clean to moderately polluted situations. For a concentration of 1,000 cm^{-3}, the characteristic time for diffusive loss of 30 nm diameter particles to other particles is over 80 seconds, greater than the residence time in the chamber.

Phoretic forces arise because of the temperature and water vapor gradients in the chamber. Thermo-diffusiophoresis imparts a velocity component toward the bottom of the chamber. However, the velocity due to these forces is an order of magnitude smaller than the settling velocity and can be neglected.

Removal by impaction in the outlet of the chamber could also bias the CCN concentration. A large droplet exiting the chamber could be removed in the bends and turns in the outlet of the chamber. From Hinds (1982), the diameter at which 50% of the particles are removed in an impactor is :

$$d_{50}\sqrt{C_c} = \left(\frac{9\eta D(Stk_{50})}{\rho_p U} \right)^{1/2} \qquad (22)$$

where d_{50} is the particle diameter having a 50% collection efficiency, C_c is the Cunningham slip coefficient, η is the kinematic viscosity of the gas, D is the particle diameter, $Stk_{50} = 0.22$ for a circular tube, ρ_p is the density of the particle, and U is the velocity of the carrier gas. This equation cannot be solved for d_{50} unless C_c is neglected. For a total flow of 3,000 cm^3 sec^{-1} through the Remover, the 50% cutoff is approximately 0.004 mm. This size droplet would fall out rapidly, but the calculation shows that haze droplets, which are in the size range of a few microns, will not be lost to impaction.

Tests of the CCNR

The performance of the CCN Remover was validated by testing it against Köhler theory, which can be used to predict the CCN activity of aerosol provided their chemical composition is known.

Köhler theory describes the equilibrium saturation vapor pressure over a solution droplet and accounts for the enhancement of the vapor pressure over a curved surface (the Kelvin effect) and the depression of vapor pressure over solutions (the Raoult effect). In equilibrium, the relationship between a particle's diameter and the supersaturation can expressed as [*Li et al.*, 1998]:

$$S_\infty \approx 1 + \frac{A}{D_{eq}} - \frac{B}{D_{eq}^3} \qquad (23a)$$

$$A = \frac{4M_w\sigma}{R_v T\rho_w} \qquad (b)$$

$$B = \frac{i\rho_s M_w}{\rho_w M_s} D_s^3 \qquad (c)$$

where M_w and M_s are the molecular weights of water and the salt, σ is the surface tension of the solution, ρ_w is the density of water, i is the van't Hoff factor which expresses the degree of dissociation of the salt in the solvent, ρ_s is the density of the salt, and D_s is the diameter of the dry salt particle. Figure 2.8 is a plot of the Köhler curve for a 50 nm ammonium sulfate particle. Note that the curve passes through a maximum. The supersaturation at which this maximum occurs is called the critical supersaturation, and the diameter, the critical diameter. The critical diameter is the point past which aerosol become CCN.

Using Equation 23, the critical supersaturation can be related to the aerosol

particle's dry size :

$$S_c = \left(\frac{D_0}{D_s}\right)^{3/2} \qquad (24)$$

where S_c is the critical supersaturation and D_0 is a constant for a given chemical composition. For ammonium sulfate, $D_0 = 28$ nm for S_c in percent.

To test the CCN Remover's performance against Köhler theory, we generated a heterodisperse ammonium sulfate aerosol with a TSI Model 3075 Constant Output Atomizer, dried the solution droplets generated with a diffusion dryer, then selected a certain size from the heterodisperse distribution with a TSI Model 3076 Differential Mobility Analyzer (DMA). This near-monodisperse aerosol was pumped into an aluminum-mylar bag, where the concentration levels could be adjusted by pumping filtered air into the bag.

We then measured the CCN spectrum from the bagged air. Since the composition and size of the input aerosol is known, the CCN spectra can be calculated and compared to those actually measured. Figure 2.9 shows two examples of the comparison between CCN spectra calculated from the aerosol distribution using Köhler theory and CCN spectra measured with the CCNR. The top panel is for 30 nm diameter particles and the lower panel is for 50 nm diameter. The calculated CCN spectrum is not a step function as would be expected for a monodisperse aerosol since the DMA does transmit an aerosol distribution of finite width. This width gives the CCN spectrum predicted from Köhler theory its S shape. Figure 2.9 demonstrates that the results from the CCNR agree with Köhler theory within the experimental uncertainty.

Further tests were conducted to verify that aerosol particles of different sizes are not interfering with each other in the chamber. To test this, particles of 200 nm diameter were pumped into the Al-Mylar bag, followed by particles of 50 nm diameter. The CCN spectra for this double-peaked aerosol distribution was measured and compared with the

predicted spectra. The result is shown in Figure 2.10. Again, the CCNR and Köhler theory agree within the error of the measurement. Though the 200 nm particles will not fall out of the chamber when exposed to the critical supersaturation, they will fall out when exposed to slightly higher supersaturations. They do not scavenge the 50 nm particles to an appreciable degree as they fall out of the sample stream. Also note that the Remover performs as predicted for particle concentrations of 2,000 cm^{-3}. Vapor depletion in the chamber introduces no appreciable error for any but the most polluted environments.

Conclusions

The Cloud Condensation Nuclei Remover (CCNR) operates on the principle that activated droplets have a greater fall speed than unactivated droplets in a thermal gradient diffusion chamber. This is used to separate unactivated aerosol from those that have become CCN.

Aerosol particles are exposed to a known supersaturation; those particles that become CCN fall out of the sample stream. Those that do not are sized and counted with a Scanning Mobility Particle Sizer. By comparing aerosol number distributions which have been exposed to a known supersaturation with distributions which have been exposed to a supersaturation of zero, the CCN concentration can be inferred. However, the number of aerosol particles which did not become CCN at a particular supersaturation is also measured so a relationship between the aerosol number distribution and the CCN supersaturation spectrum can be defined.

Errors associated with the CCNR preclude its use for measurements for supersaturations below approximately 0.1%, which corresponds to the critical supersaturation for pure, dry ammonium sulfate particles with a diameter of 130 nm. Vapor depletion and mechanisms of particle removal other than fallout are not significant.

Tests of the chamber have shown that it performs as predicted. It is a reliable instrument that provides information on the connection between atmospheric aerosol and CCN.

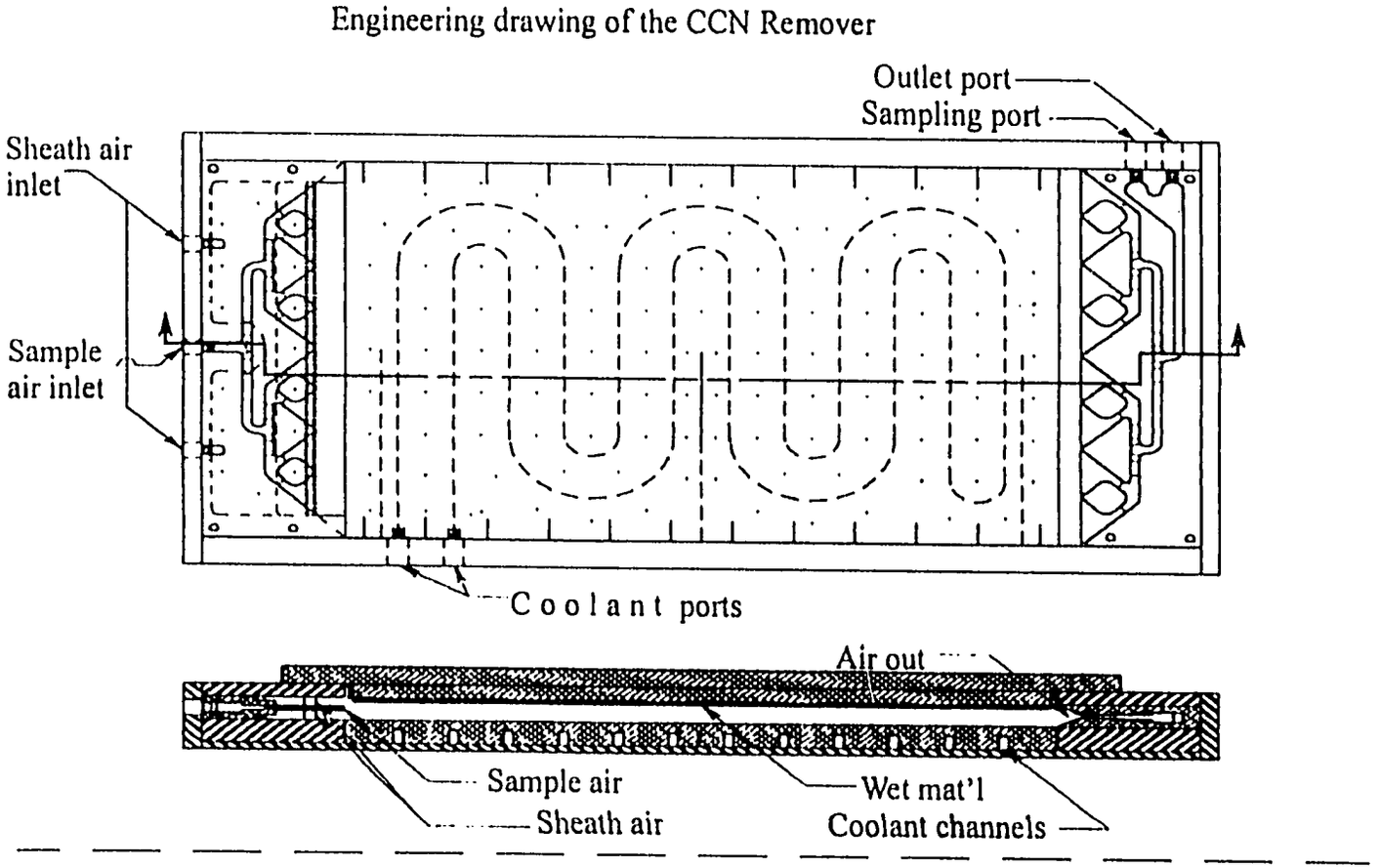

Figure 2.1 Engineering drawing of the CCN Remover, detailing the design of the sample / sheath flow inlet and outlet, which insures that the air flow is laminar and that the sample is constrained in the region of maximum supersaturation. The coolant channels are also shown.

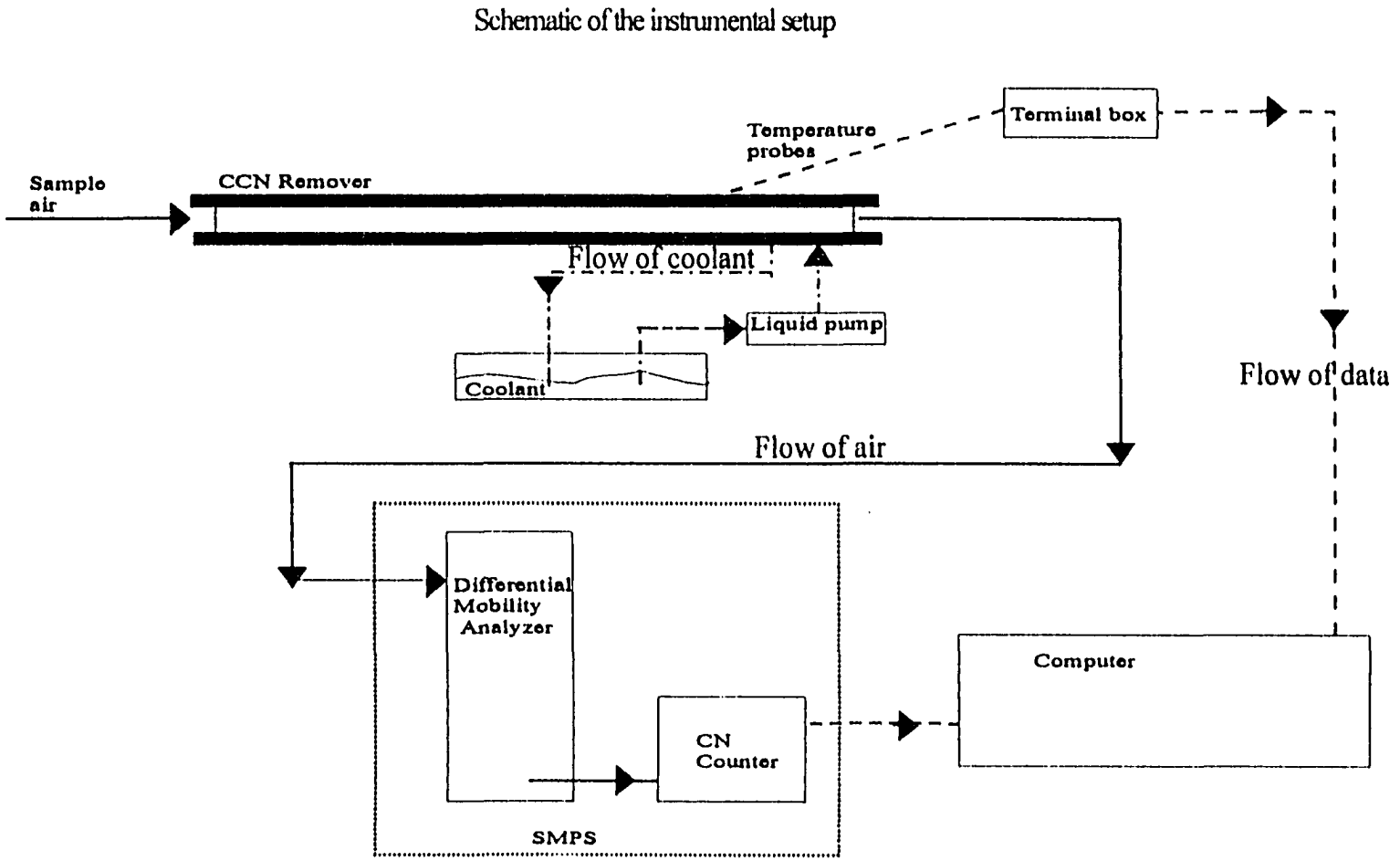

Figure 2.2 Schematic of the setup of the CCN Remover, showing the flow of air, coolant, and data. The SMPS, which consists of the a Differential Mobility Analyzer (DMA) and CN counter are computer controlled. The temperatures are recorded by computer as well. The cooling is controlled manually. The flow of air is manually set, and checked periodically.

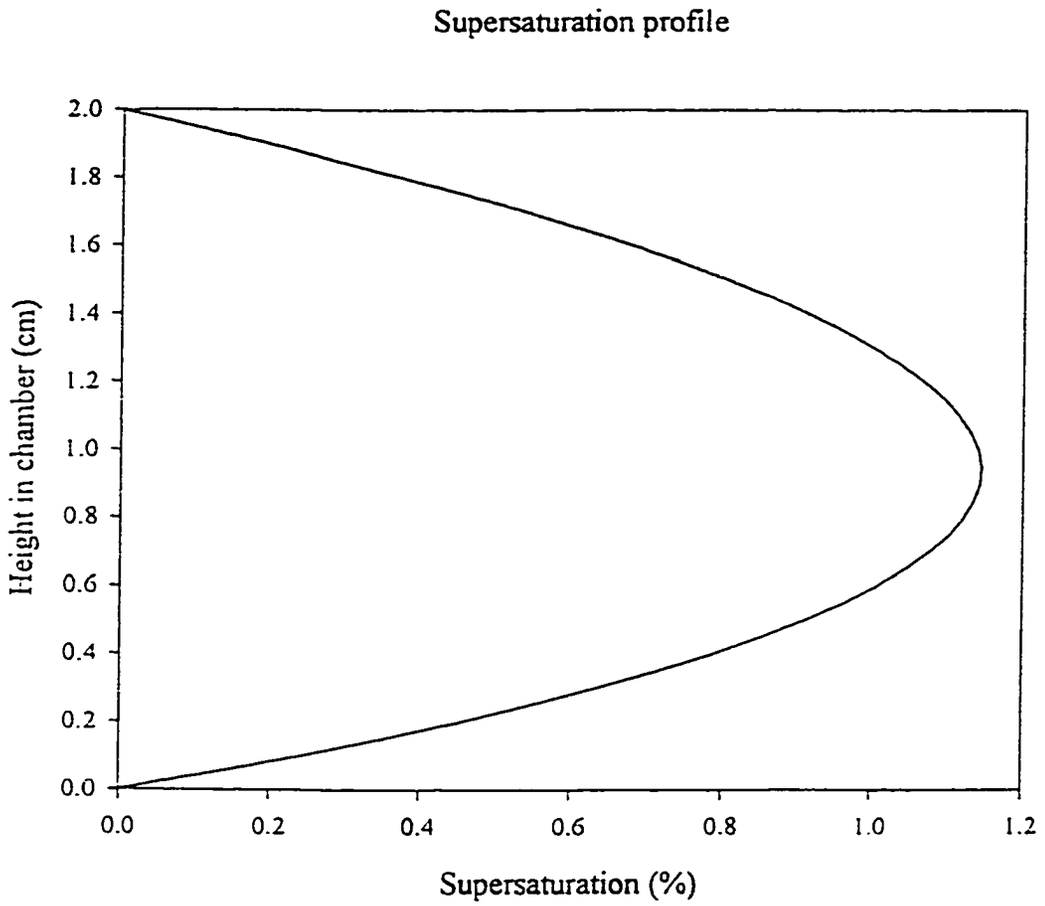

Figure 2.3 The supersaturation profile in the chamber of the CCN Remover shows a maximum near the center of the chamber. The supersaturation is zero at the top and bottom of the chamber.

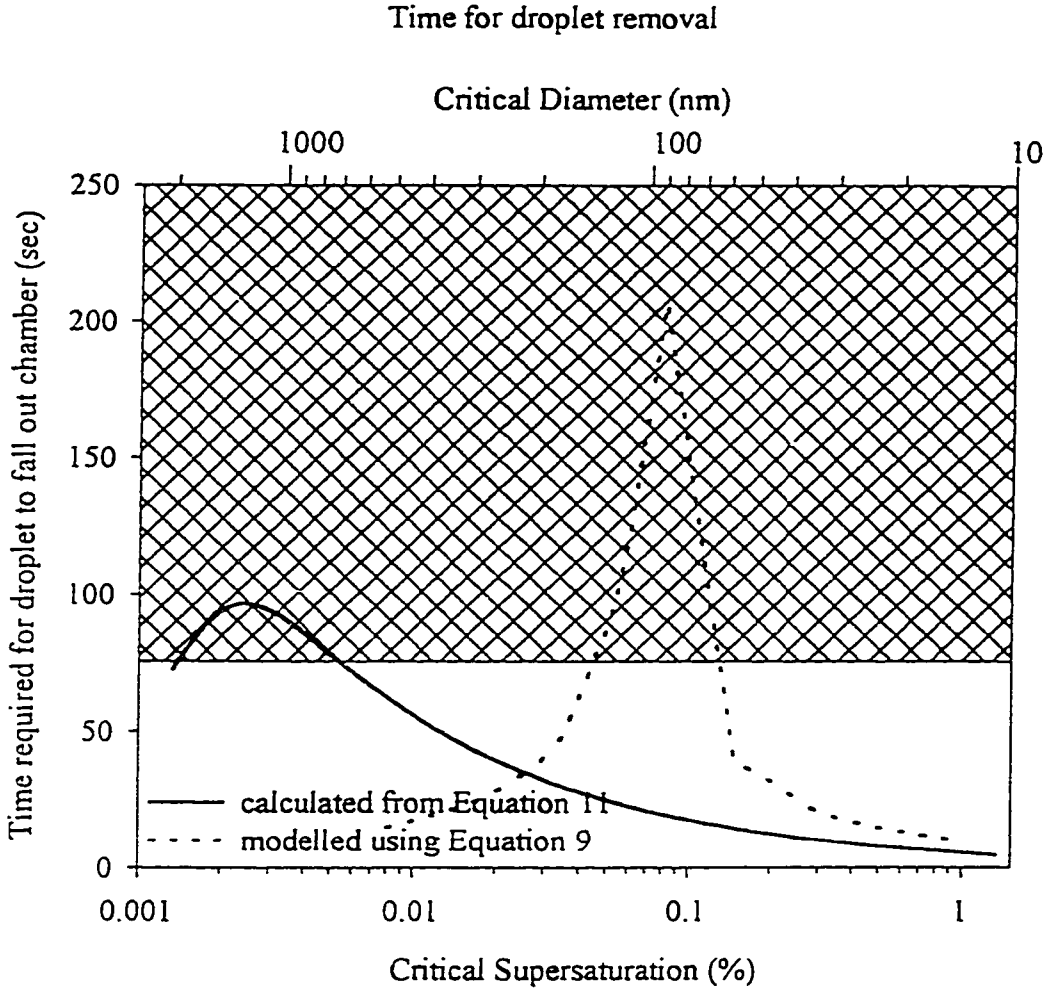

Figure 2.4 Time required for a droplet to be removed from the CCNR as a function of the particle's critical supersaturation calculated using Equations 9 and 11.

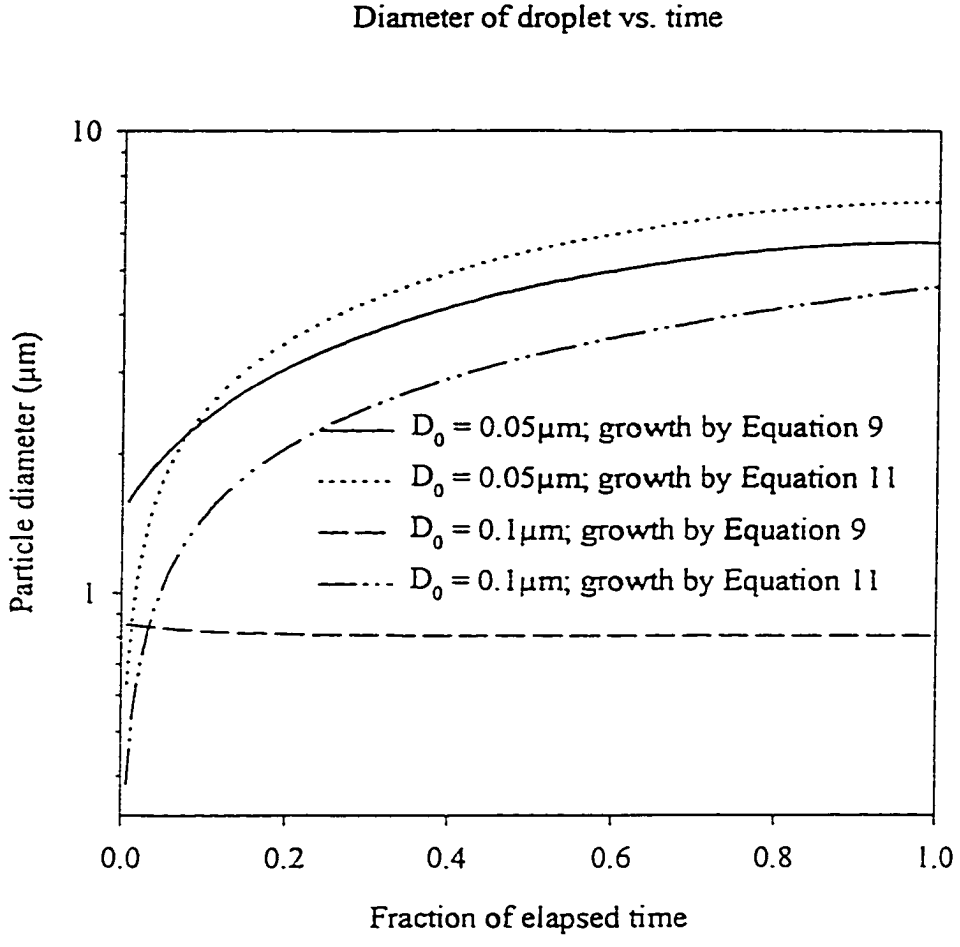

Figure 2.5 Diameter of a droplet in the chamber as a function of elapsed time calculated using Equations 9 and 11.

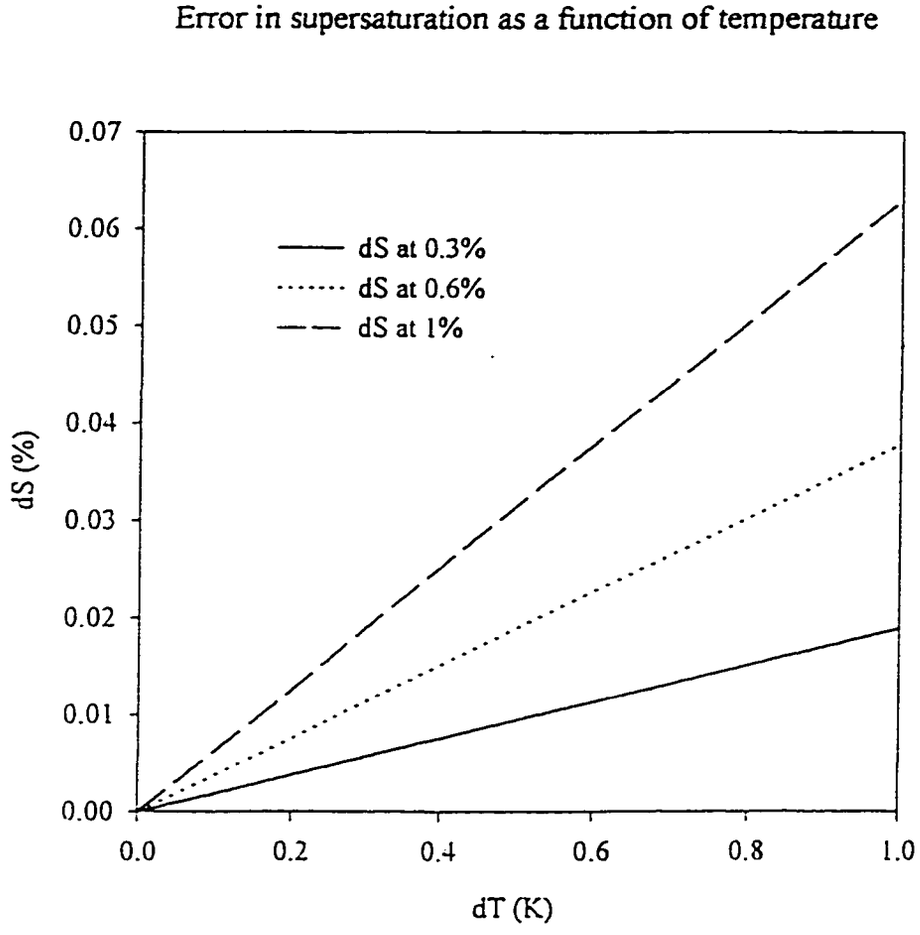

Figure 2.6 Error in supersaturation as a function of the error in temperature for three different supersaturations.

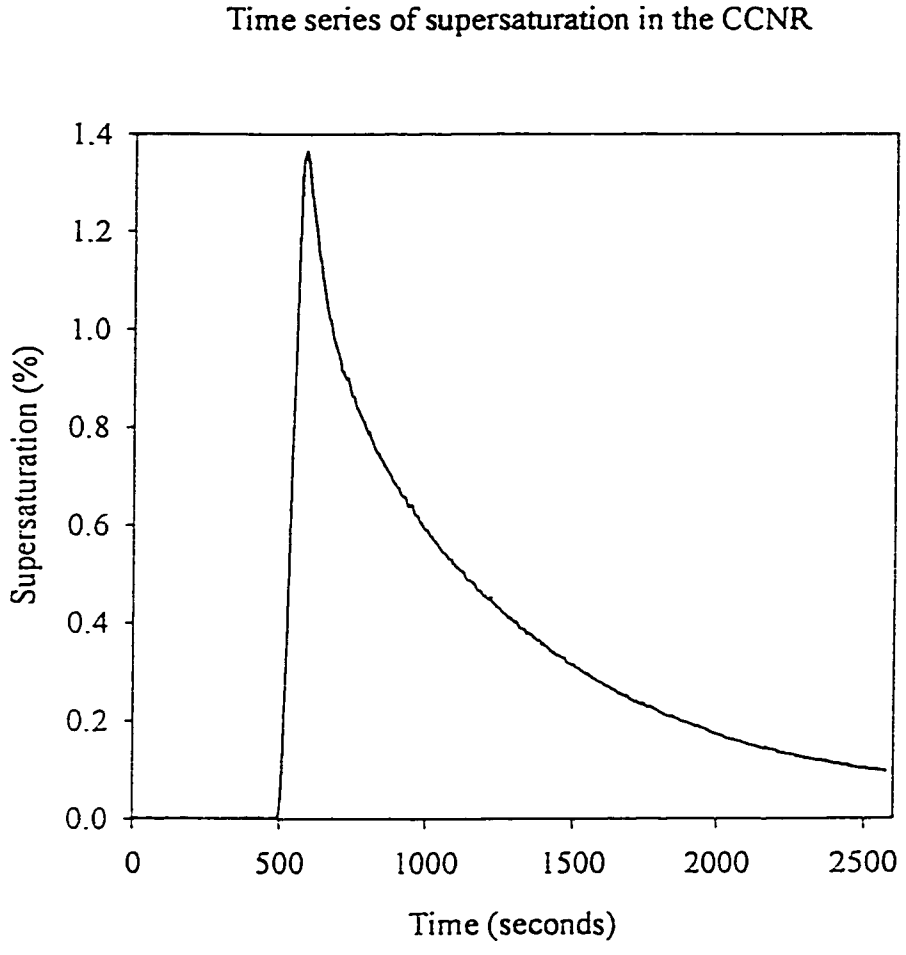

Figure 2.7 Supersaturation in the chamber as a function of time. The temperature difference between the top and bottom plate is increased rapidly, creating the rapid increase in supersaturation. The decay back to zero percent supersaturation is exponential.

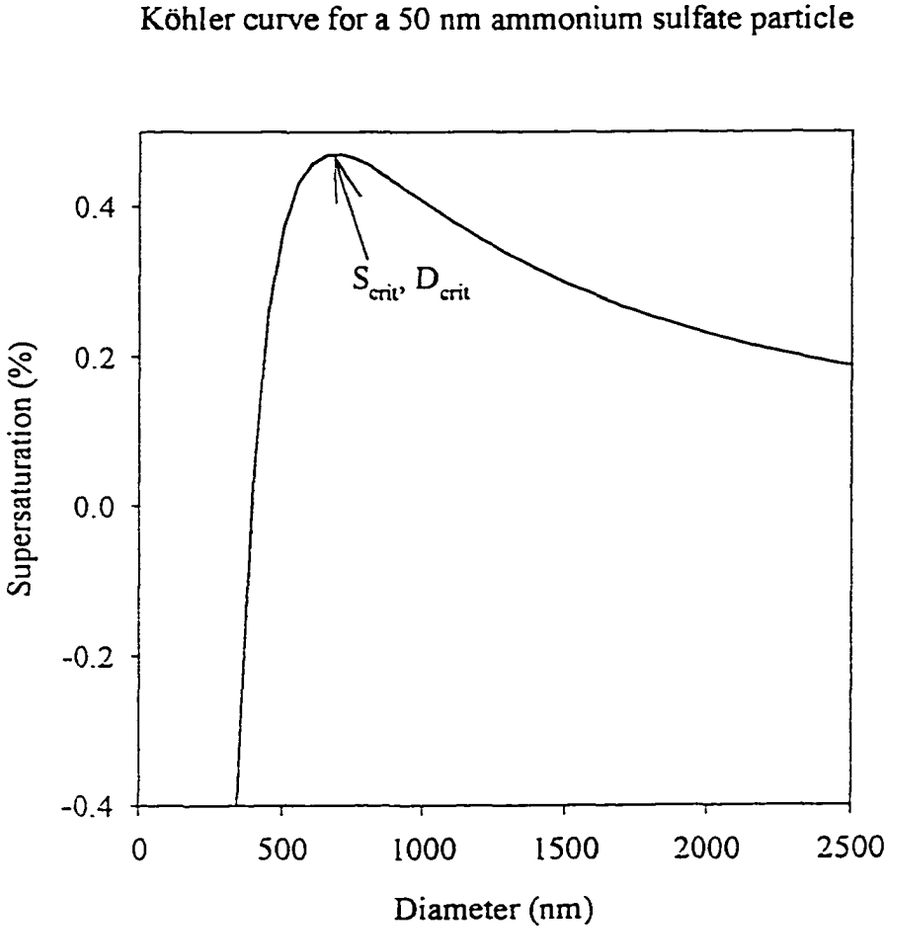

Figure 2.8 The Köhler curve describes the equilibrium relationship between particle diameter and the imposed supersaturation. Once a particle passes the maximum (at S_{crit}), it is said to be activated. Theoretically, it can grow without bound.

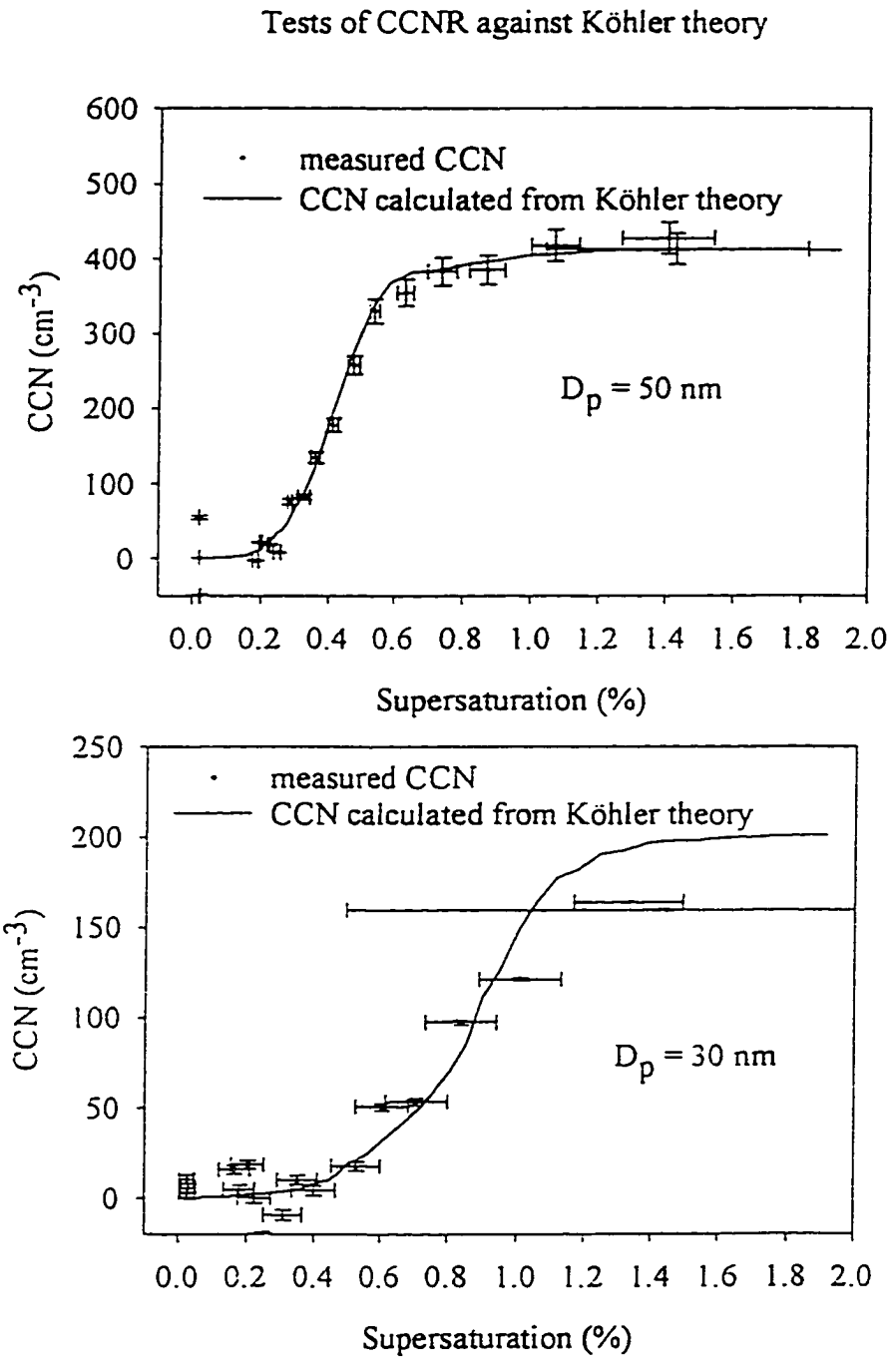

Figure 2.9 Tests of the CCN Remover against Köhler theory for ammonium sulfate particles of diameters 50 and 30 nm. The CCNR agrees with Köhler theory quite well for the 50 nm diameter particles, but not as well for the 30 nm diameter particles. The negative concentrations are artifacts of the measurement technique (see text).

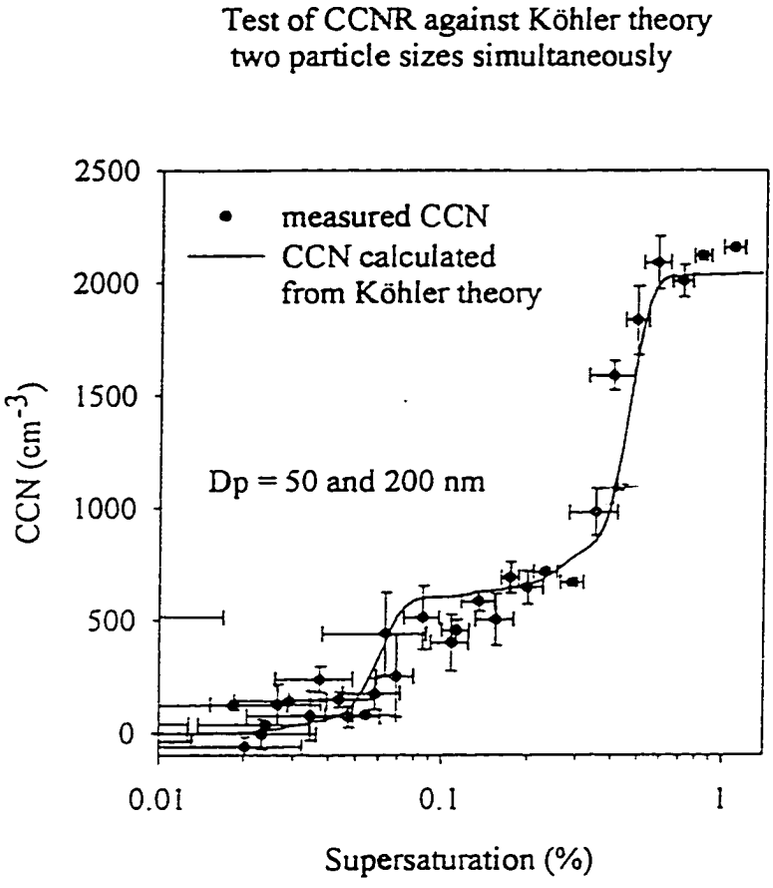

Figure 2.10 A test of the CCN Remover against Köhler theory, measuring 50 and 200 nm particles simultaneously. The measured CCN spectra and Köhler theory agree within the error of the measurement. This shows that particles of different sizes do not interfere with one another in the chamber.

Chapter 3

Aerosol Characterization Experiment 2[1]

"We're well on our way toward getting good data. I just used my first strip of duct tape." -overheard in the aerosol trailer during ACE 2

Introduction

Every liquid-water cloud in Earth's atmosphere forms when supersaturated water vapor in an air mass condenses onto aerosol particles, known as cloud condensation nuclei (CCN). Since these small particles affect cloud properties which can dominate radiative transfer in Earth's atmosphere, they have a significant impact on Earth's climate.

The ability of aerosol particles acting as CCN to modulate Earth's radiation balance by affecting cloud microphysical properties is known as the indirect effect. The magnitude of the effect is so uncertain that the International Panel on Climate Change declined to offer a "best guess", instead giving only a range for the effective flux of 0 to -1.5 W m^{-2} [IPCC, 1995]. CCN alter cloud albedo [*Twomey*, 1991], cloud lifetime and spatial extent [*Albrecht*, 1989], all of which affect the amount of incident radiation a cloud reflects away from the surface. In addition, CCN can also affect the probability that a cloud will precipitate, which can alter the dynamics [*Olsson et al.*, 1998].

Although every CCN is by definition an aerosol particle, not every aerosol particle will act as a CCN in the slight supersaturations reached in most clouds. Understanding the chemistry and physics of the aerosol particles which act as CCN is important for an adequate representation of Earth's radiative balance in climate modeling

---

[1] To be submitted to the Journal of the Atmospheric Sciences.

efforts. Some models attempt to relate emissions of trace gases and particulate matter to Earth's radiation balance. These models should be trusted to predict future climate scenarios only if they can correctly predict CCN activity from the aerosol number distribution and size segregated chemical composition. However, the ability to correctly predict CCN activity from these properties needs to be established experimentally as well as in modeling efforts. One of the key parameters needed to accomplish this goal is a direct relationship between the aerosol number distribution and the CCN supersaturation spectrum. This relationship is readily derived from Köhler theory in laboratory settings, but in the atmosphere, where size segregated aerosol composition and morphology are rarely known explicitly, the link between aerosol particles and CCN can be quite complex.

Most atmospheric measurements have concentrated on either aerosol particles or CCN. From calculations of the CCN supersaturation spectra based on assumed aerosol size distributions composed of soluble salts, Junge and McLaren [1971] concluded that the size distribution is the most important factor in determining the CCN spectra. Variations in composition were secondary as long as at least 10% of the aerosol mass was soluble. Fitzgerald [1973] found that the concentration of CCN depends critically on the aerosol chemical composition, but concurred in the judgement that the shape of the CCN spectrum is determined by the aerosol number distribution. He discovered a significant discrepancy between the measured CCN spectra and the CCN spectra calculated from the aerosol number distribution from measurements made in a small metropolitan area (Fort Collins, CO). His measurements showed that only 15 to 35% of the aerosol particles were composed of soluble material. Hoppel [1979] found that the measured and modeled CCN spectra, taken in cruises over the Atlantic and Mediterranean, were in reasonable agreement if a measured value of the aerosol soluble fraction, ϵ, and chemical composition was used to convert the aerosol number distribution to the CCN spectrum. Liu *et al.* [1996] and Covert *et al.* [1998] came to

similar conclusions.

Experimental Setup

The locations of the ACE 2 sites are shown in Figure 3.1. The measurements presented here were taken at Sagres, Portugal (36° 59' N, 8° 57' W, 50 m above sea level).

CCN spectra. Measured CCN spectra were taken with the CCN Remover (CCNR) operated in series with a scanning Mobility Particle Sizer (SMPS, TSI, Inc; Minneapolis, MN). Recall that the CCN spectrum is derived by first defining a reference aerosol number distribution, R, measured with no supersaturation in the chamber. In practice, R is an average of several distributions. Aerosol distributions measured with a supersaturation in the chamber are designated D(S). The CCN spectrum is then defined by :

$$CCN(S) = R - D(S) \qquad (1)$$

Note that deriving the concentration of CCN in this manner involves successive measurements of aerosol number distributions, which have been exposed to varying degrees of supersaturation. We not only obtain the CCN spectrum, but obtain the spectrum of particles which are **not** CCN as a function of supersaturation. These two pieces of information allow us to relate the aerosol number distribution to the CCN spectrum.

Hygroscopic growth factors. The hygroscopic growth factor is defined as the change in size of an aerosol particle in response to an increased relative humidity. It is usually written as $G = D/D_0$, where G is the growth factor, D_0 is the original diameter of the aerosol particle at some reference relative humidity, and D is the diameter after being exposed to some higher relative humidity. Growth factors were

determined with a Relative Humidity controlled Tandem Differential Mobility Analyzer (RH-TDMA) [*Rader and McMurry*, 1986; *Pitchford and McMurry*, 1994; *Covert et al.*, 1998]. A thin slice of the aerosol number distribution is selected by a DMA, which is held at some reference relative humidity, then exposed to a pre-set relative humidity (either higher or lower) in a conditioner. A second DMA, held at the same relative humidity as the aerosol conditioner, is scanned in a mobility range from 0.5 to 2.5 times that of the first DMA. Since hygroscopic particles will change in size in response to the change in relative humidity, this method can be used to ascertain the presence and relative amount of hygroscopic material in the original slice of the aerosol number distribution.

During ACE 2, the first DMA (TSI model 3071, Minneapolis, MN) was held at a relative humidity of ~10%. Particle diameters of 35, 50, 100, 150, and 250 nm were analyzed. The conditioner and second DMA (TSI model 3071) were held at 90%. The particle concentrations at the outlets of each DMA were measured with a condensation particle counter (CPC, TSI model 3760). A normalized hygroscopic growth distribution function for a relative humidity change from 10% to 90% was the result. Parameterization of the growth in terms of a geometric growth factor, defined as D/D_0, for each of the growth modes was done with the TDMAfit algorithm [*Stolzenberg and McMurry*, 1988].

Aerosol chemical composition. Chemical samples were taken on a daily or twice daily basis with a 5-stage, Berner-type low pressure impactor. The exposed Tedlar foils were cut into small pieces, leached in 1 ml of deionized water (18 MΩ cm^{-1} Nanopure Wilhelm Werner GmbH), filtrated and analyzed by capillary zone electrophoresis. Blank values for every sample were determined by analyzing a part of the foil without a sample spot. No significant blank values were ever obtained for the organic species presented in this paper. A Spectra Phoresis 1000 instrument from Thermo Separation Products (now Thermoquest, San Jose, California) with a fused silica

capillary (i.d. = 75 μm, total length = 70 cm , 63 cm to the detector) was used. The applied electrical field is 420 V cm^{-1}. The buffer used to determine anions consists of an aqueous solution of p-aminobenzoate (10 mM/l), NaOH (resulting in a pH of 9.6), and 8 mM/l. Indirect detection is performed with a diode array detector working at 254 nm. The buffer to separate the main inorganic cations contains Imidazol (5.5 mM/l), phosphoric acid (5mM/l) and ether (2.5 mM/l, to separate ammonium and potassium). Identification of organic acids is performed by adding standards to the sample. Quantification is performed by periodically running external standards, using the peak area for quantification. Because the molar response is independent of the species even unknown compounds can be quantified.

Carbon is determined with a thermographic method by a commercial system (5500 c-mat, Ströhlein, Kaarst, Germany). The sample is placed in a quartz tube and heated rapidly to a specific temperature. To separate between organic and elemental carbon, we first heat the sample under nitrogen to 500°C. Those carbon compounds which evaporate under these conditions are referred to as volatile carbon. In a second step the sample is heated under oxygen to 650 °C, where all carbon except carbonate is oxidized. The vaporized carbon is completely oxidized to CO_2 (T = 850°C, CuO - catalysator), which is analyzed with an IR-detector. Quantification is performed by running external standards.

Calculation of CCN spectra from growth factors and aerosol number distributions

Since every aerosol particle is a potential cloud condensation nucleus, the transformation of aerosol number distribution to CCN supersaturation spectra is a matter of transforming particle diameter to the supersaturation at which that particle will activate, known as the particle's critical supersaturation. This transformation can be accomplished if four specific factors are known : 1) fraction of soluble mass in the particle, 2) osmotic coefficient of the solute, usually assumed to be 1, 3) van't Hoff

factor of the solute, and 4) surface tension of the aqueous solution.

Converting particle diameter to critical supersaturation is readily accomplished in the laboratory, where the particle's chemical composition is known and the relevant factors can be measured for the specific substance. This precision cannot be achieved for atmospheric measurements. Although aerodynamic particle size can be determined accurately, chemical composition is limited to bulk measurements that usually span at least a factor of two in particle diameter (single particle mass spectrometry can provide very detailed information on single particles, but is limited by small sample size). In addition to the coarse resolution, chemical measurements have a lower cutoff at about 50 nm. The bulk composition measurements are also limited in that they do not provide information as to how chemical species are distributed across the particles, known as the degree of mixing. An external mixture indicates that there are at least two populations of particles, and each population has its own, distinct chemical composition. An internal mixture indicates that every aerosol particle is similar in composition to every other aerosol particle. This does not mean that every aerosol particle is composed of only one chemical species, only that each particle has the same mixture of species.

Hygroscopic growth measurements provide an alternative to the calculation of the critical supersaturation from a detailed knowledge of chemical composition. If the hygroscopic growth factors are referenced to the growth factors of a known chemical species (usually ammonium sulfate or ammonium bisulfate), the aerosol soluble fraction can be determined. The factors for the osmotic coefficient, van't Hoff factor, and surface tension of the solution can be taken from properties of the referenced chemical species.

The aerosol soluble fraction, ϵ, can be derived from the hygroscopic growth factors by :

$$\epsilon = \frac{G^3 - 1}{G_s^3 - 1} \qquad (2)$$

[*Pitchford and McMurry*, 1994; *Kerminen*, 1997], where G is the measured growth factor, and G_s is the growth factor for a particle composed solely of a soluble material.

G_s can be derived from :

$$G_s = \left(\frac{100\,\rho_0}{x\,\rho} \right)^{1/3} \tag{3}$$

$$\%RH = 100 a_w \exp\left(\frac{4\gamma M}{\rho R T D} \right) \tag{4}$$

$$\rho = 0.9971 + \Sigma A_i x^i \tag{5}$$

$$a_w = 1.0 + \Sigma C_i x^i \tag{6}$$

[*Tang*, 1996], where ρ is the density of the aqueous solution, x is the weight percentage of solute in the solution, a_w is the water activity, γ is the surface tension of the solution, M is the molecular weight of water, R is the gas constant, T is the temperature, D is the diameter of the particle, and A_i and C_i are experimentally determined coefficients taken from Tang and Munkelwitz [1994].

Using the aerosol soluble fraction and an assumed composition of ammonium bisulfate, the critical supersaturation is given by :

$$S_c = \frac{K}{\sqrt{\epsilon}} \left(\frac{2}{D} \right)^{3/2} \tag{7}$$

[*Hoppel et al.*, 1996], where S_c is the supersaturation and $K = 1.59 \times 10^{-11}$ $cm^{3/2}$ for ammonium bisulfate. Once particle diameters are converted to critical supersaturation, the number of CCN active at a particular supersaturation, S, is the number of aerosol particles with critical supersaturation less than S. We used the ambient aerosol number distributions, used in the definition of R in Equation 1, to construct the CCN spectra based on the hygroscopic growth factors.

Results

There are 20 cases for comparison between measured and modeled CCN spectra. Figure 3.2 is a scatter plot of the modeled CCN using the hygroscopic growth data and aerosol number distributions vs. measured CCN. The least squares fit to the data and the 1:1 lines are shown on the plot. Overall, the measured and modeled CCN concentrations agree within the combined experimental error of the CCN concentrations, hygroscopic growth measurements, and aerosol number distribution. Table 1 shows the parameters for the least squares fit performed for the individual cases. In some of the cases, the y-intercept is quite high, reflecting the inability of the CCN Remover to accurately characterize CCN concentrations at supersaturations below approximately 0.1% [*Ji et al.*, 1998]. Cases from specific episodes are presented below.

June 28. One of the objectives of ACE 2 was to characterize the plume from Europe which is frequently swept out over the south Atlantic Ocean in the summer months. Pristine air masses were rarely encountered at Sagres. However, on June 28 (day of year 179) we were briefly under the influence of a clean, marine air mass.

Figure 3.3 shows that the modeled and measured CCN agree within the experimental error. Also shown in Figure 3.3 is the CCN spectrum calculated from the aerosol number distribution, assuming an aerosol soluble fraction of 1. This CCN spectrum is about 30% greater than the measured spectrum at 1% supersaturation. Figure 3.4 illustrates the time series for selected chemical species.

The concentrations of black carbon were less than 200 ng m^{-3}. While this is not a pristine airmass, it is relatively clean. Concentrations of volatile and nonvolatile carbon were near zero, and sulfate and ammonium concentrations were both low. MSA, a biogenic sulfur species, was relatively high. The concentration of oxalate measured during this time period are not inconsistent with levels found in other marine air masses [*Matsumoto et al.*, 1998].

July 3-4. Figure 3.5 illustrates the CCN spectra for another relatively clean time period (based on black carbon concentrations less than 200 ng/m^3). In contrast to the previous case, both volatile and nonvolatile carbon species were increasing, though not exceptionally high. However, concentrations of sulfate and ammonium were relatively low. The organic species contributes less than 10% of the total mass in the 50 to 420 nm size range.

The CCN spectra show that the agreement between modeled and measured CCN is not as good. The modeled CCN spectra generally predict slightly higher concentrations than were actually measured. Again, the CCN spectra calculated simply assuming an aerosol soluble fraction of 1 are substantially greater than the measured spectra.

July 6. Figure 3.6 shows the CCN spectra for a polluted episode. Black carbon concentrations were 500 to 600 ng/m^3, and sulfate concentrations in the 140 to 420 nm size range were greater than 2 $\mu g/m^3$. Volatile and nonvolatile carbon were relatively high, as was oxalate, consistent with a polluted air mass.

The agreement between the modeled and measured CCN spectra in this case is somewhat better than the previous case. The CCN spectra modeled using the measured aerosol soluble fraction are higher than the measured spectra in three of the cases, and lower in two. The spectra modeled assuming an aerosol soluble fraction of 1 are higher in all cases.

June 24. Figure 3.7 illustrates the CCN spectra for another polluted episode. Black

carbon concentrations were greater than 500 ng/m^3, and sulfate was increasing to 5 μg/m^3. Oxalate and volatile carbon were also high, but nonvolatile carbon was relatively low.

The modeled and measured CCN spectra agree quite well for two of cases when the measured aerosol soluble fraction is used, but the modeled spectrum is substantially greater than the measured in the last case.

Discussion

Usually, in clean situations the dominant chemical species in the size range contributing the majority of the CCN number is either sulfate or sea-salt, though there is some evidence that organic species may play a role even in background air masses [*Matsumoto et al.*, 1997]. In the case of sulfate or sea-salt, the activation characteristics are well known [*Seinfeld and Pandis*, 1998]. The transformation from aerosol number distribution to CCN supersaturation spectrum is a straightforward process because particle diameter can be unambiguously converted to a particle's critical supersaturation. The activation characteristics of organic species are still being explored [*Cruz and Pandis*, 1997, 1998; *Li et al.*, 1998; *Shulman et al.*, 1996]; calculation of the critical supersaturation of particles composed of organic compounds may not be possible with the physical data currently available. To further complicate the matter, organic species may inhibit or actually prohibit the well characterized salts from activating as they would in the absence of the organic species through either kinetic or thermodynamic effects.

Bigg [1986] compared the CCN spectrum calculated from the aerosol number distribution with the measured CCN spectrum at Cape Grim, Tasmania, and suggested that a suppression in the activation of aerosol particles due to surface-active organic compounds could explain the factor of two to three between the calculated and measured CCN spectra. In a laboratory study, Li *et al.* [1998] concluded that sodium dodecyl sulfate, a surface-active organic compound, did increase critical supersaturation

from 0.1% to 0.25% as sodium chloride was displaced by the organic.

Kerminen [1997] concluded that water-inhibiting compounds in aerosol particles reduce the particle's uptake of water through thermodynamic rather than kinetic effects. Through comparison of hygroscopic growth measurements with chemical composition of the aerosol, Saxena *et al.* [1995] found that organics diminished the water uptake of inorganic species in some situations. Cruz and Pandis [1998] found that dioctylphthalate, a nonhygroscopic organic compound, did not prohibit ammonium sulfate particles from activating even though it completely coated the particle.

Covert *et al.* [1998] found that the agreement between their modeled and measured CCN concentrations at Cape Grim during the first Aerosol Characterization Experiment was better in pristine air masses. In air masses which had continental, anthropogenic, or biomass burning characteristics, the agreement was not as good. Their hygroscopic growth measurements showed that there was not enough insoluble material to explain the discrepancy between the modeled and measured CCN spectra. They hypothesized that surface-active organic species might be responsible for the differing results. At a site in the northern Atlantic, Liu *et al.* [1997] also compared modeled and calculated CCN spectra, but only in the supersaturation range from 0 to 0.1%. The agreement was good for nine of the 12 cases they considered. The three cases in which the agreement was marginal or poor were not distinguished by exceptionally high or low concentrations of organic species. Both Covert *et al.* and Liu *et al.* concluded that the agreement between the modeled and measured CCN concentrations was improved by incorporating the aerosol soluble fraction, which was less than 1.

As expected from the previous studies, the agreement between the modeled and measured CCN spectra was good (see Figure 3.3) on June 28, the cleanest time period encountered. Concentrations of volatile and nonvolatile organic compounds were below detection limits. However, we also obtained reasonable agreement in a polluted air mass on June 24 (Figure 3.7). In this case, the concentration of volatile carbon was relatively

high, but the sulfate loading was quite substantial, almost an order of magnitude higher than the carbon mass.

In another polluted episode on July 6, the agreement between our modeled and measured CCN spectra was not as good (Figure 3.6). Though the concentration of volatile carbon was comparable to the case measured on June 24, the sulfate concentration was lower. The organic species were a higher fraction of the total mass. The agreement between modeled and measured CCN spectra was also not as good on July 4. Though not pristine, this day was relatively clean. It is distinguished from June 28 by slightly higher levels of black carbon and higher levels of volatile and nonvolatile carbon. The poor agreement between the modeled and measured CCN spectra may be due to the presence of these elevated levels of carbon.

How these elevated levels of organic species are affecting the activation of aerosol particles is unclear. Even if the organic species were nonhygroscopic or inhibited the uptake of water by hygroscopic compounds, the effect should be seen in the hygroscopic growth data. Incorporation of the aerosol soluble fraction into the calculation of the modeled CCN spectra accounts for this effect. Surface-active compounds could be inhibiting the activation of the aerosol particles, but with the present data set we cannot confirm or refute this hypothesis.

Conclusions

We have compared the measured CCN spectra with CCN spectra calculated from the aerosol number distribution and aerosol soluble fractions calculated from measured hygroscopic growth factors for Sagres, Portugal during the second Aerosol Characterization Experiment. Overall the agreement between the measured and modeled CCN concentrations is within the experimental uncertainties of the two techniques. In all cases, the agreement between the modeled and measured CCN spectra was improved when the aerosol soluble fraction calculated from the measured hygroscopic growth

factors was included.

Agreement between measured and modeled CCN spectra was better during time periods when the concentrations of organic species were low. The measured hygroscopic growth factors should account for any insoluble organic species, so the reason for this discrepancy is unknown. Surface-active organic compounds which inhibit the transport of water from the vapor to the liquid phase may be responsible for the inconsistency.

Locations of sampling stations during ACE 2

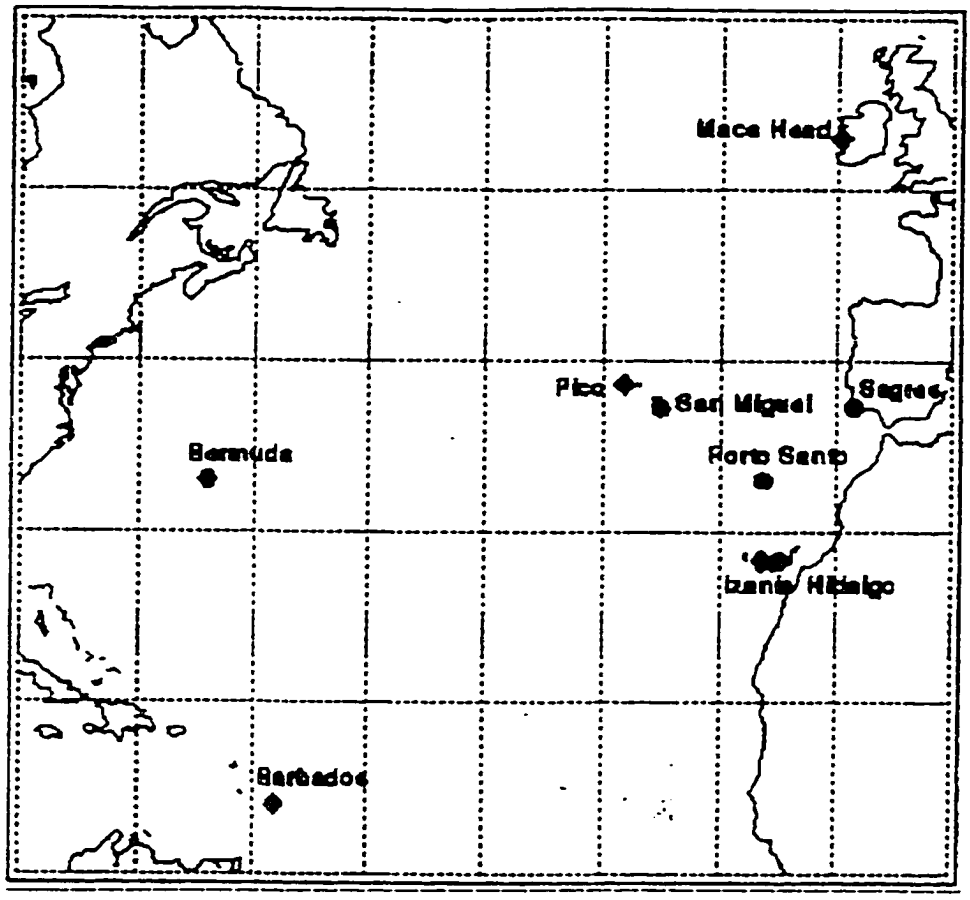

Figure 3.1 Locations of the sampling stations during ACE 2. Our data was collected at Sagres, Portugal, the southwestern-most point of the European continent. During the summer months of June and July, the Azores High quite frequently sweeps pollution off the European out over the south Atlantic Ocean. One objective of ACE 2 was to observe the evolution of this pollution plume.

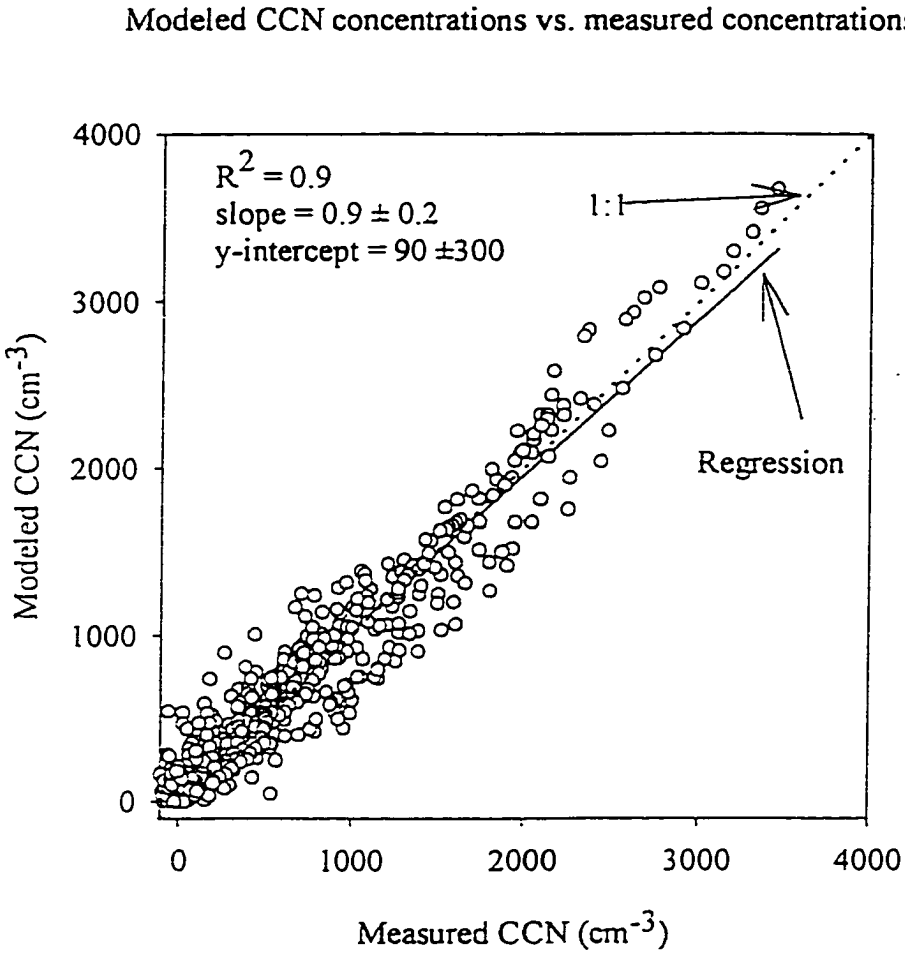

Figure 3.2 Scatter plot of the modeled vs. measured CCN concentrations. The two agree overall, though there is substantial scatter.

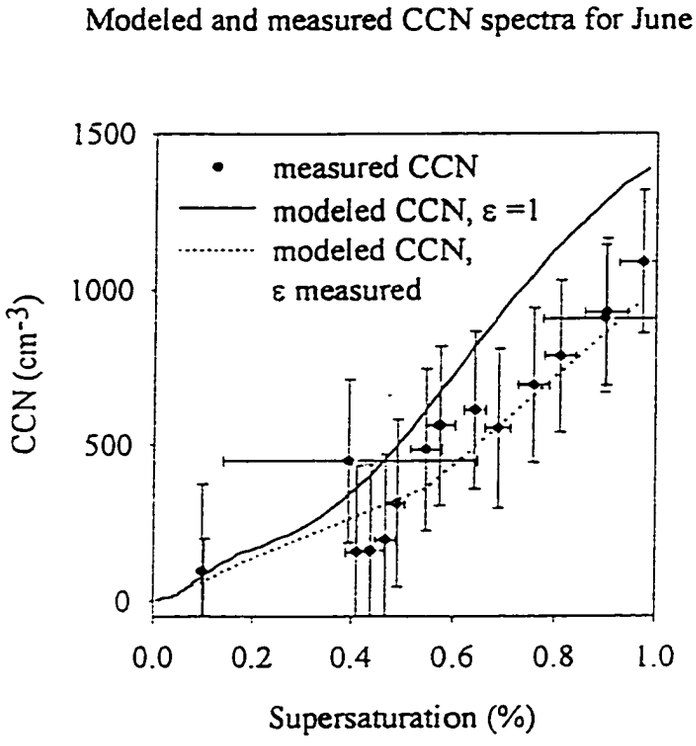

Figure 3.3 CCN spectra at Sagres, Portugal for June 28 (day of year 179). In this relatively simple air mass (modified marine) the agreement between the modeled and measured CCN spectra was within the errors of the measurements.

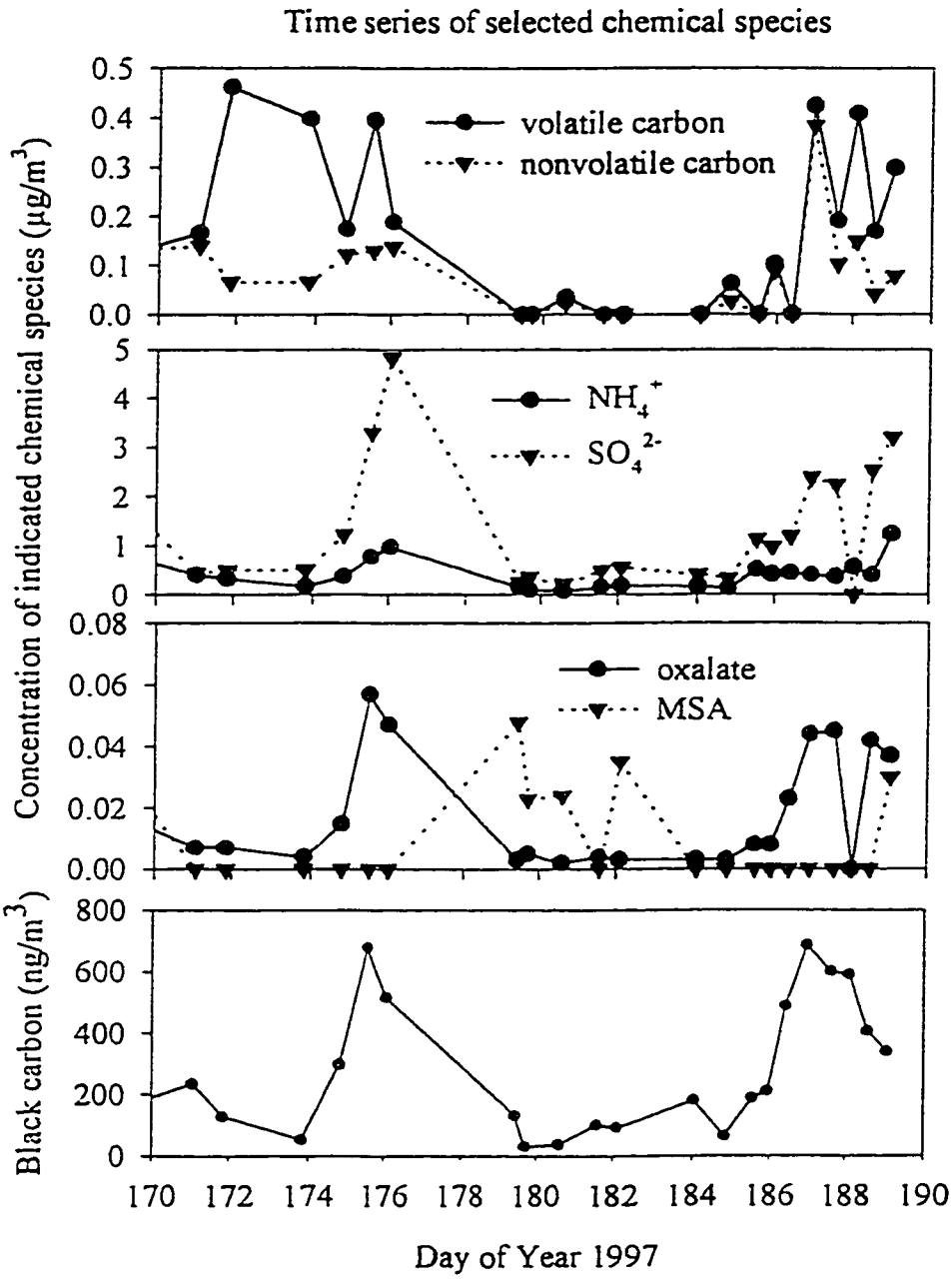

Figure 3.4 Time series for selected chemical species at Sagres for day of year 170 to 190. The measurements presented are for stage 4 of the impactor, which covers the size range $0.14 < D_p < 0.42$ µm.

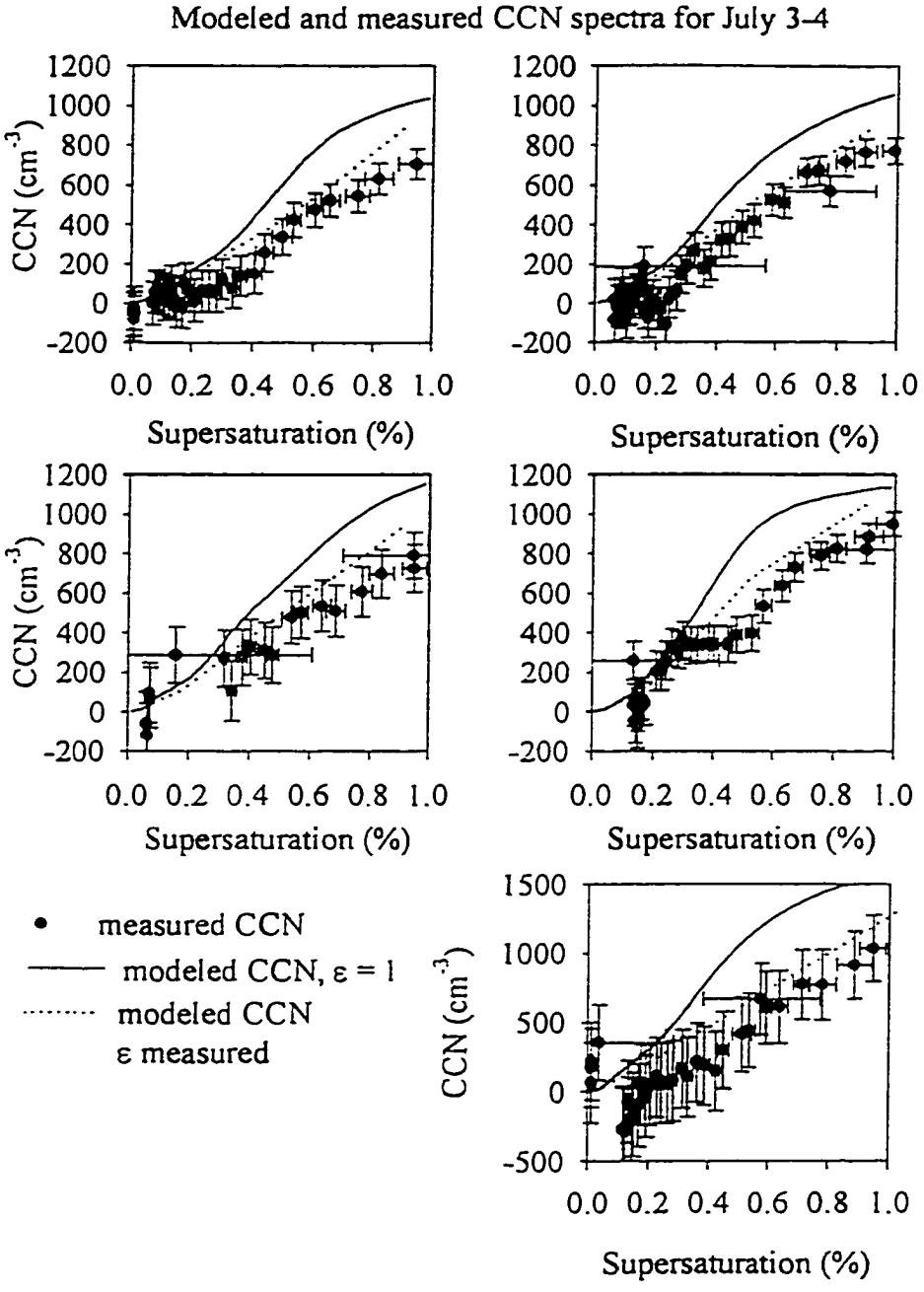

Figure 3.5 Modeled and measured CCN spectra for July 3 - 4 (day of year 184 -185). The agreement between the two is not as good as for June 28 (Figure 3.3). The pulse of carbon mass seen in Figure 3.4 may be responsible for the poor agreement between the modeled and measured CCN spectra.

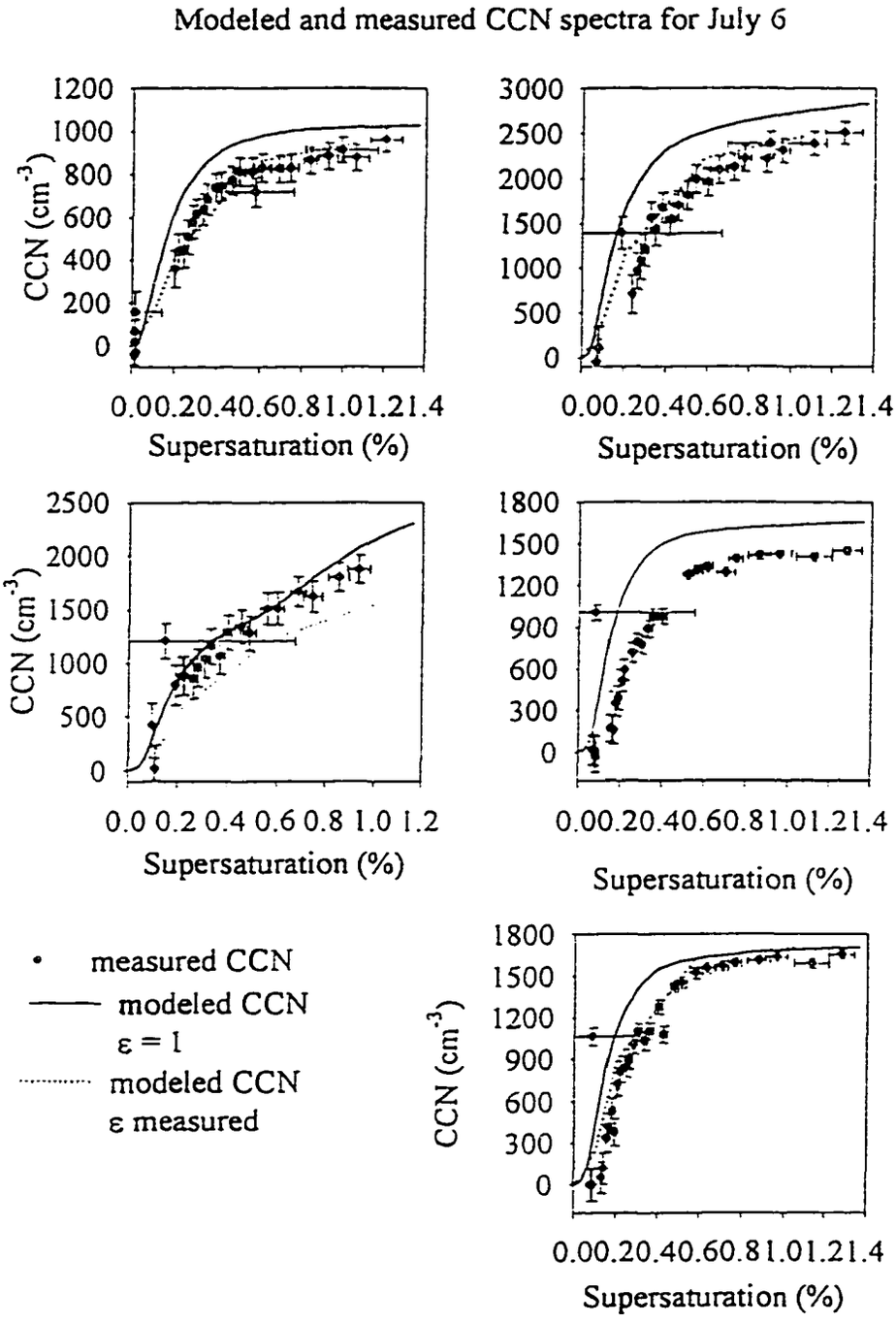

Figure 3.6 Modeled and measured CCN spectra for July 6 (day of year 187). The agreement between modeled and measured CCN spectra is good overall, even though black carbon concentrations were quite high, indicating a polluted air mass.

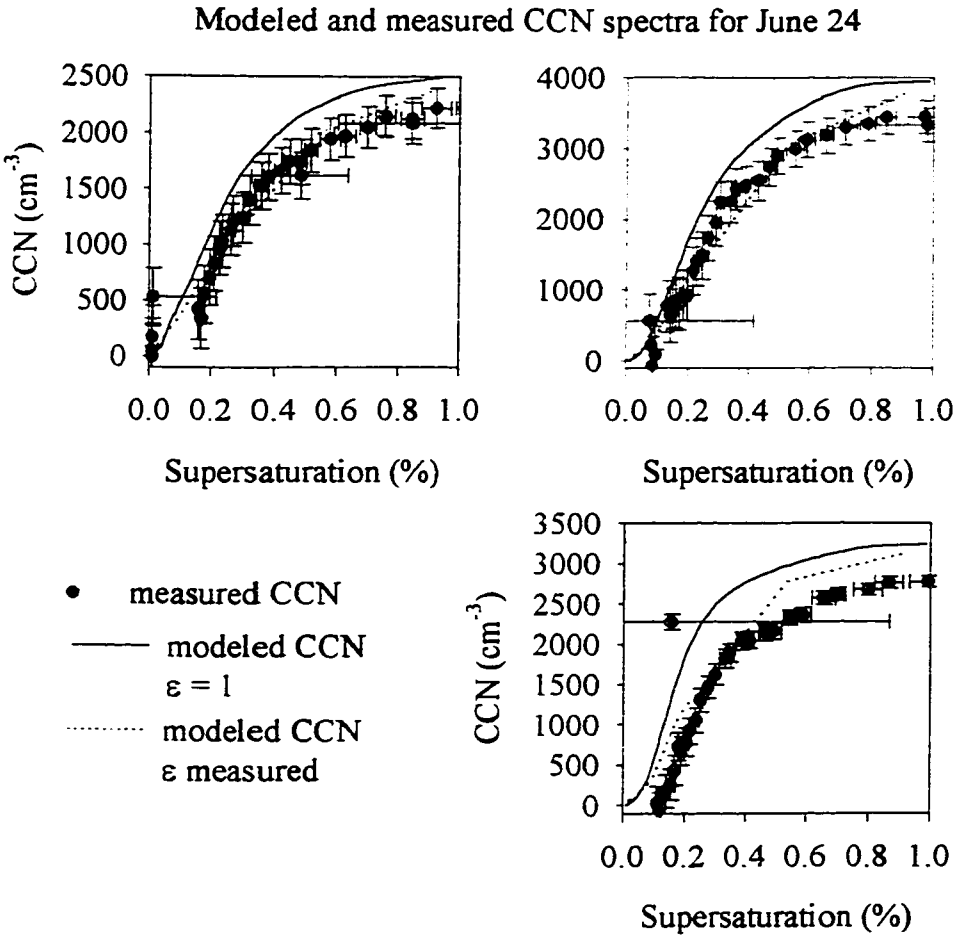

Figure 3.7 Modeled and measured CCN spectra for June 24 (day of year 175). Note that the concentrations are quite high (> 3000 cm^{-3} at 1% supersaturation) and that black carbon concentrations are also quite high (see Figure 3.4).

Parameters for equation CCN(modeled) = Y + A*CCN(measured)

Day	y-intercept	slope	R^2
June 20	24	1.2	0.98
23	-24	0.79	0.89
24	1	1.01	0.95
24	87	0.94	0.96
24	486	0.90	0.96
28	79	0.78	0.89
29	-3	0.69	0.84
30	76	1.02	0.94
July 3	73	1.08	0.92
3	96	0.96	0.92
3	50	1.10	0.86
3	40	1.10	0.87
4	213	0.95	0.75
5	40	0.67	0.92
6	-25	1.03	0.88
6	311	0.90	0.95
6	119	0.68	0.91
6	232	0.84	0.98
6	293	0.84	0.97
7	-29	0.93	0.92

Table 3.1 Y-intercept, slope, and correlation coefficients for modeled vs. measured CCN concentrations. Many of the y-intercept values are significantly different from zero, probably because the CCNR is not accurate for supersaturations less than 0.13%

Values for A_i and C_i for NH_4HSO_4

$C_1 = -3.05 \times 10^{-3}$	$A_1 = 5.87 \times 10^{-3}$
$C_2 = -2.94 \times 10^{-5}$	$A_2 = -1.89 \times 10^{-6}$
$C_3 = -4.43 \times 10^{-7}$	$A_3 = 1.763 \times 10^{-7}$

Table 3.2 Values for A_i and C_i, used in the calculation of the activity and density of a solution (see Equations 5 and 6). The values are from Tang and Munkelwitz, 1994.

Chapter 4

The Indian Ocean Experiment[2]

"It (cloud formation) is just air and water vapor and aerosols." -Jasper Kirkby

Introduction

There are few places on Earth with a more pronounced juxtaposition of air masses than in the mid-Indian Ocean during the Asian winter monsoon. From January to April, the dominant circulation in the Northern Hemisphere is a low level flow from the subcontinent out over the ocean toward the InterTropical Convergence Zone (ITCZ). A mixture of aerosol particles derived from urban pollution, natural organic species, biomass burning, and dust is carried with the air streaming out from over the subcontinent. The flow in the Southern Hemisphere is from the open ocean. Though this region is relatively free from anthropogenic influences, long range transport from Madagascar and Australia can perturb the "background" conditions (V. Ramanathan, personal communication). These two air masses, with their strikingly different characteristics, meet at the ITCZ, and their confluence provides an opportunity to study the role of the ITCZ in interhemispheric transport of trace gases and aerosol [*Krishnamurti et al.*, submitted; *Rhoads et al.*, 1997]. It is also a unique natural laboratory for the investigation of how anthropogenic activities may affect Earth's radiative balance through the perturbation of cloud microphysical properties.

For a given dynamic forcing and liquid water content, increasing the number of cloud condensation nuclei (CCN) can increase a cloud's droplet concentration, its albedo, and therefore, the amount of radiation it reflects [*Twomey*, 1991]. Spreading the

---

[2] Prepared for submission to Tellus.

liquid water over a greater number of CCN results in smaller cloud droplets, which can decrease the chance of collection and coagulation between droplets, leading to a decreased chance of precipitation. This can result in increased cloud thickness and lifetime [*Albrecht*, 1989], which can also enhance a cloud's reflectivity [*Pincus and Baker*, 1994].

The close proximity of a polluted and clean air mass at the ITCZ provides the chance to test this hypothesis because, except for the differing aerosol sources, the synoptic situation is often symmetrical about the ITCZ. On either side of the ITCZ, which is dominated by cumulonimbus clouds, the prevailing cloud type is marine stratocumulus, which are susceptible to changes in the concentration of CCN. We expect the marine stratocumulus to the south of the ITCZ to have substantially lower reflectivities and higher probability of precipitation than those to the north. Cloud droplet radii derived from AVHRR data from the NOAA-9 and NOAA-10 satellites show a marked north/south gradient in the Indian Ocean/Arabian Sea during the winter monsoon [*Han et al.*, 1994]. Droplet radii near the Indian coast were almost a factor of two smaller than radii in air masses south of the ITCZ. For the same liquid water content, this implies eight times more cloud droplets with four times the surface area in the Northern Hemisphere.

I observed this in a qualitative way during the cruise. A few degrees south of the ITCZ, rain shafts were frequent, and the clouds appeared greyish in color when forward-lit (*i.e.* the light reaching me was backscattered from the cloud), the sun approximately 20 degrees above the horizon. The greyish color suggests a relatively sparse number concentration of large cloud droplets (*i.e.* a relatively small optical depth, which excludes a high concentration of small drops). A few degrees north of the ITCZ, very few rainshafts were observed, and clouds of similar size and depth viewed under similar conditions appeared noticeably brighter, indicating a higher concentration of small cloud droplets (*i.e.* a relatively high optical depth).

We present the first (to our knowledge) CCN spectra from this region of the Indian Ocean/Arabian Sea, aerosol mass concentrations for four major ionic species, and the mass concentration of black carbon and total carbon. Our CCN measurement technique also relates CCN to the aerosol number distribution. This additional piece of information indicates that aerosol particles in the Northern Hemisphere air mass appeared to have soluble fractions as low as 0.05.

Cruise Track and Experimental Setup

The measurements were made aboard the Indian research vessel *Sagar Kanya* in February and March of 1998 as part of the INDian Ocean EXperiment (INDOEX), a multinational research effort culminating in an intensive field campaign in the winter/spring of 1999. Previous results from this project are described in Rhoads *et al.* [1997], Jayaraman *et al.* [1998], and Krishnamurti *et al.* [submitted].

The cruise track, shown in Figure 4.1, spanned almost 35 degrees of latitude, providing the opportunity to sample north/south gradients in aerosol properties, radiation, and trace gases over the Arabian Sea and Indian Ocean. We penetrated the ITCZ enabling us to sample both Northern and Southern Hemisphere air masses and to investigate possible cross-ITCZ transport of aerosol from north to south.

Because of difficulties with the sampling setup and following winds for most of the journey from Goa to Mauritius, only data from the last leg of the cruise (March 19 to 28) will be presented here. That section of the cruise track is marked in bold in Figure 4.1.

Air was drawn through a 30 meter long sampling duct (5.7 cm inner diameter) from a position well forward on the ship. The duct's inlet was approximately 15 meters above the surface of the water. The residence time in the duct was approximately 2 minutes, and air was subsequently drawn from the center line to minimize particle losses. To eliminate the possibility of contamination from the ship's exhaust, the CCN

spectrometer was operated only at times when the ship was underway.

CCN spectra were measured with the CCN Remover, described in Chapter 2. Recall that to construct a CCN spectrum, we measure distributions with no supersaturation in the CCNR. These ambient distributions are defined as the reference, R. Then, we force a temperature difference between the two plates by cooling the bottom one. Distributions measured with a temperature difference in the chamber experience some degree of supersaturation. These distributions are D(S). The CCN spectrum is defined by :

$$CCN(S) = R - D(S) \qquad (1)$$

Since CCN and the unactivated aerosol particles are measured, the soluble fraction, ϵ, which is the ratio of the volume of soluble material to the total volume of the dry particle, can be inferred from the measurements by comparing the measured CCN spectrum with CCN spectra calculated on the basis of the ambient aerosol number distributions and size segregated aerosol chemical composition.

Results and Discussion

South/north gradients in CCN and aerosol soluble fraction. We observed an increase of an order of magnitude in the number concentration of cloud condensation nuclei on the south to north transect through the ITCZ. There was also a change in the apparent aerosol soluble fraction, ϵ. The latitudinal dependence in both is shown in Figure 4.2. South of the ITCZ, the CCN concentrations were 100-200 cm^{-3} at 0.5% supersaturation, comparable to those measured in clean, "baseline" conditions at Cape Grim, Tasmania [*Gras*, 1995], the central, south Indian Ocean [*Bigg et al.*, 1995], the remote Atlantic [*Hoppel*, 1979], and the northwest Pacific Ocean [*Matsumoto et al.*, 1997]. North of the ITCZ, CCN concentrations ranged between 1,000 and 2,000 cm^{-3} at

0.5% supersaturation. Liu *et al.* [1996] report comparable values during the North Atlantic Regional Experiment for a station frequently impacted by polluted air masses. The increase in CCN concentration also corresponded to an increase in the aerosol mass loading. The latitudinal variation in four ionic species (SO_4^{2-}, NH_4^+, Na^+, and Cl^-) and the mass of carbon is shown in Figure 4.3. The transition between the two regimes on our cruise was relatively sharp, and corresponded to the position of the ITCZ.

Similar latitudinal variations in trace gases and aerosol mass were observed in previous experiments in the Indian Ocean/Arabian Sea. Jayaraman *et al.* [1998] detected a drop in the aerosol mass upon entering the ITCZ from the north and a commensurate increase upon exiting the region. Rhoads *et al.* [1997] report a sharp increase in the concentrations of carbon monoxide, carbon dioxide, nitrate, non-sea-salt sulfate, and nitrate upon crossing the ITCZ going from south to north. Our peak value of approximately 2 $\mu g\ m^{-3}$ SO_4^{2-} is comparable to their average value of 2.96±1.04 for Northern Hemisphere continental tropical air masses.

The concentrations of CCN and mass loading of the ionic species (Figures 4.2 and 4.3) indicate a sharp transition between the clean air mass of the Southern Hemisphere and the more polluted one of the North. This transition corresponded to the position at which we crossed the ITCZ. We cannot infer the existence of such an abrupt change in the concentration of the carbonaceous aerosol mass because of the coarse time resolution in that measurement.

The ITCZ has conventionally been viewed as a wall, preventing air masses from the Northern and Southern Hemisphere from mixing. A more accurate analogy is that it may be a wall, but it is a wall with holes in it. Eddies within the ITCZ allow some transport and mixing between the two hemispheres [*Krishnamurti et al.*, submitted; *Rhoads et al.*, 1997]. CCN rich, Northern Hemisphere air can be injected into the clean conditions of the Southern Hemisphere, while CCN depleted, Southern Hemisphere air can be transported to the north. Only a portion of the aerosol loading from the Northern

Hemisphere will survive transport through the ITCZ because of the high probability of precipitation there; some fraction of the CCN in Northern Hemisphere air mass will be washed out as they leak through the ITCZ. This process not only reduces the number of CCN which are transported to the Southern Hemisphere, but will fractionate them according to solubility. Aerosol particles with the most soluble material, or highest ϵ, are the most likely to act as CCN. They have a higher probability to be incorporated into cloud droplets and washed out. Figure 4.2 suggests a broad minimum in ϵ around the equator, the latitude at which we crossed the ITCZ. This latitudinal dependence is consistent with aerosol particles with initially low solubilities transported toward the ITCZ from the north, then scavenged in the ITCZ. Rhoads *et al.* [1997] also concluded that the northern hemisphere air masses were substantially depleted in soluble species.

Figure 4.4, which is a plot of the ratio of the mass of sulfate to the mass of carbon, also shows the depletion in soluble species. There are two minima in the plot. The first corresponds to the southern edge of the ITCZ; the second corresponds to the latitude of Bangalore, India and will be commented upon further in the next section. Black carbon particles are inefficient as cloud condensation nuclei because it is insoluble. It can be removed from the atmosphere through wet deposition processes either by being associated with a soluble species which will be more likely to participate in the cloud activation process or by precipitation scavenging. In either case, it will be removed less efficiently than a soluble species in a similar sized particle. In the absence of sources, the ratio of the mass of soluble species to black carbon should show a decrease after passing through a region of frequent precipitation. Figure 4.4 also indicates that some of the organic carbon mass was insoluble since the ratio of sulfate to the organic carbon also showed a minimum at the ITCZ.

Though still rather low, the maximum in ϵ of 0.3 to 0.2 in the Southern Hemisphere reflects the higher background values of ϵ in relatively unpolluted air masses. Aerosol particles with low solubilities which "leak" through the ITCZ will

contribute to the apparent aerosol soluble fraction we infer. The total aerosol distribution will be an external mixture of aerosol particles with a low ϵ, originating in the Northern Hemisphere, and aerosol particles with a higher ϵ, originating in the Southern Hemisphere. There is also evidence that biomass burning from eastern Africa and Madagascar and pollutants from Australia can be transported to this region (V. Ramanathan, personal communication). Aerosol particles associated with such anthropogenic influences could have a lower ϵ.

Mixing Northern Hemisphere air across the ITCZ could have a substantial impact on cloud optical properties in the Southern Hemisphere. That air mass is susceptible to modification by injection of aerosol pollutants because of its low CCN concentration. The sensitivity of cloud reflectance to droplet concentration is inversely proportional to the cloud droplet concentration for a constant liquid water content [*Twomey*, 1991]:

$$\left(\frac{dR}{dN}\right)_W = \frac{R(1-R)}{3N} \qquad (2)$$

where R is cloud reflectance, N is cloud droplet concentration, W is liquid water content, and dR/dN is the cloud susceptibility. This expression shows that the susceptibility is highest in "clean" clouds. For clouds which already have high droplet concentrations, increasing the CCN concentration has very little effect on the cloud reflectance; the cloud is already saturated with respect to CCN. However in clouds with low droplet concentrations, adding as few as one droplet cm^{-3} can change the reflectance by almost one percent [Twomey, 1991].

Even though aerosol particles which act efficiently as CCN are likely to be removed in the passage through the ITCZ, those that survive can still have a significant impact on cloud optical properties on the south side of the ITCZ because of the susceptibility argument just outlined. Clouds forming in clean air are likely to experience

higher maximum supersaturations [*Seinfeld and Pandis*, 1998, *Cantrell et al.*, submitted], which could activate even the slightly soluble CCN which survive transport through the ITCZ.

Relationships among CCN and chemical species. The most striking feature in the plot of latitude vs. CCN, SO_4^{2-}, NH_4^+, total carbon, and black carbon is the strong gradient (see Figures 2 and 3). The concentrations jump by an order of magnitude across the ITCZ from south to north and increase with latitude, indicating a source in the Northern Hemisphere. The peak at approximately 13 °N in CCN, ionic species, and mass of carbon corresponds to the latitude of Bangalore, an industrial and transportation center in southern India with a population of approximately 2.6 million people. Figure 4.4 shows a minimum in the ratio of sulfate mass to carbon mass at this latitude. This can be explained by the oxidation of sulfur gases to sulfate as the plume ages, increasing the ratio. Both Na^+ and Cl^- showed relatively low concentrations, and had no significant latitudinal gradient. The source of these species over the open ocean is sea spray, and wind speeds were relatively low from March 19 - 28, suppressing production of spray.

Table 4.1 shows correlation coefficients for CCN, ionic species, and mass of carbon. The highest correlation was between NH_4^+ and SO_4^{2-}, not an unexpected result since ammonium is frequently associated with sulfate. The slope of 0.75 in Figure 4.5, a plot of sulfate vs. ammonium, indicates a composition between ammonium bisulfate, NH_4HSO_4, which is partially neutralized, and ammonium sulfate, $(NH_4)_2SO_4$, which is fully neutralized. Sulfate and ammonium were positively correlated with black and total carbon with R^2 values near 0.50 in all four cases. Since black carbon can be used as a tracer for pollution, this suggests that a substantial fraction of the ammonium sulfate mass is anthropogenic. Black carbon and total carbon were also positively correlated (R^2 = 0.91), also suggesting that a significant portion of the total carbon mass was anthropogenic in origin.

Plots of CCN vs. NH_4^+, SO_4^{2-}, total carbon, and black carbon are shown in Figure

4.6. Cloud condensation nuclei active at 0.5% supersaturation were significantly correlated with ammonium/sulfate with R^2 values of approximately 0.70. Sulfate has been identified as a principal component of CCN in a variety of air masses. An increase in sulfate does not *a priori* indicate an increase in aerosol or CCN number concentration. The increased mass could simply result in larger aerosol particles, not more of them. However, aerosol number distributions clearly show an increased number concentration; the jump in the mass of sulfate and ammonium upon entering the Northern Hemisphere corresponds to a jump in the number concentration of CCN.

The CCN concentrations were also highly correlated with the mass of carbon with R^2 values of approximately 0.80. Though elemental carbon is not efficient as CCN [*Andrews and Larson*, 1993], organic carbon has been shown to be a component of CCN. In air masses influenced by anthropogenic sources, organic carbon was shown to contribute over half of the CCN activity [*Rivera-Carpio et al.*, 1996; *Novakov and Penner*, 1993]. However, organic carbon has also been shown to diminish the water absorption of inorganic species in an urban air mass [*Saxena et al.*, 1995].

Aerosol soluble fraction, ϵ, exhibited a latitudinal trend with a minimum at the ITCZ, but failed to show a significant correlation with any of the other measured parameters. The minimum at the ITCZ is expected since aerosol particles with higher soluble fractions will be more likely to nucleate cloud droplets and be removed in precipitation. The weak correlation between ϵ and CCN shows that ϵ does not control the CCN concentrations. The CCN apparently start with a low soluble fraction; their number concentration is controlled through dilution of the source plume and removal processes. It should be noted that both CCN and ϵ pass through a minimum at the ITCZ. The aerosol soluble fraction may control the fraction of CCN which survive transport through the heavily precipitating region around the ITCZ. The aerosol soluble fraction also failed to show a significant correlation with ammonium or sulfate, both of which are soluble species. This is probably because both were also associated with the mass of

carbon, which was shown above to have a significant insoluble fraction.

Measured CCN spectra and CCN spectra calculated from ambient aerosol number distributions. The shape of the CCN spectra and its relationship to the aerosol number distribution also showed a substantial change from the Southern to Northern Hemisphere. Figure 4.7 shows representative CCN spectra from the "background" air mass in the Southern Hemisphere, the transition airmass in the ITCZ, and the "polluted" air mass of the Northern Hemisphere. Measured CCN concentrations are shown along with CCN concentrations calculated from the ambient aerosol number distributions, using Köhler theory and assuming a composition of pure ammonium sulfate. We calculate CCN spectra based on an assumed composition of ammonium sulfate to serve as a benchmark. Sulfate is frequently assumed to be the dominant chemical species in atmospheric aerosol [*Charlson et al.*, 1992, *Pinnick et al.*, 1987], and CCN spectra calculated from the aerosol distributions assuming a composition of another readily soluble chemical species would be very similar to those calculated based on ammonium sulfate.

In all three instances shown in Figure 4.7, there is a substantial difference between calculated and measured CCN spectra. Apparently, the ambient aerosol particles are not activating as efficiently as ammonium sulfate would, indicating the presence of some other chemical species. To serve as another benchmark, we calculate the CCN spectra again, this time assuming an internally mixed aerosol (every aerosol particle in the distribution has a similar composition to every other one) composed of ammonium sulfate and some insoluble substance. These calculated spectra are shown in Figure 4.7 as dotted lines. Aerosol soluble fractions (*i.e* fraction of ammonium sulfate) as low as 0.05 to 0.1 were necessary to get agreement between our measured spectra and those calculated from the aerosol number distribution.

Measurements made with a Hygroscopic Tandem Differential Mobility Analyzer have also shown that some portion of the atmospheric aerosol can have a relatively low

ϵ. In most cases, two modes in the solubility are found, designated "more soluble" and "less soluble". In air masses influenced by anthropogenic activity, the "less soluble" mode had values of ϵ ranging from 0.02 to 0.14, and constituted up to 60% of the aerosol number concentration [*Svenningsson et al.*, 1994, 1992]. The "more soluble" fraction at a site near Frankfurt am Main, Germany had an ϵ as low as 0.37 [*Svenningsson et al.*, 1994]. Over the remote Pacific Ocean south of Australia, aerosol soluble fractions were close to unity, with growth factors less than non-sea-salt sulfate reported only when sampling anthropogenically influenced air masses [*Berg et al.*,1998]. Other investigators, using different methods, have found ϵ between 0.15 and 0.5 in mid-sized towns in the U.S. [*Alofs et al.*,1989; *Fitzgerald*, 1973].

This insoluble mass could be from the mass of carbon associated with the ammonium and sulfate. Mineral dust is usually in particles with diameters larger than one micrometer, and so would be a very minor component of any insoluble material in the size range (diameter < 1 μm) which contributes the majority of the CCN number. As shown above, the mass of particulate carbon was high in the Northern Hemisphere (see Figure 4.3). We also inferred that a substantial fraction of the carbon mass was insoluble (see Figure 4.4). Saxena *et al.* [1995] showed that organic mass in urban air masses can actually inhibit the water uptake of soluble species, further contributing to the low apparent aerosol soluble fractions we observe.

An alternative explanation of the large discrepancy between the measured CCN spectra and the spectra calculated from aerosol number distributions is the presence of hydrophobic films on the surface of aerosol particles, which could inhibit the transfer of water from the vapor to the liquid phase. Organic films on aerosol particles and hydrometeors are not uncommon in the atmosphere [*Gill et al.*, 1983]. In a comparison between measured CCN spectra and CCN spectra calculated from aerosol number distributions, Bigg [1986] concluded that activation of the aerosol particles was inhibited by the presence of some surface-active organic component. Shulman *et al.* [1996]

showed that slightly soluble chemical substances, which include a wide range of organics, can alter droplet growth. However, recent laboratory results have been ambiguous. In one study, ammonium sulfate particles coated with dioctylphthalate, a nonhygroscopic organic, were not prevented from activating, nor was the activation appreciably delayed [*Cruz and Pandis*, 1998], while in another study sodium dodecyl sulfate, which was used as a surrogate for atmospheric surfactants, did have a substantial effect on the activation of inorganic salts [*Li et al.*, 1998].

Though the difference between the calculated and measured CCN spectra is as much as a factor of two in some instances, the impact of this discrepancy on cloud albedo is probably rather small. Clouds forming over the northern Indian Ocean would already be saturated with respect to CCN. Though more CCN would activate if the aerosol soluble fraction were higher, the resulting increased number concentration of cloud droplets would have little effect on cloud reflectivity. Equation 2 shows that the reflectivity of clouds with droplet concentrations greater than about 200 cm^{-3} are relatively insensitive to a further increase in droplet concentration.

However, the low aerosol soluble fractions could have implications for the direct scattering of solar radiation by aerosol particles, since the aerosol optical depth is dependent upon the efficiency at which aerosol particles take up water with increasing relative humidity. Relative to pure sulfate, aerosol particles over the northern Indian Ocean would be much less efficient as scatterers because of their low soluble fraction.

Conclusions

On a south/north transect of the Indian Ocean we observed a gradient of an order of magnitude in the concentrations of CCN, sulfate, ammonium, black carbon, and total carbon. The transition from low to high concentrations was sharp and corresponded to crossing the ITCZ into the Northern Hemisphere air mass. The observed variation is consistent with the findings of previous studies [*Jayaraman et al.*, 1998; *Rhoads et al.*,

1997]. The inferred aerosol soluble fraction was low (< 0.5) throughout the cruise; it passed through a minimum at the ITCZ.

Sulfate and ammonium were correlated with the mass of black and total carbon, indicating a common source in the Northern Hemisphere, which we presume is the Indian subcontinent. The concentration of CCN correlated with the mass of ammonium and sulfate, which is not unexpected since both species have been shown to be associated with CCN activity. CCN also correlated with the mass of carbon. This may simply be a result of a common source for carbon and ammonium and sulfate, or may be because organic carbon is participating in the activation process.

The relationship between the aerosol number distribution and the CCN spectra showed that the aerosol particles are not activating as efficiently as ammonium sulfate. By calculating the CCN spectra from the aerosol number distribution using an assumed composition of ammonium sulfate and an insoluble component, we infer aerosol soluble fractions as low as 0.05 in the ITCZ, with relatively higher values to the north and south.

The low aerosol soluble fraction may contribute to the transport of some portion of the aerosol in the Northern Hemisphere air mass through the ITCZ. Despite their low soluble fractions, these aerosol particles could influence cloud properties in the Southern Hemisphere air mass because of the low, "background" concentration of CCN there. The low aerosol soluble fraction will have little impact on cloud properties in the Northern Hemisphere air mass because the CCN concentration is already quite high. Clouds in the Northern Hemisphere air mass are already saturated with respect to CCN.

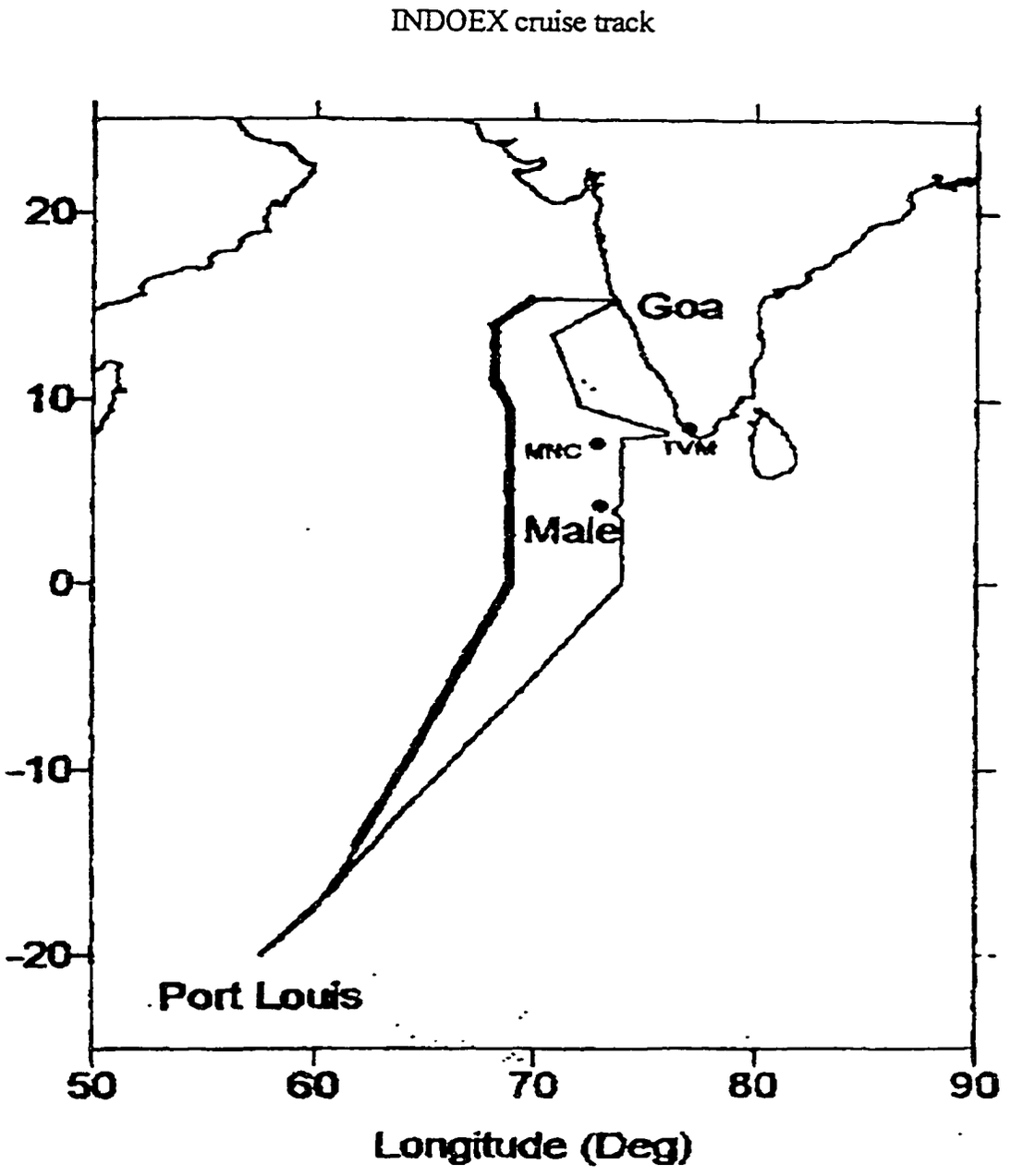

Figure 4.1 Cruise track for the R/V Sagar Kanya during the 1998 first field phase of the INdian Ocean EXperiment. Because of problems with the instrument and following winds, data from the first leg of the cruise is not presented. Only the section marked in bold is presented.

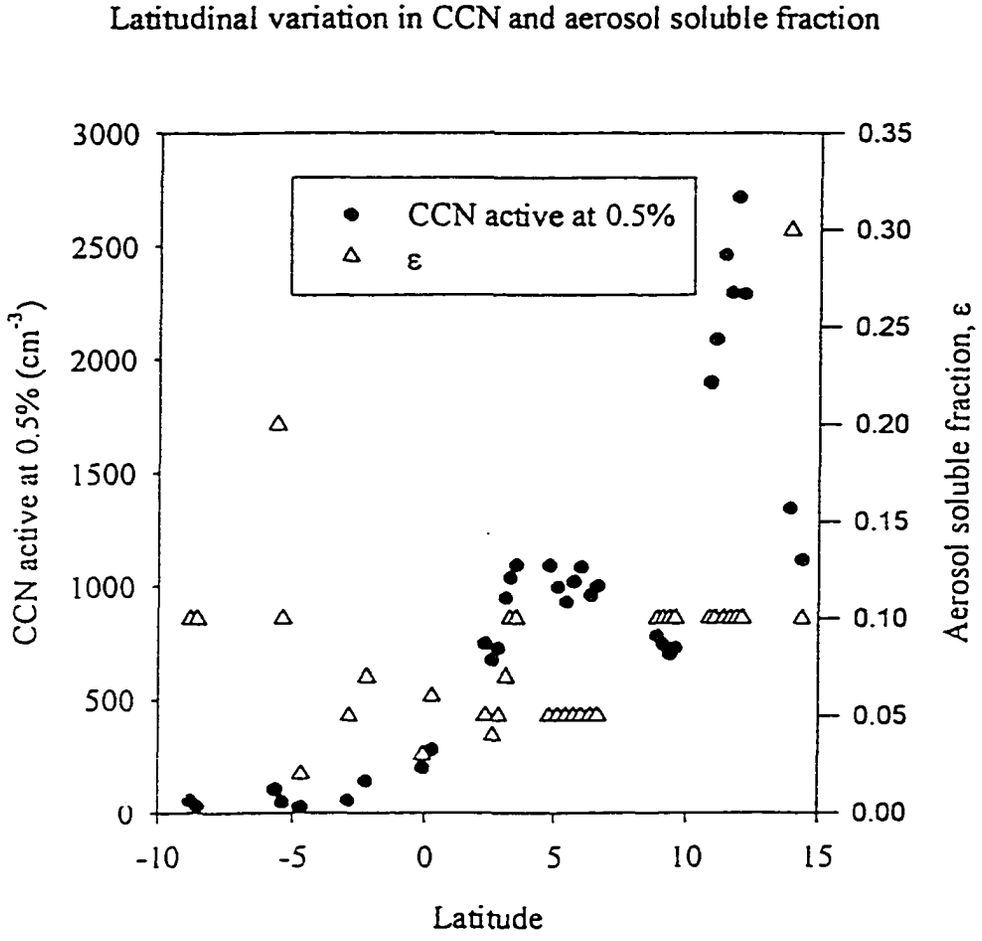

Figure 4.2 The south / north variation in CCN active at 0.5% and in the inferred aerosol soluble fraction, ε. The concentrations of CCN are lower in the cleaner Southern Hemisphere, and increase sharply in the Northern Hemisphere. The transition occurs at the position at which we crossed the ITCZ. There is a suggestion of a broad minimum in ε at the ITCZ.

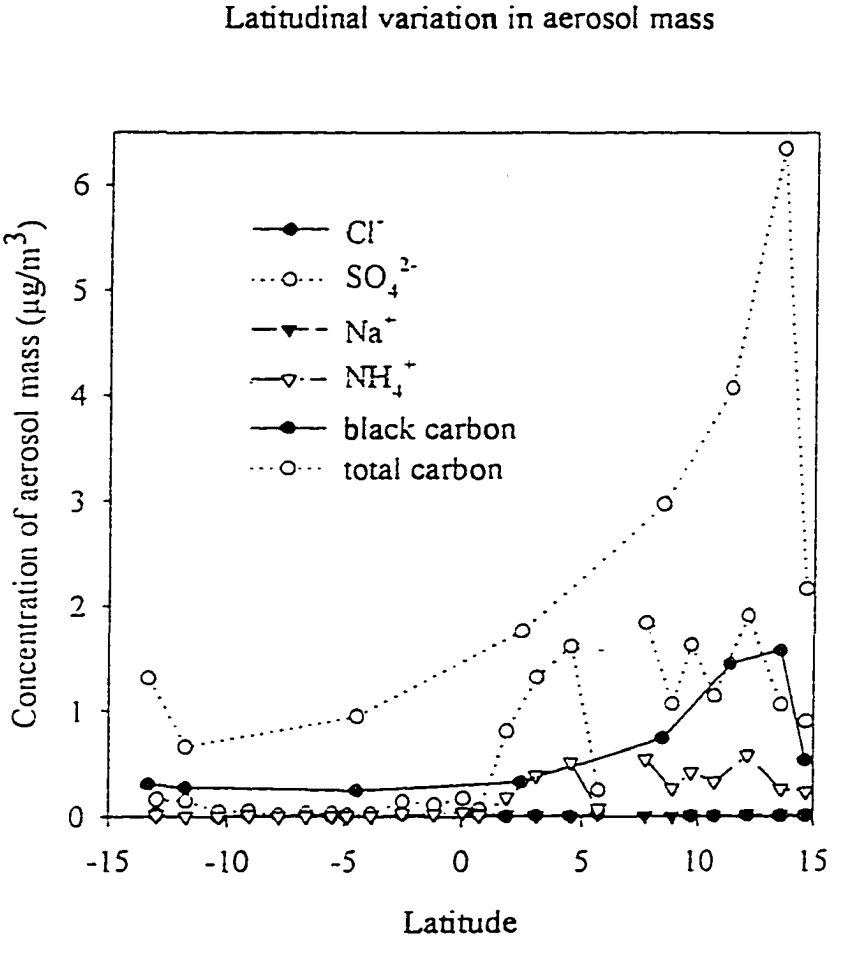

Figure 4.3 South / north variation in aerosol mass. Low wind speeds suppressed production of sea spray, so Na^+ and Cl^- were low throughout the cruise. SO_4^{2-} and NH_4^+ increased dramatically in the Northern Hemisphere, as did black and total carbon. The transition for the carbon species upon crossing the ITCZ was not as sharp because of the lower time resolution for carbon samples.

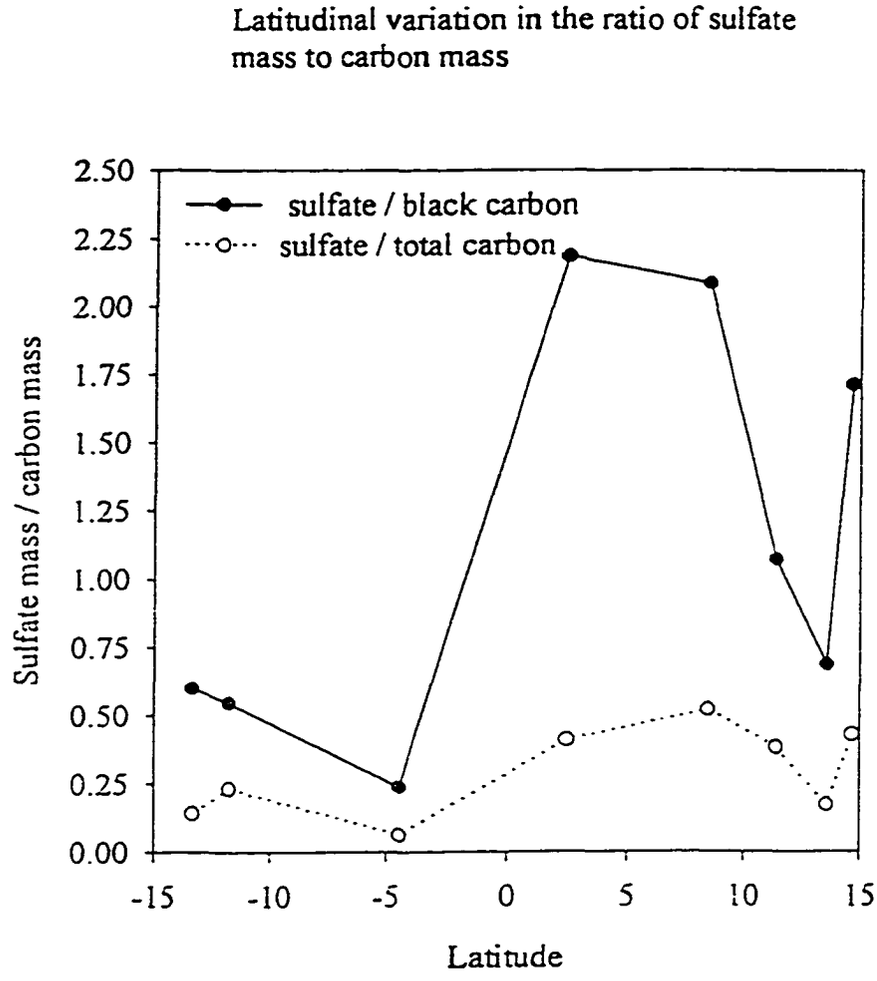

Figure 4.4 Latitudinal dependence of the ratio of sulfate mass to carbon mass. The decrease between 0 and -5 degrees is because the sulfate is preferentially removed in the heavy precipitation associated with the ITCZ. The dip at approximately 13 degrees is because we passed through the plume of Bangalore, India (see text for details).

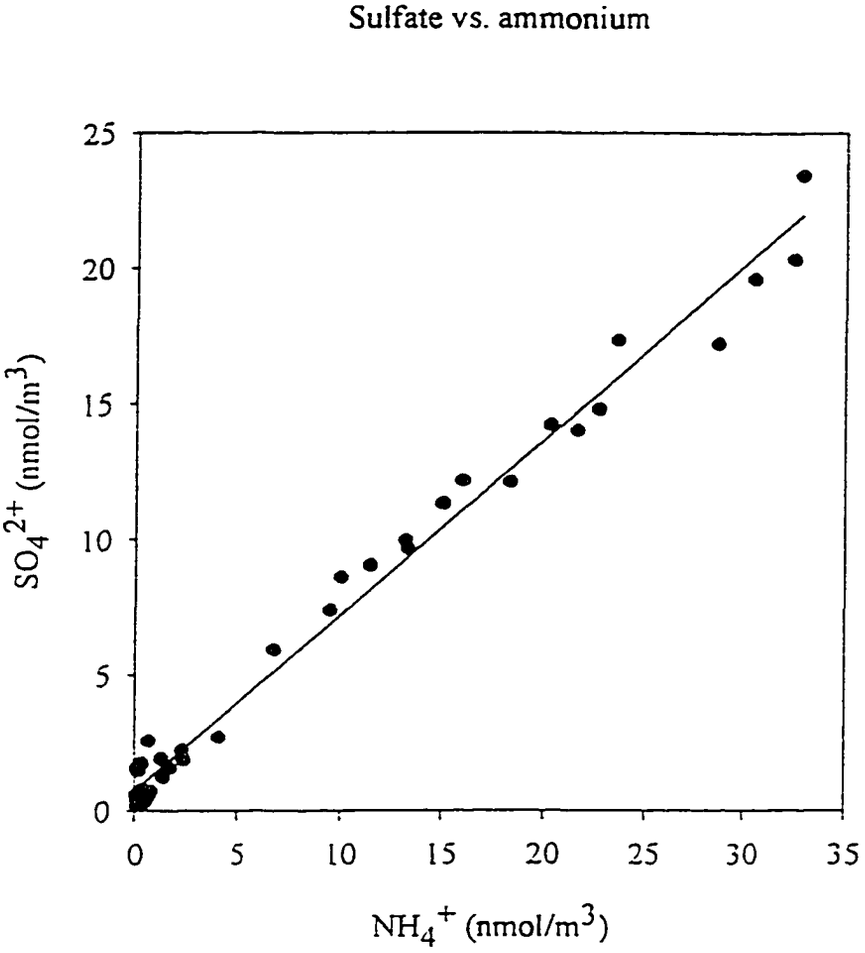

Figure 4.5 Regression of sulfate concentration to to ammonium concentration, showing that the sulfate in the air mass is probably not fully neutralized.

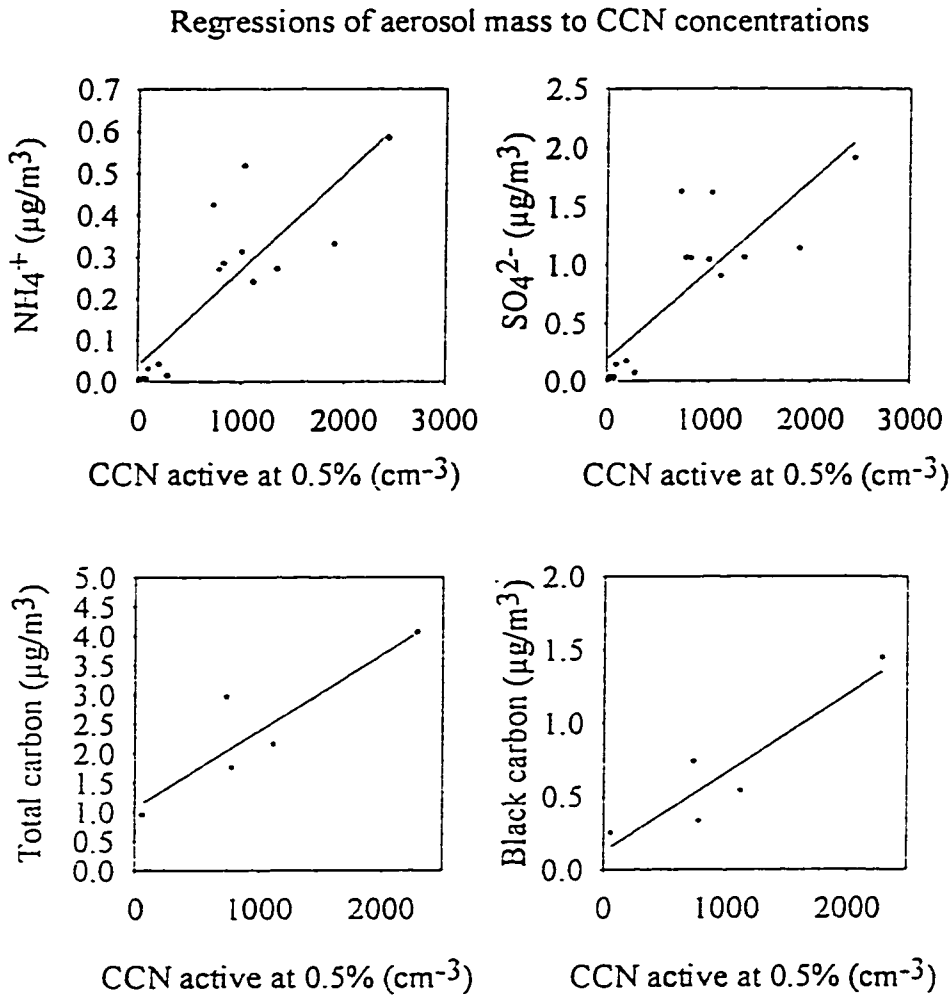

Figure 4.6 Regressions of aerosol mass to the concentration of CCN active at 0.5% supersaturation. The correlation coefficients are shown in Table 4.1.

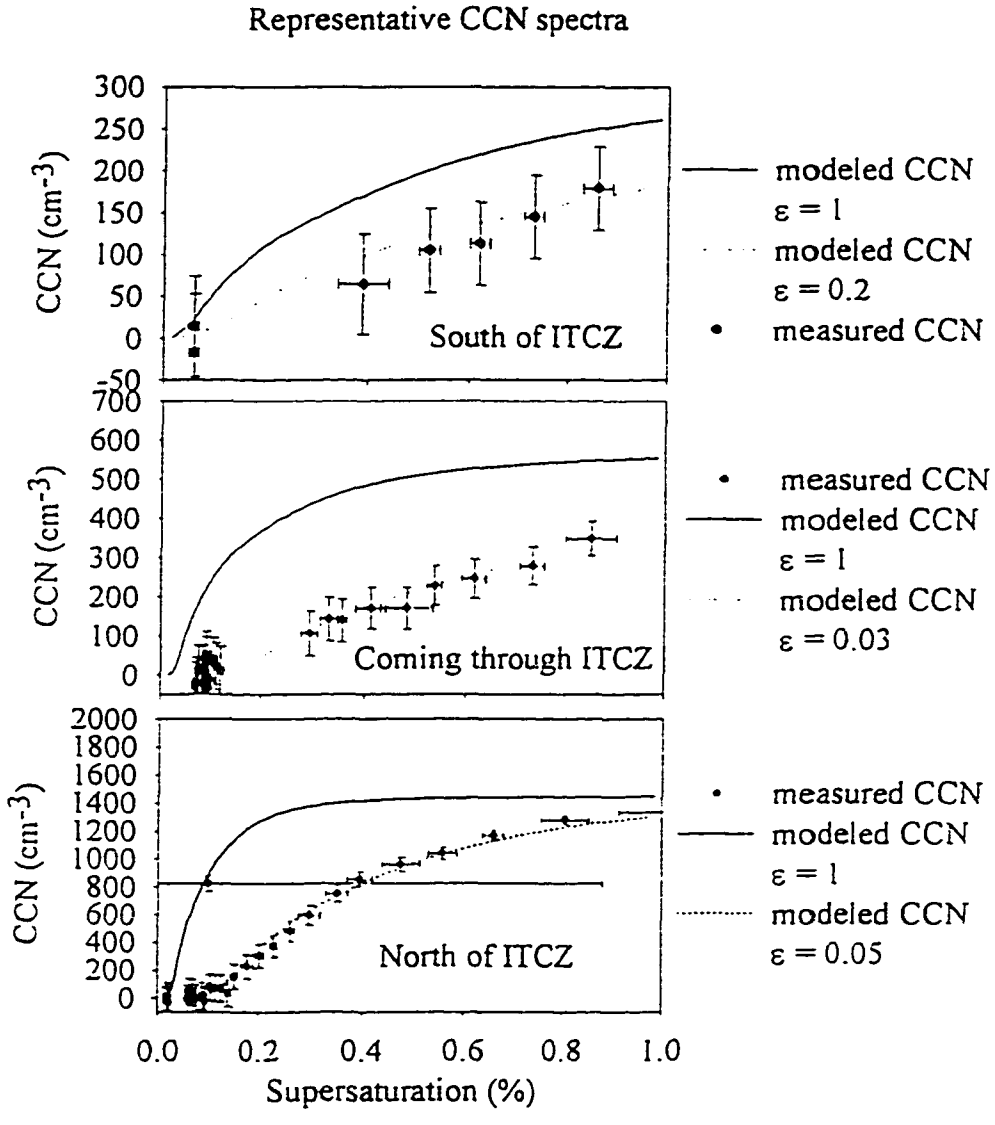

Figure 4.7 Representative CCN spectra, both measured and calculated from south, in, and north of the ITCZ. Concentrations of CCN increase from south to north, while the inferred aerosol fraction, ε, goes through a minimum at the ITCZ.

INDOEX correlation coefficients

	ϵ	SO_4^{2-}	NH_4^+	Cl^-	Na^+	TC	BC	CCN @ 0.5%
ϵ	1							
SO_4^{2-}	0.04 15	1						
NH_4^+	0.02 15	0.99 40	1					
Cl^-	0.001 15	0.02 40	0.02 40	1				
Na^+	0.11 15	0.07 40	0.06 40	0.63 40	1			
TC	0.09 5	0.50 8	0.46 8	0.01 8	0.36 8	1		
BC	0.15 5	0.55 8	0.53 8	0.03 8	0.29 8	0.91 8	1	
CCN @ 0.5%	0.04 34	0.68 15	0.70 15	0.18 15	0.33 15	0.80 5	0.84 5	1

Table 4.1 Correlation coefficients between parameters measured on the cruise are shown with the number of observations used in each case.

Chapter 5

Evidence for sulfuric acid coated particles in the Arctic air mass [3]

"... the dust counter was used just as a dog uses its nose when quartering the ground in searching for game." -John Aitken

Introduction

Size and chemical composition determine whether an aerosol particle will become a cloud condensation nuclei at a given supersaturation. Determining the size is relatively straightforward with a differential mobility analyzer and condensation particle counter (see Chapter 1). Information about the composition of aerosol particles can be inferred by measuring the size and concentration before and after they are exposed to an elevated temperature field. This is usually done by passing the aerosol sample through a heated tube. During the passage through the tube, the aerosol particles evaporate or decompose to an extent dependent upon the temperature and residence time in the tube. This method has been used to infer aerosol chemical composition as a function of size. Twomey [1968] used the method to infer that a large fraction of cloud condensation nuclei are ammonium sulfate and ammonium chloride. Other researchers using this method have inferred ammonium sulfate or bisulfate to be a common constituent of atmospheric aerosol in the accumulation mode ($100<D_{particle}<1000$ nm) at locations as disparate as the Northeast Atlantic [*O'Dowd and Smith*, 1993], south-central New Mexico [*Pinnick et al.*, 1987], and the remote Pacific [*Clarke et al.*, 1987].

However, interpreting the results of volatility experiments in which particles of all

---

[3] Originally published as Cantrell, W., G. Shaw, and R. Benner, Evidence for sulfuric acid coated particles in the Arctic air mass. *Geophys. Res. Lett.*, 24, 3005-3008, 1997.

sizes are subjected to the heat treatment is difficult. A number of complications can arise because of the aerosol particles' heterogeneity in size and composition. For example, compounds with similar volatility characteristics such as ammonium sulfate and ammonium bisulfate are difficult to separate. Trace species and mixtures of compounds can also be difficult to identify. Because particles of different sizes but similar composition can volatilize at different rates, they can end up the same size after heat treatment, leading to ambiguous and perhaps faulty interpretation of the results.

We present results of a volatility experiment, conducted at a clean station in the interior of Alaska in March of 1996. The behavior of the aerosol number distribution upon heating was unusual in our experience and was such that an unambiguous interpretation is possible - the individual aerosol particles were composed of at least three chemical species. We hypothesize that the submicron aerosol particles were coated with a volatile substance, which we assume is sulfuric acid although an organic substance of similar vapor pressure cannot be ruled out. The presence of a coating on the aerosol particles has important implications, which will be discussed later. It is the **surface**, not bulk, properties of aerosol particles that govern their growth as a function of water vapor concentration.

Experiment

Aerosol physical and chemical characteristics were measured at Poker Flat Research Range (64.18 N, 147.72 W, 497 m asl). This site provides an excellent opportunity to monitor air masses of different origins which contain aerosol of different types, including background continental aerosol, modified marine aerosol advected from the Pacific ocean, and aged pollution, which builds up in the Arctic air mass over the winter [*Shaw*, 1983].

Aerosol size spectra were measured continuously with a TSI (Minneapolis, MN) Scanning Mobility Particle Sizer (SMPS). Distributions with the SMPS were integrated

over 10 minutes to assure adequate counting statistics in the clean conditions which were prevalent during the field campaign. The volatility apparatus, similar to that of Clarke [1991], consisted of three 0.635 cm ID stainless steel heated tubes. One tube was maintained at room temperature, another at 130 °C, and the other at 300 °C. The tubes were surrounded by sand, which was heated to the desired temperature by a heater controlled with an Omega Engineering (Stamford, CT; Model CN4400) temperature controller. Ambient aerosol distributions were sampled without heat treatment for 30 minutes. Next a computer controlled solenoid valve was activated to divert flow through the 300 °C tube, and distributions were sampled at this temperature for 30 minutes. Finally, another solenoid was used to divert flow through the 130 °C tube. After 30 minutes in this configuration, both solenoids were returned to their original positions, to sample the aerosol at room temperature once again. A complete cycle took two hours.

Temperatures of 130 and 300 °C were chosen to differentiate between volatile chemical species such as sulfuric acid and possibly organics, intermediately volatile species such as ammonium sulfate and ammonium bisulfate, and more refractory substances such as elemental carbon, mineral dust, or sea salt. Laboratory calibrations of our apparatus show that sulfuric acid is volatilized from particles exposed to 130 °C, but ammonium sulfate is not. However at 300 °C, sulfuric acid and ammonium sulfate volatilize, leaving refractory substances. Comparison of the distributions taken at the three temperatures provides information on the aerosol's chemical composition, including degree of mixing.

Black carbon concentrations were measured with a Magee Scientific Aethalometer (Berkeley, CA; Model AE-10) with a time resolution of 15 minutes. The number concentration of particles with diameters greater than approximately 10 nm was monitored with a TSI Condensation Nucleus Particle Counter (Model 3020).

During the period of investigation, ambient temperatures reached almost 0 °C in the afternoon, and overnight lows were -8 to -10 °C. Relative humidity ranged from 60

to 70% at night, and dipped to less than 20% in the afternoon. Surface winds were light and variable from the east. The ground was still snow-covered.

Figure 5.1 shows that condensation nuclei and black carbon concentrations were stable and indicative of background levels. The mean annual value for 1986-94 for black carbon concentrations at Barrow, a remote site on the northern coast of Alaska, is 41 ng/m^3 [*Bodhaine*, 1995], while Barrow's geometric mean condensation nuclei concentration for 1975-81 is 169 cm^{-3} [*Bodhaine*, 1983]. The spike in black carbon concentration near the end of day 62 (local noon at the site) is probably due to a vehicle passing on the access road to the site. We do not believe that these spikes affect our aerosol measurements significantly because the black carbon levels were low even during the spike and the condensation nuclei were not affected during the same period.

Results

Figure 5.2 is an example of typical size distributions at various temperatures, illustrating the difficulties in interpreting this type of data. The peak in the aerosol distribution exposed to 130 °C has shifted to a smaller size, and the integrated number is reduced. There is more than one explanation of this result. The ambient aerosol particles could be composed of a group which is completely volatile at 130 °C and a group which is only partially volatile at 130 °C. This could produce the reduction in number and shift in peak diameter at 130 °C shown in Figure 5.2. However, an equally plausible explanation is that some particles greater than 200 nm in diameter were completely volatile at 130 °C, while those less than 200 nm in diameter were not volatile at that temperature. This would also produce the result shown in Figure 5.2. There is no way to discriminate between the two scenarios based on the data.

Figure 5.3 shows a representative size distribution of aerosol volatility representing conditions during the coated particle episode. There are two characteristics of the curves that make interpretation of the thermography of the aerosol unambiguous.

First, there is a clear shift in the peak of the aerosol distribution upon heating to 130 °C. Second, the integrated number concentration in the accumulation mode is unchanged. The aerosol is composed of at least three chemical species. A plausible explanation is that the aerosol particles are coated with a volatile film which evaporates upon heating. However, we stress that the morphology of the particles cannot be determined with the volatility technique. The presence of a volatile coating on the aerosol particles is only conjecture, though consistent with the data presented here and with other results in Arctic locations. Bigg [1980] concluded that large fractions of aerosol particles sampled at Barrow, Alaska were coated with sulfuric acid.

The ambient and 130 °C distributions were fit with lognormal distribution functions. The peak diameters given by these fits are shown in Figure 5.4. The position of the ambient peak was constant, but the peak diameter of the 130 °C distributions increased steadily from 100 to 120 nm over one day. The total volume of aerosol was calculated from the distributions. Figure 5.5 shows the percentage of mass volatile at 130 °C decreased from 65% to 50% over the course of the episode, while the mass volatile at 300 °C decreased slightly from 80 to 75%.

Discussion

These volatility measurements are not precise enough to unambiguously identify chemical composition of the particles. The only certainty in the interpretation of these results is there is a component to the aerosol particles comprising at least 50% of the volume or mass which was volatile at 130 °C, and this apparently was a coating on less volatile particles. Through comparison with laboratory tests, certain inferences can be made about the composition of the aerosol particles.

Previous studies in the Arctic have suggested aerosol to be externally mixed with respect to volatility [*Covert and Heintzenberg*, 1993]. Typically, our results indicate that the aerosol are externally mixed (see Figure 5.2). The aerosol distributions in Figure 5.3

are very close to internally mixed, though they do not meet the criteria for a pure internal mixture.

The results of the heating are not consistent with a pure ammonium bisulfate composition. The aerosol's behavior is consistent with an aerosol component which is refractory at 300 °C, and a component of ammonium bisulfate coated with a substance which is volatile at 130 °C. The mixture of refractory and volatile components appears to be uniform across the aerosol distribution.

The relative humidity in the sample manifold averaged less than 10%, insuring that aerosol particles were at their dry diameter when sampled. Tang and Munkelwitz [1994] report that NH_4HSO_4 aerosol particles sometimes do not recrystallize until a relative humidity of 0.05%, though some recrystallize at relative humidities as high as 22%. Because of the consistency of the shift in peak diameter shown in Figure 5.4 upon heating the samples to 130 °C, we do not believe it is the result of recrystallization of hydrated NH_4HSO_4.

The two most likely substances for the volatile coating that disappeared upon heating to 130 °C are sulfuric acid or an organic species. Given the time of year, we favor sulfuric acid. In early March, the Arctic is still snow covered and temperatures are rarely above freezing, making production of organics highly unlikely. Sulfate undergoes a strong seasonal variation in the Arctic, reaching a maximum in the spring. Barrie and Barrie [1990] have reported that virtually all of the sulfate is secondary. Photochemical conversion of sulfur dioxide to sulfuric acid with subsequent condensation onto the aerosol particles is consistent with the results reported here. Sulfur dioxide mixing ratios in the Arctic during the winter are in the range of 100 to 2000 pptv (parts per trillion by volume) [*Barrie and Hoff*, 1984], and the observed change in aerosol volume between ambient and 130 °C distributions is equivalent to 34 pptv of sulfuric acid vapor condensed onto the aerosol particles.

The peak diameter of the aerosol exposed to 130 °C increased from 100 to 120

nm over the event. This behavior is consistent with ammonia reacting with sulfuric acid to produce ammonium bisulfate and would be difficult to understand if the coating were an organic compound. Measurements of ammonia in the Arctic are unavailable, but the ammonium ion (NH_4^+) has been observed. Ogren and Rodhe [1986] inferred 1 to 14 pptv of ammonia through analysis of cloud water composition in summer. Approximately 10 pptv of ammonia would have been sufficient to neutralize the volume of sulfuric acid necessary to produce the change in peak diameter observed. The corresponding ammonia to sulfate ratio increased from 0.14 to 0.39.

Regardless of the chemical species, the existence of a coating on atmospheric aerosol particles has significant implications. Though Pilinis *et al.* [1995] calculate that external vs. internal mixing in aerosol has little influence on direct radiative forcing, they conclude that chemical composition modulates radiation through its influence on the uptake of water with increasing relative humidity. However, it is the surface properties of aerosol particles, not bulk composition, which exert the largest influence on how they respond to changes in water vapor concentration. Surface properties of aerosol particles also affect their ability to act as cloud condensation nuclei, and thus the magnitude of the indirect climate effect. This makes bulk composition measurements of the aerosol difficult to interpret in terms of the potential climatic impact of the aerosol.

Conclusions

The volatility behavior is consistent with partially neutralized aerosol particles with an initial ammonium to sulfate ratio of 0.14, which increased to 0.39 over one day. The values of sulfuric acid and ammonia required to explain this behavior are consistent with those found in the Arctic at this time of year.

Our results show that aerosol particles in natural systems are sometimes coated. We have concluded that this coating is likely to be sulfuric acid, which could have consequences for the direct radiative forcing of the aerosol since sulfuric acid hydrates

more readily than ammonium sulfate or bisulfate at low relative humidities. If the volatile coating is an organic (which we think is unlikely), the hygroscopic behavior could be very different, perhaps reducing the ability of the aerosol particles to absorb water [*Saxena et al.*, 1995]. The difference in activation between sulfate and an organic could be considerable [*Schulman et al.*, 1996], modifying the aerosol particles' ability to act as cloud condensation nuclei and influencing the indirect effect.

Better methods are needed to identify the chemical species present at the aerosol particles' surface, since that is what controls the response to changes in water vapor concentration which, in turn, has important implications for both the direct and indirect climate effect.

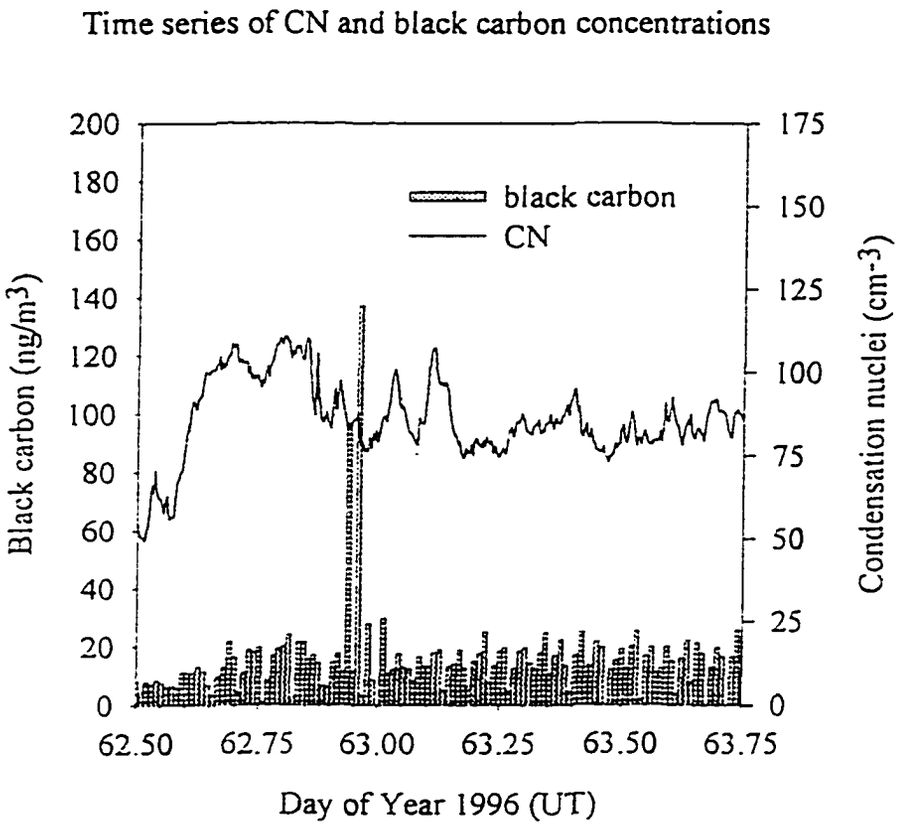

Figure 5.1 Time series of CN and black carbon concentrations for March 2 and 3 1996. Both are representative of background conditions (see text for details).

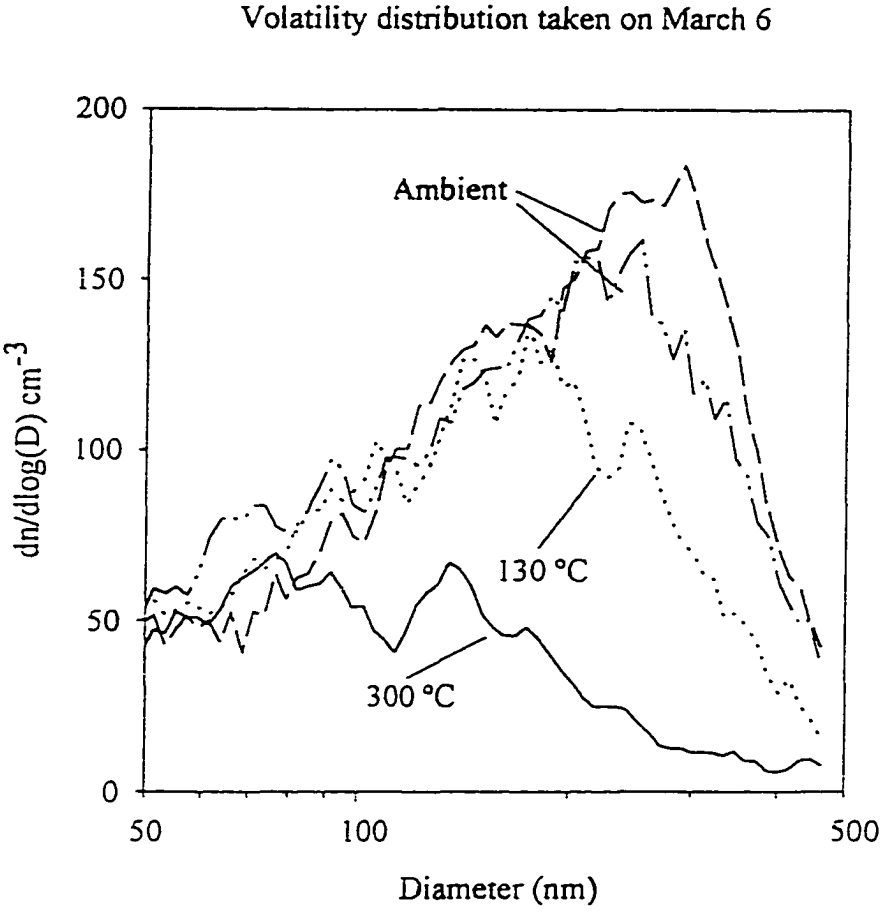

Figure 5.2 Volatility distributions taken on March 6, illustrating the difficulties in interpretation that can arise (see text). An ambient temperature distribution is taken, followed by one at 300 °C, one at 130 °C, then another at ambient temperature.

Volatility distributions from March 2 and 3

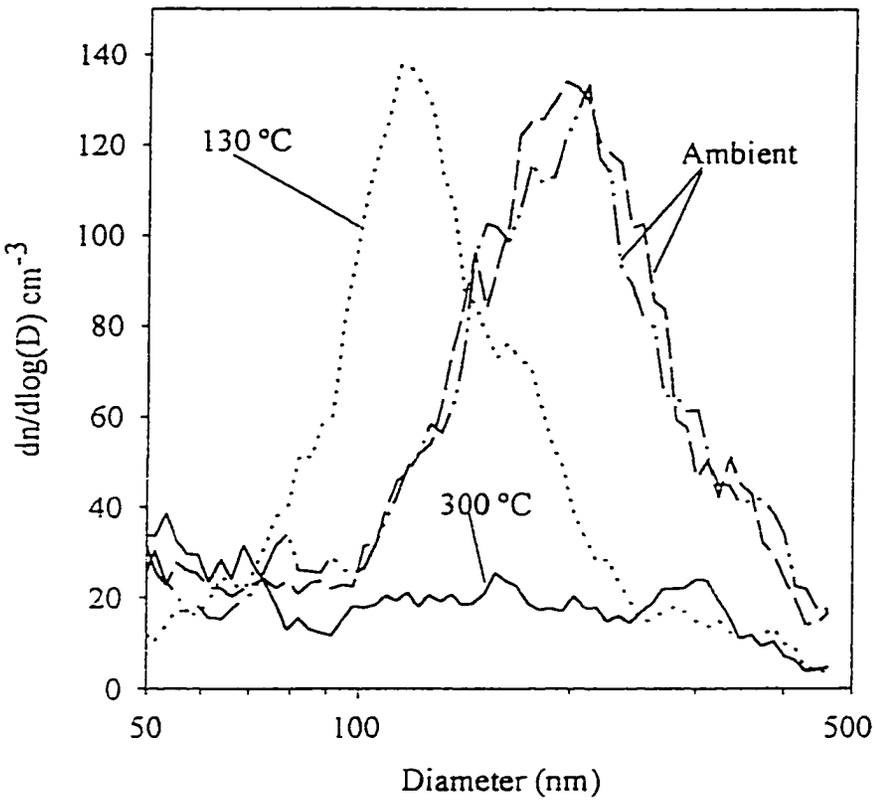

Figure 5.3 Volatility distributions from March 2 and 3, illustrating the marked shift in peak diameter between the ambient temperature distribution and 130 °C. The interpretation is simplified because the number concentration does not change upon heating to 130 °C.

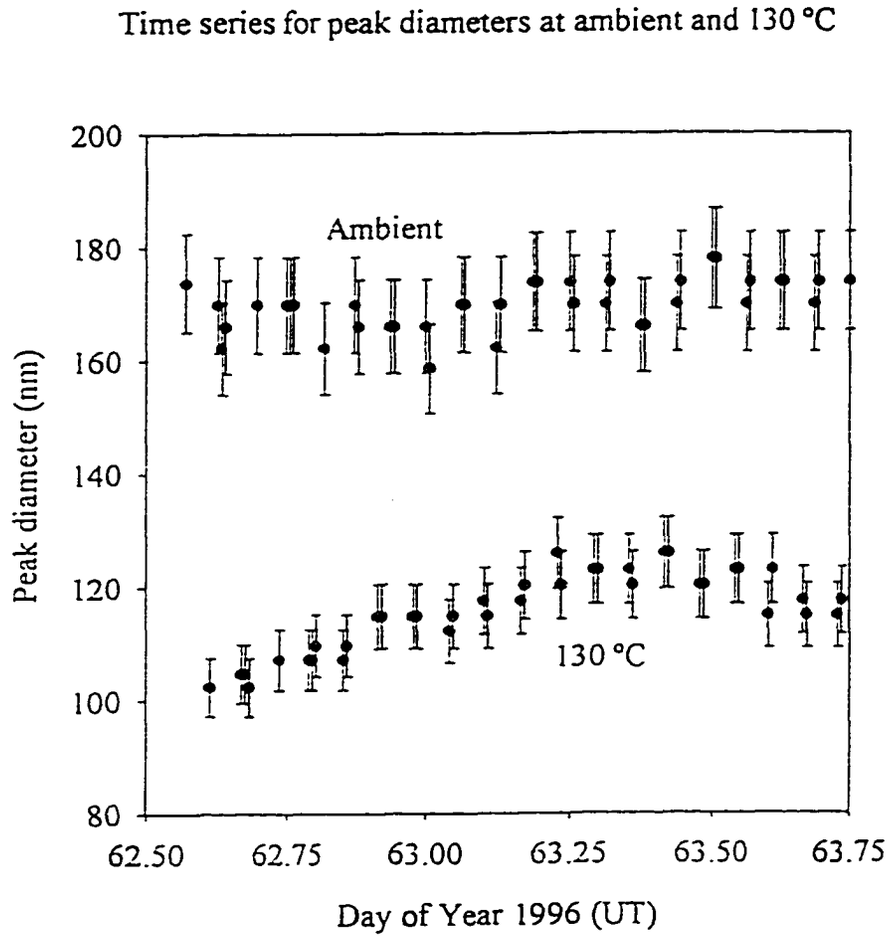

Figure 5.4 Time series of the peak diameter of the aerosol number distribution at ambient temperature and 130 °C.

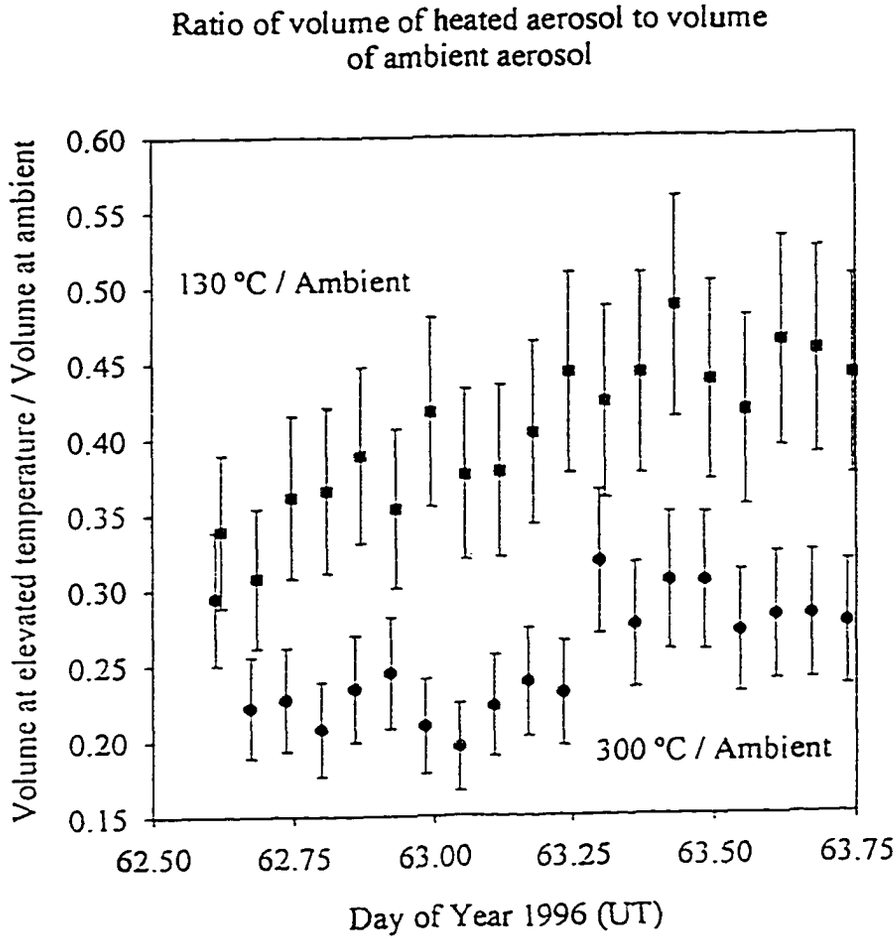

Figure 5.5 The ratio of the volume at 130 °C and 300 °C relative to the volume of the room temperature aerosol. The percentage of volume remaining at 300 °C increases from 20% to 25%.

Chapter 6

Cloud properties inferred from bimodal aerosol number distributions[4]

"Every cloud engenders not a storm." -William Shakespeare, Henry VI

Introduction

Aerosol particles are known to affect cloud properties such as droplet concentration, lifetime, and liquid water content [*Twomey*, 1984; *Albrecht*, 1989], but since most clouds evaporate without precipitating [*Pruppacher and Jaenicke*, 1995], the particles which were incorporated into cloud are returned to the atmosphere. Hoppel *et al.* [1986] hypothesized that double-peaked aerosol distributions, observed frequently in the marine boundary layer, were due to cloud processing of gaseous sulfur species to sulfate. They observed that when boundary layer clouds were not present in the back trajectory of the sampled air mass, there was no double-peaked feature, whereas bimodal distributions were sampled when boundary layer clouds were present in the back trajectory. In that paper, Hoppel *et al.* pointed out that cloud properties could be inferred from these double-peaked aerosol number distributions, and subsequently, demonstrated that bimodal distributions could be created from cloud processing of aerosol particles and trace gases by simulating non-precipitating cloud cycles in a large cloud chamber [*Hoppel et al.*, 1994b].

In the cloud activation process, air becomes supersaturated with respect to water as an air parcel cools. Aerosol particles nucleate and grow into cloud droplets, serving as an increasing sink for the water vapor. The maximum supersaturation, S_{max}, reached

---

[4] Submitted to Journal of Geophysical Research - Atmospheres as Cantrell, W., G. Shaw, and R. Benner, Cloud properties inferred from bimodal aerosol number distributions.

during activation, is determined through the feedback between the source and sink of the water vapor supersaturation. Once S_{max} is reached, usually a few tenths of a percent, the aerosol is divided into two populations of particles - those that activated and became cloud droplets and those that did not and remained interstitial in the cloud. As *Hoppel et al.* [1994b] demonstrated, additional mass can be added to the aerosol particles incorporated into cloud droplets through liquid phase oxidation of sulfur gases to sulfate. Droplet scavenging of interstitial aerosol particles and coalescence of droplets can also add mass to the particles which are included in the cloud droplets. When the cloud evaporates, the population of aerosol particles that were incorporated into cloud droplets is larger in size, while those that remained unactivated do not change in size. This creates a split in the aerosol number distribution which delineates those aerosol particles that were activated in the cloud formation process from those that were not. The minimum in the aerosol number distribution separating the two populations or modes of aerosol is related to S_{max}. Assuming a homogeneous chemical composition, aerosol particles larger than the diameter, D_{min}, at which the minimum in the aerosol number distribution occurs have been incorporated into cloud droplets, and those smaller have not. By using the minimum between the two modes as a proxy, S_{max} and the cloud droplet concentration, N_c, can be inferred from bimodal aerosol number distributions. This information can be used to validate modeling efforts on a regional and global scale [*Ghan et al.*, 1997].

Data and Data Analysis

We collected aerosol number distributions in field campaigns over a period of two years at five different locations, ranging from two pristine sites in Alaska to a polluted site on the east coast of the United States. Figure 6.1 shows the location of the five stations.

Cheeka Peak is a Climate Monitoring Diagnostics Laboratory (CMDL) station

located on the northwest tip of the Olympic Peninsula in Washington state. The station is approximately two km inland from the Pacific coast and 100 km from the nearest industrial centers of Port Angeles, Washington and Victoria, British Columbia. Clean marine air masses are frequently sampled at the site, though continentally influenced and polluted air masses are also encountered. The duration of the experiment was September 23 to November 16, 1995.

Poker Flat Research Range is in central Alaska, 50 km north of Fairbanks. Pollution from Fairbanks is rarely seen at the site, especially during the winter. Local contamination is occasionally seen, but has been screened out of the data set based on measurements of black carbon concentration and the total number of condensation nuclei. The data presented here are from a 10 day (7th - 17th) episode in April 1995, when low pressure systems in the Gulf of Alaska advected air masses over the Alaska Range into the interior of the state.

The site in Hawaii is located on the eastern (upwind) tip of the island of Hawaii. The nearest anthropogenic influence to the east is the western seaboard of the United States. Thirty km to the northwest is Hilo, the largest metropolitan area on the island. Mauna Loa volcano is approximately 70 km to the west. The data presented here were collected April 19-23, 1994.

As part of the Tropospheric Aerosol Radiative Forcing Observational Experiment (TARFOX), we sampled from a station on Wallops Island, Virginia from July 16 to 26, 1996. The air mass affected by the eastern seaboard of the United States is one of the most polluted in the world. Condensation nucleus concentrations at Wallops Island frequently exceeded 10,000 cm^{-3}.

Homer, Alaska is located on Kachemak Bay, which is an offshoot of Cook Inlet approximately 50 km from the Gulf of Alaska. The sample site, on a bluff overlooking the bay, was frequently impacted by local influences, but these were screened from the data based on black carbon and condensation nucleus concentrations. The Gulf of Alaska

and Kachemak Bay are biologically productive regions. High concentrations of dimethyl sulfide and methane sulfonic acid, which are biologically derived sulfur species, have been found in both regions [*Jodwalis*, 1998]. The duration of the experiment there was June 10 - 30, 1996.

The aerosol number distributions at all the sites were measured using a Scanning Mobility Particle Sizer, SMPS, (TSI, Inc., Minneapolis, MN). The instrument automatically collected number distributions on a nearly continuous basis with a time resolution optimized to insure adequate counting statistics for the conditions prevalent at the particular site. The measured aerosol number distribution covered the diameter range between 20 and 600 nm. In all of the field campaigns, we took measures to ensure that aerosol particles were sized at their dry, not hydrated, diameter. We used either diffusion dryers, dried sheath air in the SMPS, or a combination of both to dry the aerosol sample. The relative humidity in the SMPS was less than 20%. Ammonium sulfate and bisulfate usually recrystallize at relative humidities greater than 22%, though occasionally ammonium bisulfate will exist as a metastable droplet down to humidities of about 0.05%. No indication is given as to the fraction of ammonium sulfate droplets which exist in the metastable state [*Tang and Munkelwitz*, 1994].

The first step in the data analysis was to visually inspect all ambient distributions and select those that had a bimodal character. Approximately 30% of the distributions had a bimodal character. Only distributions with a clear minimum between modes were selected for further analysis.

Next, both modes were fit to a lognormal distribution:

$$f(D)\,dD = \frac{1}{\log \beta_g \sqrt{(2\pi)}} \exp\left(\frac{-(\log D - \log D_g)^2}{2(\log \beta_g)^2} \right) d(\log D) \qquad (1)$$

[*Fuchs*, 1989], where :

f(D)dD = the fraction of particles in size range D to D + dD

β_g = standard deviation of logarithm of the diameters

D_g = geometric mean of the particle diameters (cm)

D = particle diameter (cm)

Once β_g and D_g were determined for both modes, the diameter at which the modes intersect was calculated, and this was defined as the minimum between the two modes, D_{min}. The number of particles smaller than D_{min} was defined to be members of the small or Aitken mode while larger ones were categorized as members of the cloud-processed mode. An example distribution with lognormal fits to each mode is shown in Figure 6.2. The fitted curves capture the salient features in the aerosol number distribution. The large discrepancy between the data and fitted curve at the smallest diameters indicates the presence of another mode of aerosol with diameters less than 20 nm.

Once the minimum is determined, S_{max} is deduced from Köhler theory :

$$S_{max} = \left(\frac{D_0}{D_{min}}\right)^{3/2} \qquad (2)$$

[*Twomey*, 1977], where

S_{max} = the maximum supersaturation experienced by the aerosol (%)

$D_0 = 2.8 \times 10^{-6}$ cm for ammonium sulfate

D_{min} = diameter of the minimum between the two modes (cm)

Figure 6.2 also shows that representing the ambient data with two lognormal distributions and solving for the diameter at which they cross introduces an average error of approximately ±5% in our determination of the diameter of aerosol at the minimum between the modes. This translates into an error of ±10% in S_{max}. We have assumed that ammonium sulfate is a surrogate for the composition of the aerosol particles, which corresponds to a specific value of D_0 in Equation 2. We estimate this assumption causes

an error of less than 4% in the inferred value of S_{max}.

In Equations 1 and 2, D_{min} is assumed to be the dry diameter of the aerosol particles. If the aerosol are actually hydrated, the inferred value of S_{max} will be lower than the true value. In all of the data presented here, the relative humidity in the Scanning Mobility Particle Sizer was less than 20%, insuring that the aerosol particles were at their dry diameter when sized. Failure to recrystallize would lead to an error of about 30% in the inferred supersaturation.

The inferred N_c does not necessarily correspond to the number of cloud droplets activated at S_{max}. Coalescence can reduce N_c before the cloud evaporates, which will bias our value of N_c low. However, aerosol particles will have undergone multiple cloud cycles before being sampled. The most vigorous of those cycles will determine the number of particles in the larger mode of the bimodal aerosol number distribution such that our inferred N_c will be biased toward higher values associated with stronger updrafts or more rapid cooling. These two competing biases plus the assumption that all particles larger than the calculated minimum between the two modes in the number distribution were incorporated into a cloud as droplets are expected to contribute an error of approximately ±10% to N_c.

The validity of three assumptions used in this analysis will be discussed below.

1) *The bimodal distributions are created by cloud processing.*

Cloud processing has been shown to create a bimodal structure in aerosol number distributions [*Hoppel et al.*, 1986; *Hoppel et al.*, 1994a,b] through the aqueous phase oxidation of sulfur dioxide to sulfate. However, this is not the only mechanism by which a bimodal distribution can be produced. Mixing of air masses could produce a bimodal character in a number distribution, for example a pollution plume mixing with background air [*Fassi-Fihri et al.*, 1997]. Another possible mechanism for production of multiple modes in the number distribution is through nucleation of new particles [*Covert et al.*, 1996]. However, the effects of these mechanisms are transient and can be

differentiated from those of cloud processing by examining a time series of number distributions. Cloud processing produces number distributions in which the size and position of the two modes remain relatively constant. In mixing or nucleation events, the size and position of the modes change relatively quickly. Figure 6.3 is an example of the two types of bimodal distributions. The distributions in the top panel are bimodal, but their relative size and position change significantly over the three hour time period. In contrast, the lower panel shows bimodal distributions which do not change significantly over a three hour time period. This compares favorably with the variation in bimodal distributions shown by Hoppel *et al.* [1996].

2) ***Ammonium sulfate is a good surrogate for the composition of the majority of aerosol particles. This assumption affects the inferred supersaturation.***

Sulfate has been found to be the dominant component of aerosol mass in the Aitken and accumulation mode size range ($20 < D_p < 1000$ nm) [*O' Dowd et al.* 1997, *Pinnick et al.*, 1987, *Charlson et al.*, 1992]. Though sea salt can dominate aerosol mass in the marine boundary layer, it is generally found in particles whose diameters are greater than one micron, which are usually not significant in terms of particle number.

Novakov and Penner [1993] concluded that organic material could make up a large fraction of the aerosol mass in air masses which have been anthropogenically influenced. Matsumoto *et al.* [1997] found that water soluble organic carbon could contribute a significant fraction of the cloud condensation nuclei in clean marine air masses, and Rivera-Carpio *et al.* [1996] found that multicomponent aerosol particles (containing organics) have nucleation properties similar to that of ammonium sulfate. They also found that in air masses which contained significant fractions of organic material, the agreement between measured cloud condensation nuclei concentrations and those calculated from size distributions using the nucleation properties of ammonium sulfate was within 15%. This agreement could break down in highly polluted situations, where sulfate is only a minor constituent of the aerosol mass and where the dominant

constituent is hydrophobic or only slightly soluble.

3) *The aerosol particles in the larger mode are all cloud processed i.e. were incorporated into cloud droplets. This assumption affects the inferred cloud droplet number.*

We assume that all of the aerosol particles larger than the minimum between the two modes in the number distribution were incorporated into the cloud as droplets. It is possible that particles larger than the minimum between the modes could remain interstitial within the cloud if they are insoluble or only slightly soluble. However, the number of interstitial aerosol particles is generally greatly outnumbered by those incorporated into droplets, especially in clean situations [*Gillani et al.*,1995]. This assumption may break down in highly polluted situations, depending on the cloud type and dynamic forcing. We have also assumed that aerosol particles have not been removed by precipitation.

Kinetic limitations may prohibit some soluble particles from activating in some clouds if they are large [*Chuang et al.*, 1997]. Detailed microphysical simulations, using marine and rural continental aerosol distributions as input, have shown that a fraction of the aerosol particles with critical supersaturations less than the maximum supersaturation reached in cloud did not activate [*Bott*, 1997]. However, this effect became important only at diameters greater than approximately 600 nm. The relative contribution of particles of this size to the cloud processed mode is small. We estimate that counting particles of this size and larger as having activated, when in fact, they might not have, will introduce an error of +10% or less.

Results

Table 1 shows the average and standard deviation of S_{max}, N_c, and geometric mean diameter of the cloud-processed mode. The average value of S_{max} was in the range 0.27% to 0.4% at the four remote, clean stations, slightly higher than those reported by

Hoppel *et al.* [1996], who found that 70% of their supersaturation values fell between 0.13% and 0.22% for two cruises over the Atlantic and Pacific Oceans. The average was 0.12% at Wallops Island, a polluted site. The histograms of the frequency of occurrence for S_{max} are shown in Figure 6.4. The average N_c was 70 to 120 cm^{-3} at all stations with the exception of Wallops Island, where it was over 1000. Figure 6.5 shows histograms of the frequency of occurrence of N_c for the five sites. The two peaks in the histogram of N_c for Wallops Island reflect two distinct episodes when the sampled air masses had different histories. A similar split is observed in the histograms of geometric mean diameter of the cloud-processed mode, which are shown in Figure 6.6, at Wallops Island, Poker Flat, and Homer. The average geometric mean diameter of the cloud-processed mode is approximately 135 nm for Cheeka Peak, Poker Flat, and Hawaii, while the mode was at 150 and 220 nm for Homer and Wallops Island respectively.

Poker Flat. Although Poker Flat is more than 400 km from the Gulf of Alaska, low pressure systems in the Gulf frequently advect air from the south over the Alaska Range, an approximately 3000 m barrier, or from the west between the Alaska and Brooks Ranges. The data from Poker Flat were taken in April of 1995 during a time period when a series of low pressure systems consistently forced air from the Gulf into interior Alaska. The intervening land mass is still largely snow covered at that time of year, so the continental influence is minimized. Marine air masses can penetrate that far inland and still retain their marine characteristics [*Shaw*, 1988].

The histogram of N_c for this site is rather narrow as shown in Figure 6.5. The histogram of S_{max} has a slightly bimodal character, seen in Figure 6.4. The higher supersaturations are associated with rapid transport over the Alaska Range, which would produce strong uplift and lead to higher supersaturations. The lower supersaturations are associated with air that originated in the Gulf, but did not cross the Alaska Range, instead coming from northern British Columbia, across the Yukon and eastern Alaska.

Cheeka Peak. In contrast to the narrow frequency distribution of N_c at

Poker Flat, the histogram at Cheeka Peak is broader, with a tail that extends to concentrations as high as 400 cm^{-3}. The Cheeka Peak data were collected over a period of almost three months, while the Poker Flat data were collected over a time period of just 15 days. The distributions taken at Cheeka Peak represent a wider range of meteorological situations and source regions, so a wider distribution of N_c is expected. The histograms of the geometric mean diameter of the cloud-processed mode for Poker Flat and Cheeka Peak are similar, though the histogram at Cheeka Peak does not have two peaks, reflecting the longer sampling period.

Hawaii. The Hawaii data set was collected in April of 1994. The supersaturations greater than 0.5% encountered there could be due to the clean conditions and vigorous updrafts encountered in the island chain [*Szumowski et al.*, 1997]. The histograms of the N_c and S_{max} for Hawaii are broader than all of the other "clean" sites, but the histogram of the geometric mean diameter of the cloud-processed mode is slightly more narrow. The standard deviation of N_c sampled at the site is 40, comparable to the standard deviations for Poker Flat, Cheeka Peak, and Homer. However, the standard deviation in the geometric mean diameter of the cloud-processed mode is 10, half that of Poker Flat, Cheeka Peak, and Homer (see Table 1).

Wallops Island. Wallops Island is coastal, but certainly not "clean". The total aerosol number concentration frequently exceeded 10000 cm^{-3}. The duration of our experiment at Wallops Island was only 14 days, and in that time we had only two time periods in which we sampled bimodal aerosol number distributions. There were clear differences in the episodes, evident in Figures 5 and 6. The two peaks in the Wallops Island data for N_c and geometric mean diameter of the cloud-processed mode correspond to different events.

The higher values of N_c, sampled on July 23, occurred during a time period when air from the northeast of Wallops Island, a heavily industrialized area, was advected over the Atlantic then back to the coast. The back trajectory is shown in the lower panel of

Figure 6.7. The high droplet concentrations sampled during this time period seem to be indicative of cloud processed pollution. In a polluted environment, N_c is expected to be higher [*Coakley et. al*, 1987; *Twomey*, 1984] than it would be in a clean air mass. Droplet concentrations of greater than 1000 cm^{-3} have not been reported for stratus or stratocumulus clouds to our knowledge, but there are reports of concentrations in excess of 2500 cm^{-3} for fair weather cumulus clouds [*Seidl*, 1994 and references therein]. Lower supersaturations are consistent with the inferred droplet concentration. Supersaturations of approximately 0.1% are all that is needed to activate a large number of aerosol when the mean diameter and number concentration are so high.

The lower values of N_c, sampled on July 19, are indicative of a continental air mass. Back trajectories, shown in the upper panel of Figure 6.7, indicate that the air mass originated over the Gulf of Mexico and traveled across the Southeast before being sampled at Wallops Island.

Homer. The Homer data also fall into two distinct episodes, which can be seen in the histograms of the geometric mean diameter of the cloud-processed mode and S_{max}. The two modes in the histograms of both parameters correspond to different air mass histories.

The air mass sampled on June 9, 1996 originated over the Gulf of Alaska and was sampled at Homer with a minimum of continental influence. The air mass sampled on June 17 originated over Alaska's north coast, came across the west coast, and looped out over the Gulf briefly, before being sampled at Homer. The back trajectories are shown in Figure 6.8. The values of N_c inferred from the clean marine case are significantly lower than the modified continental case, while S_{max} in the clean marine case is higher than the modified continental. This is probably due to differences in the cloud activation process, which will be discussed below. The geometric mean diameter of the cloud-processed mode is clearly separated into two peaks. The larger geometric mean diameters correspond to the continentally influenced aerosol while the smaller

correspond to the marine case.

Discussion

The process of cloud formation is dynamic. The interplay among vertical velocity in the cloud, lapse rate, available water vapor, shape of the aerosol number distribution, chemical composition of the aerosol, and total concentration of the aerosol determines S_{max} and N_c [*Hänel*, 1987]. We do not have independent information on speed of the updraft, water vapor, lapse rate, or chemical composition of the aerosol. However with this comparatively large data set, we can explore relationships among supersaturation, cloud droplet concentration, aerosol concentration, and shape of the aerosol number distribution. We compare the data we collected with the relationships predicted by a theoretical formulation.

The time evolution of supersaturation during cloud activation is described by [*Twomey*, 1977]:

$$\frac{dS}{dt} = \alpha v - \beta S \Sigma D \qquad (3)$$

α,β = constants of proportionality

v = updraft velocity (cm s^{-1})

S = supersaturation

ΣD = summation over diameters (cm)

In situations where lapse rate and vertical velocity are relatively constant, maximum supersaturation and cloud droplet concentration will be inversely correlated. Competition between activated droplets for available water vapor limits the maximum supersaturation, which determines the smallest aerosol which will activate. For a constant updraft velocity, S_{max} will be lower if more particles are nucleated. Figure 6.9 illustrates this relationship, generated by coupling Equation 3 with Equation 2. Abdul-

Razzak *et al.* [1998] found a similar relationship from a parameterization of aerosol activation suitable for inclusion in a general circulation model.

It seems counter-intuitive that low supersaturations would be correlated with high droplet concentrations, but S_{max} and N_c are determined simultaneously through a feedback process during cloud formation. If the aerosol number concentration is high, many particles will nucleate early in the cloud activation process, contributing a large surface area which acts as a significant sink for water vapor. The resultant supersaturation will be lower than if fewer aerosol particles had activated. Conversely, if the aerosol concentration is low, relatively few particles will activate early in the cloud activation process. With a lower initial sink for the supersaturated water vapor, the supersaturation will become greater before eventually being reduced by the growing cloud droplet concentration.

Figure 6.10 is a plot of N_c vs. S_{max} for all of the bimodal distributions collected at Cheeka Peak. There is no clear relationship between the two in the overall ensemble of data. Day-to-day variations in updraft velocity, lapse rate and other parameters obscure any trends. However, if specific time periods are chosen, the correlation between S_{max} and N_c becomes clearer. Figure 6.11 illustrates the trends that emerge when specific time periods are examined. Though there is scatter, the data show that S_{max} and N_c can be inversely correlated in natural systems.

In contrast, the frequently used parameterization for the number of cloud condensation nuclei (CCN) activated as a function of applied supersaturation [*Twomey*, 1977] :

$$N_{CCN} = CS^k \qquad (4)$$

N_{CCN} = number concentration of CCN (cm^{-3})

C = empirically derived constant (cm^{-3})

k = empirically derived constant

S = supersaturation (%)

might seem to predict a positive correlation between N_c and S_{max}. However, it is the **CCN** concentration which is predicted, not N_c. CCN, a subset of the aerosol, are potential cloud droplets, but will only become cloud droplets if they are subjected to a supersaturation larger than some critical value. They are usually measured by subjecting the aerosol particles to a specific supersaturation, then counting the number which become droplets. In the measurement device, there is no feedback between the activated aerosol and the supersaturation because the vapor source is essentially infinite. If the aerosol particles are exposed to lower supersaturation, fewer of them will become droplets, and conversely, if they are exposed to a higher supersaturation, more will become drops.

The inverse relationship illustrated in Figures 9 and 11 highlights a potential shortcoming of many CCN measurements, which are frequently made at a single supersaturation, typically 0.5%. Because the cloud supersaturation and droplet concentration are determined through a feedback process, increasing the number concentration of CCN in an air mass will result in lower maximum supersaturations given the same dynamical forcing. To accurately assess a cloud's response to an increase in the CCN concentration, the CCN supersaturation spectrum must be measured, or alternatively, a relationship between the aerosol number distribution and CCN spectrum could be specified [*Abdul-Razzak et al.*, 1998].

The shape of the aerosol number distribution also affects the cloud droplet concentration. Again, these two variables cannot be considered to be independent because the cloud droplet concentration can affect the shape of the aerosol distribution through in-cloud processes like conversion of sulfur gases to sulfate.

Figure 6.12 illustrates the relationship between geometric mean diameter of the aerosol and the number of aerosol activated predicted by Equations 2 and 3. As the

aerosol number distribution is shifted to larger diameters, more particles are nucleated in the cloud activation process, in agreement with results obtained by Abdul-Razzak *et al.* [1998]. Data taken at Homer and Cheeka Peak, shown in Figure 6.13, point to an inverse correlation between the geometric mean diameter of the cloud-processed mode and N_c, suggesting that some process other than cloud activation is controlling this relationship. In-cloud conversion of sulfur gases to sulfate would produce a trend like that seen in Figure 6.13. If there are fewer cloud droplets, each will gain more mass than if there had been more cloud droplets. Sulfate (or any mass added to the aerosol particles by aqueous phase reactions in-cloud) split between fewer aerosol particles will result in a larger diameter once the cloud evaporates.

Conclusions

Non-precipitating clouds alter the aerosol particles which cycle through them. The fraction of aerosol particles which are incorporated into cloud droplets frequently gains mass through aqueous conversion of sulfur gases to sulfate. When the cloud evaporates, the aerosol particles which have gained sulfate mass have an increased diameter, while aerosol particles which were interstitial in the cloud return to their original size, creating a bimodal aerosol number distribution. By making a few reasonable assumptions, cloud characteristics can be inferred from the bimodal aerosol number distributions. The number of aerosol particles in the larger of the two modes can be used as a proxy for N_c, and the location of the minimum between the two modes serves as an indicator of S_{max} experienced in cloud.

We analyzed over 1700 bimodal aerosol number distributions from five locations for these properties. Though N_c and S_{max} varied across geographic regions and air mass history, station averages for both were within a factor of three with the exception of the Wallops Island data set, which was taken in polluted conditions on the eastern seaboard of the U.S.

The inferred values of S_{max} and N_c have implications for experimental work. If at all possible, measurements of cloud condensation nuclei should include a range of supersaturations, not a single value. The process of cloud activation is a dynamic process, so cloud supersaturation and droplet concentration are determined through a feedback process. To accurately assess how the number concentration of droplets in a cloud will change with a change in CCN, the number of CCN as a function of supersaturation must be specified.

The average geometric mean diameter of the cloud-processed mode was remarkably constant from station to station. Four of the five stations agreed within the standard deviation of the geometric mean diameter determined at the station. The outlier, again, was Wallops Island.

We also examined relationships among cloud properties by inspecting specific episodes in the data. An inverse correlation between S_{max} and N_c is apparent, which can be explained by the cloud activation process. An inverse correlation between geometric mean diameter of the cloud-processed mode and N_c is presumably due to addition of mass through aqueous phase reactions.

Analyzing bimodal distributions for cloud properties can provide a large database across a wide variety of geographic regions, seasons, and time scales. In addition, the method is relatively inexpensive, requiring only a differential mobility analyzer and particle counter. It provides one tool for validation of cloud processes on a regional and global scale in modeling efforts.

Locations of the five sampling stations

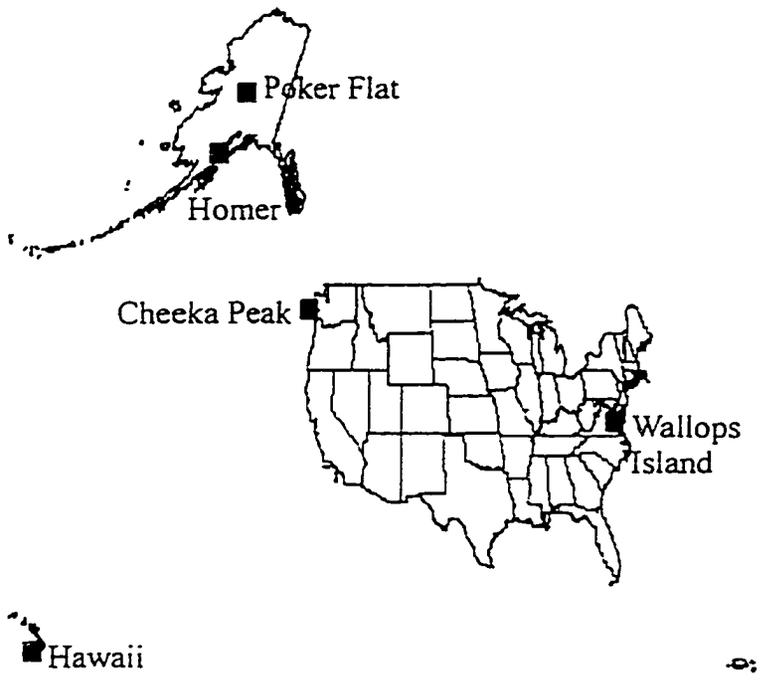

Figure 6.1 The five sampling stations from which we infer cloud properties based on the bimodal aerosol number distributions collected there.

Example aerosol number distribution with lognormal fits

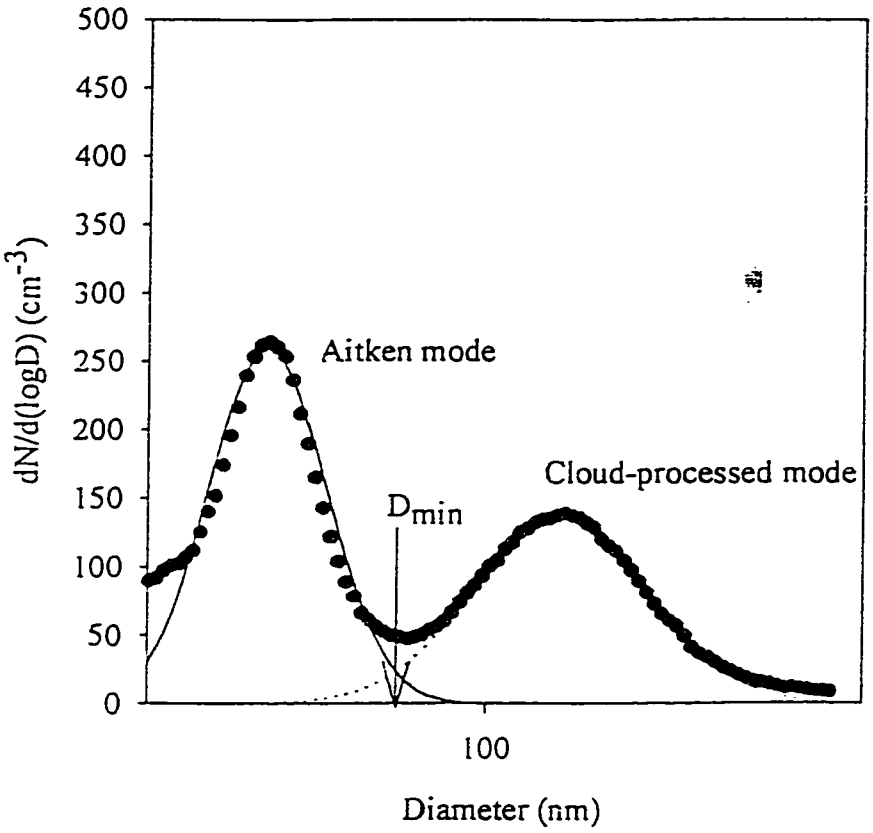

Figure 6.2 Example of a bimodal aerosol number distribution and the lognormal fits to each mode. The point at which the two fitted curves cross is defined as D_{min} in the subsequent analysis.

Examples of bimodal aerosol number distributions

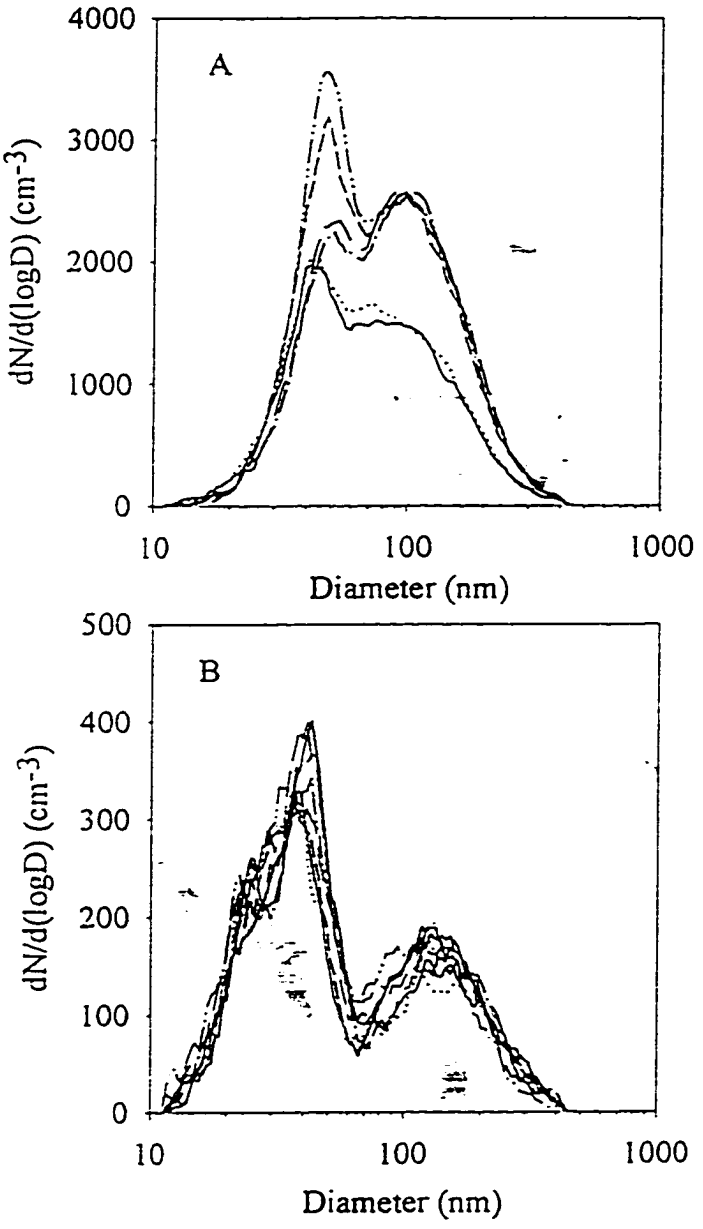

Figure 6.3 Examples of bimodal aerosol number distributions. The distributions in panel A changed significantly in size and position over a time period of three hours. Distributions such as these were excluded from further analysis as they could result from mixing processes. The distributions in panel B, assumed to be cloud processed, were stable over three hours.

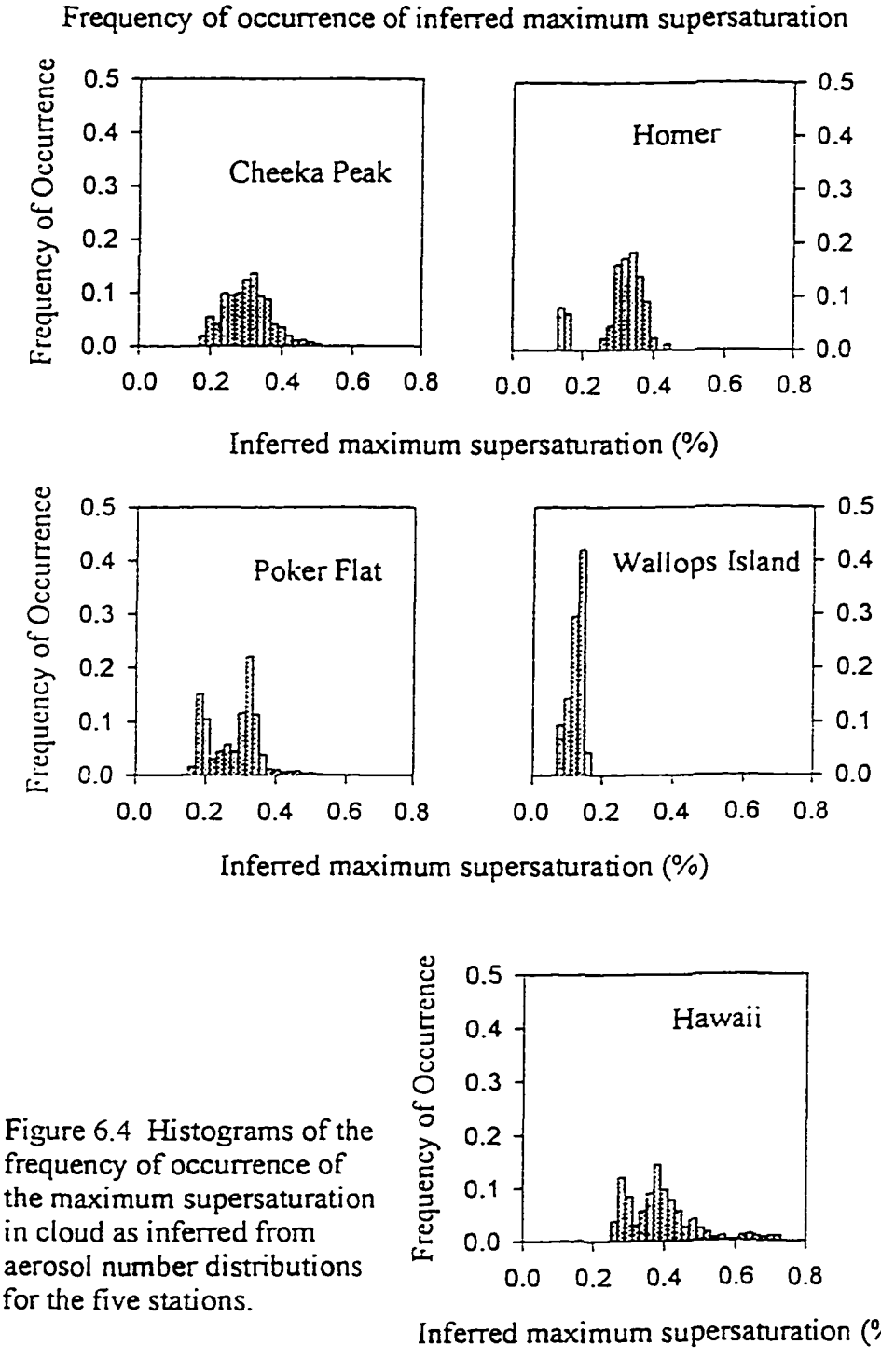

Figure 6.4 Histograms of the frequency of occurrence of the maximum supersaturation in cloud as inferred from aerosol number distributions for the five stations.

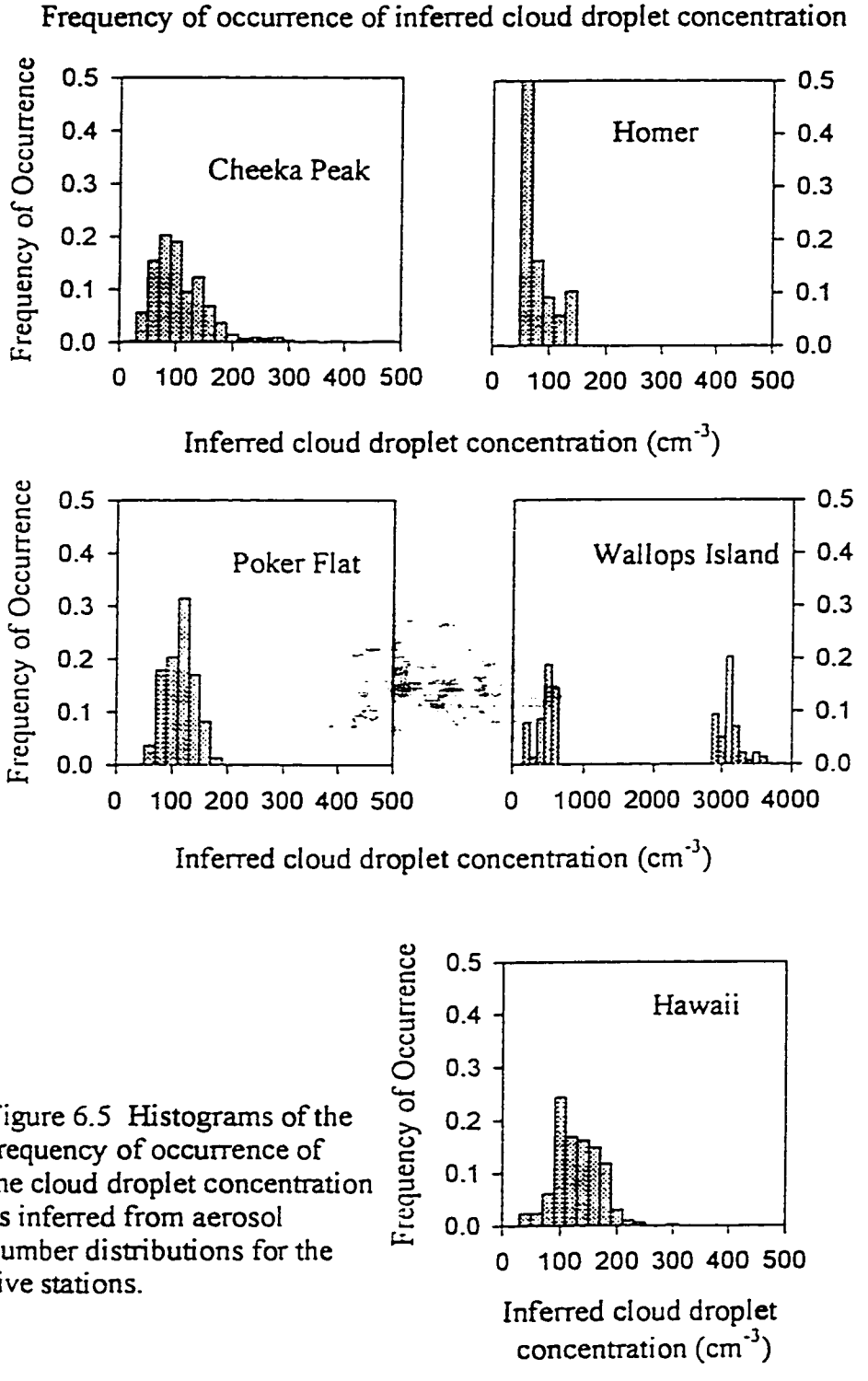

Figure 6.5 Histograms of the frequency of occurrence of the cloud droplet concentration as inferred from aerosol number distributions for the five stations.

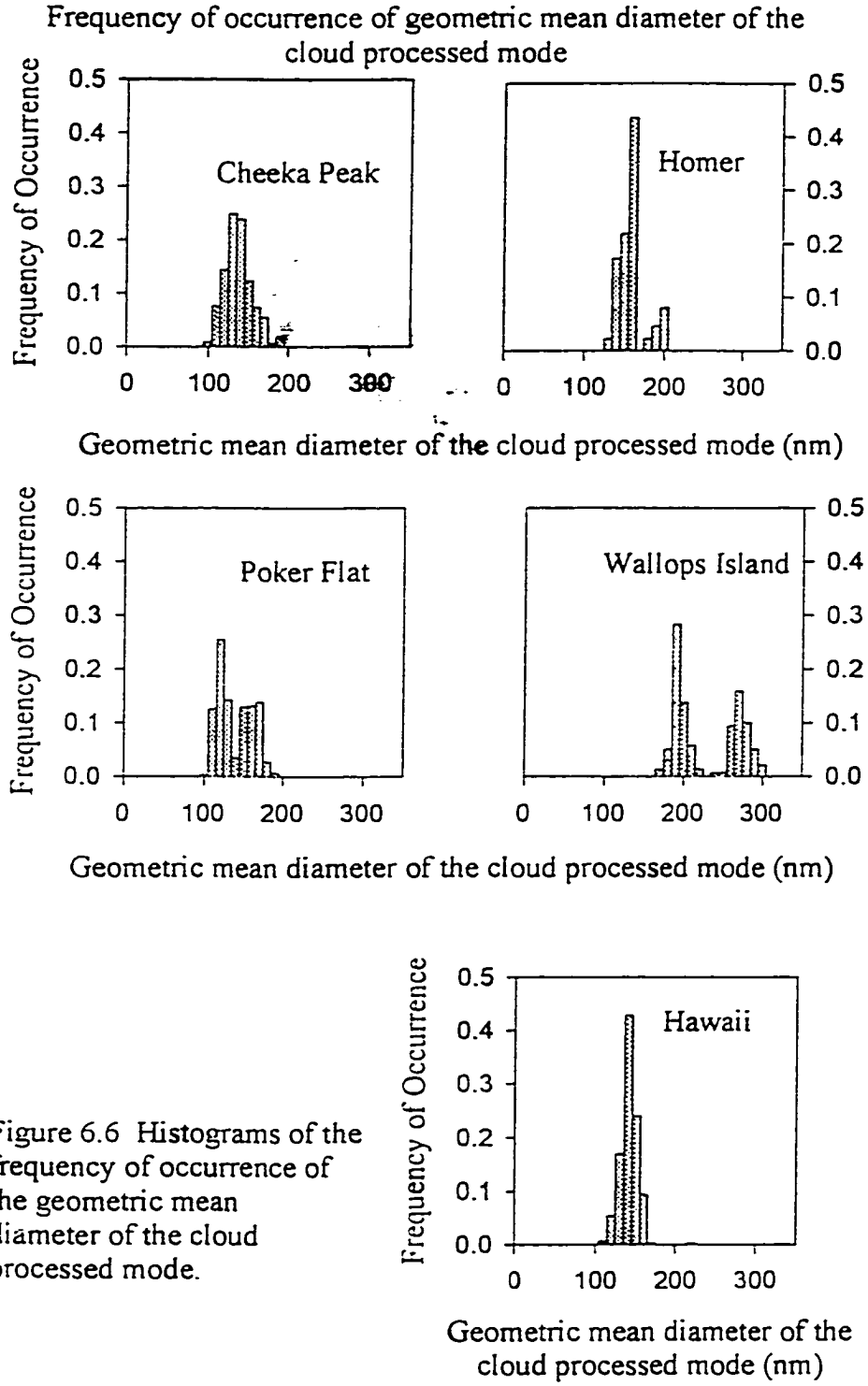

Figure 6.6 Histograms of the frequency of occurrence of the geometric mean diameter of the cloud processed mode.

Back trajectories for air masses sampled at Wallops Island

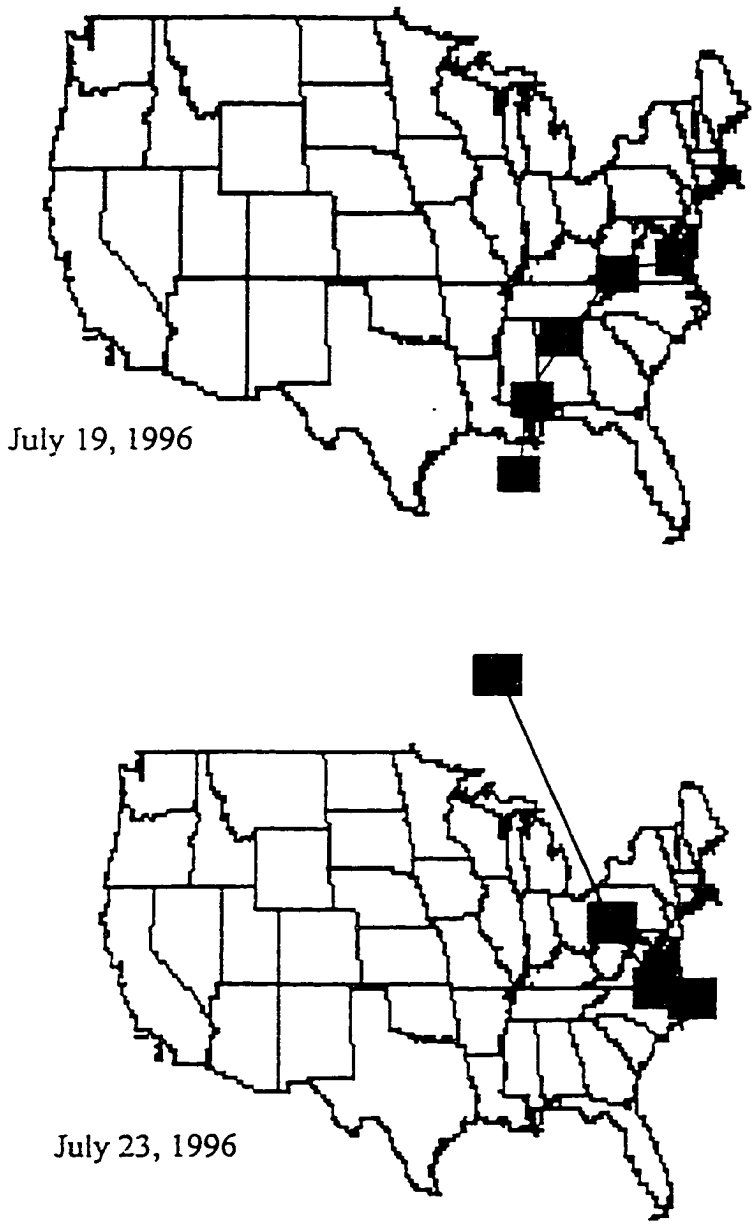

Figure 6.7 Back trajectories for the air masses sampled at Wallops Island. The air mass sampled on June 19 originated over the Gulf of Mexico and was continentally influenced before being sampled. The air mass sampled on June 23 originated over the continent, but looped out over the Atlantic Ocean briefly before being sampled.

Back trajectories for air masses sampled at Homer

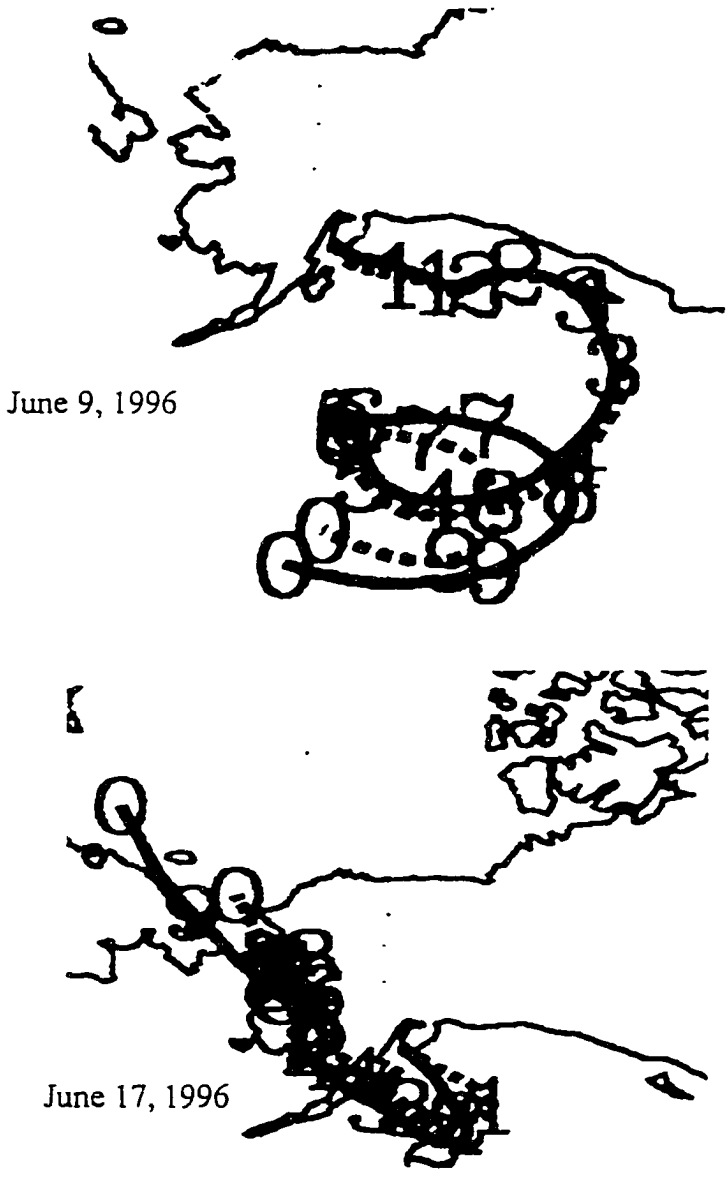

Figure 6.8 The back trajectories for the air masses sampled at Homer indicate that the air mass sampled on June 9 was relatively free of continental influence. The air mass sampled on June 17 was influenced by the Kamchatka and Alaskan peninsulas. The numbers along the trajectories indicate days back from Homer.

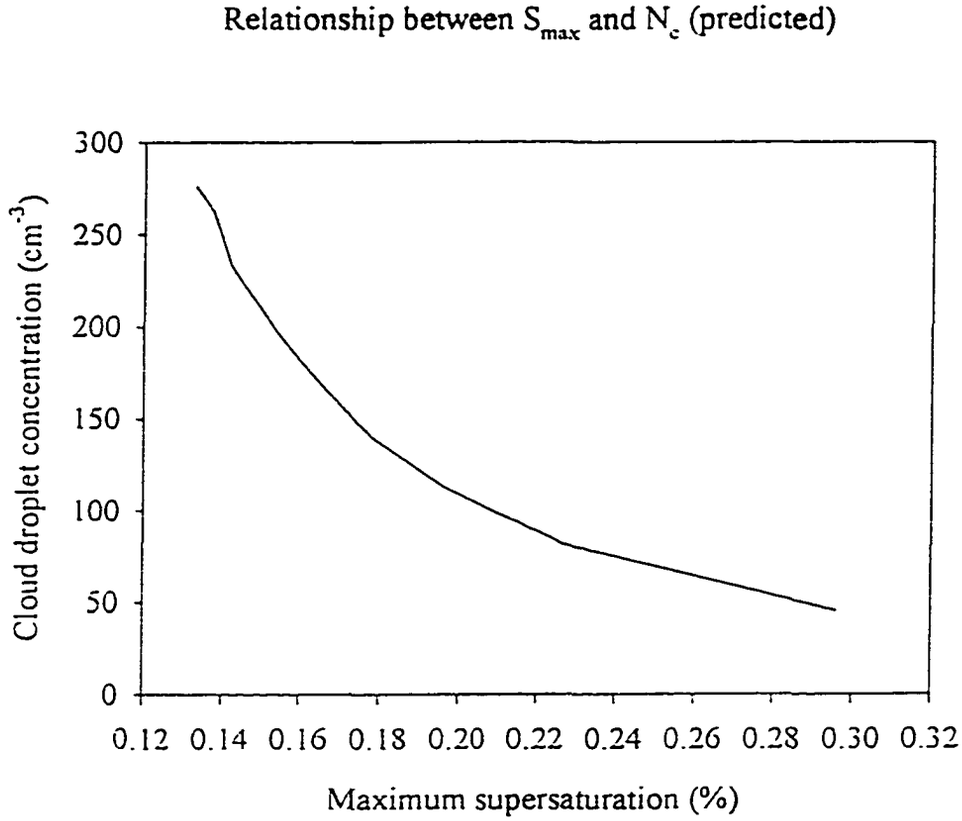

Figure 6.9 The relationship between S_{max} and N_c predicted by Equations 2 and 3. If more aerosol are nucleated, the droplet population is larger, which increases the sink term in Equation 3. The sink becomes the dominant term more quickly, so the maximum supersaturation in the cloud is lower. The updraft velocity used for this case is 30 cm s^{-1}. The geometric mean diameter of the aerosol number distribution is 100 nm, and the total aerosol number concentration varies between 50 and 500 cm^{-3}.

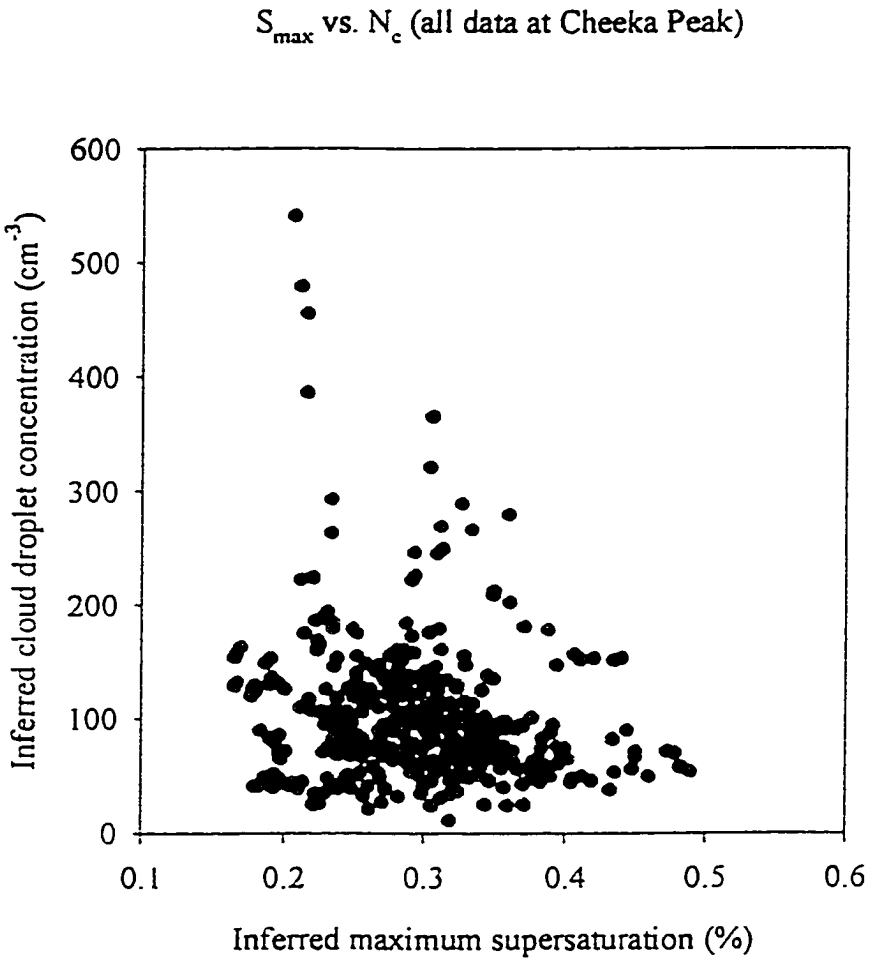

Figure 6.10 Maximum supersaturation vs. cloud droplet concentration for all data collected at Cheeka Peak. Any trend is obscured by day-to-day variations in other parameters such as updraft velocity and lapse rate.

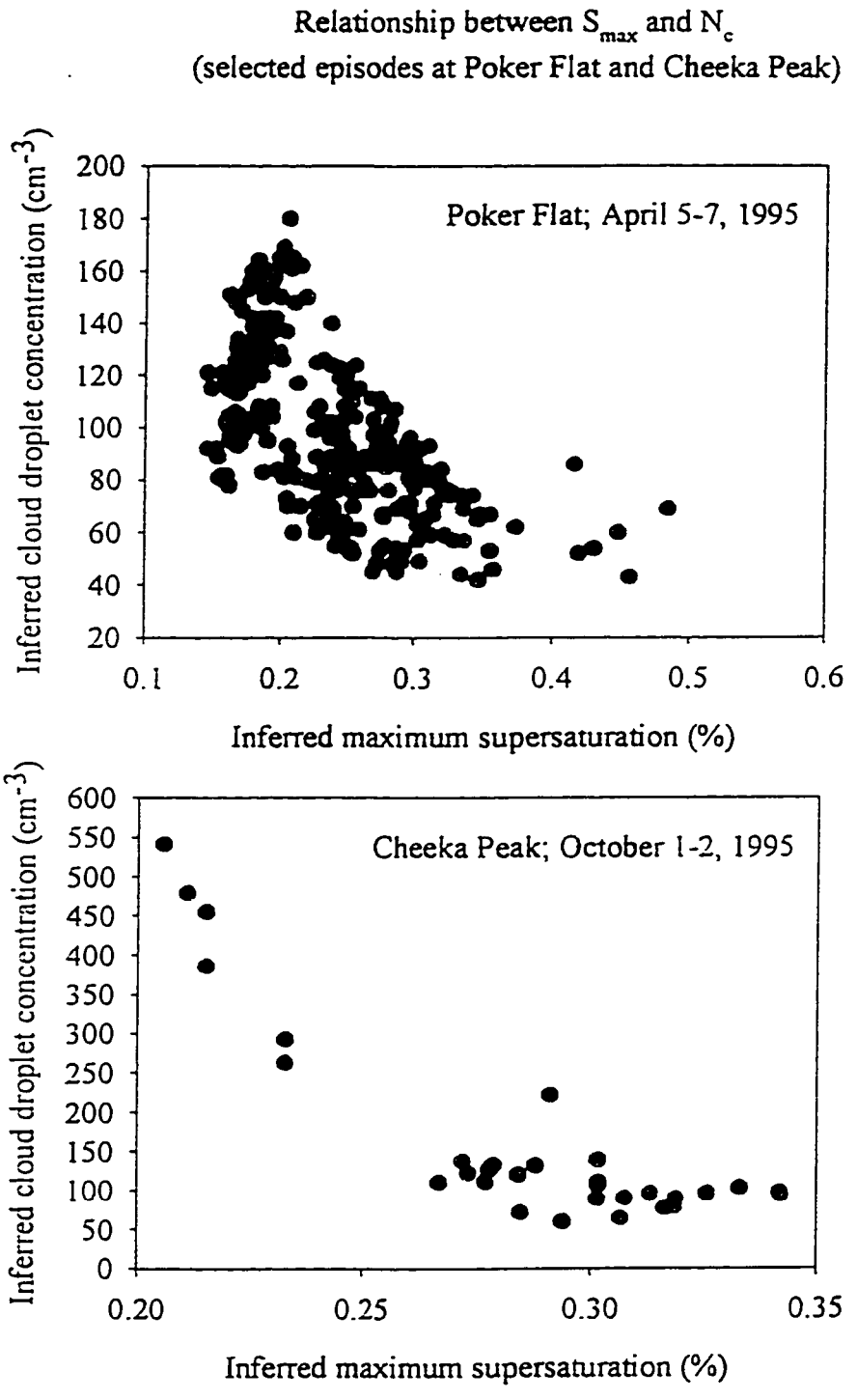

Figure 6.11 Relationship between maximum supersaturation and Nc, seen in selected episodes at Poker Flat and Cheeka Peak. The inverse correlation predicted by Equations 2 and 3 is apparent.

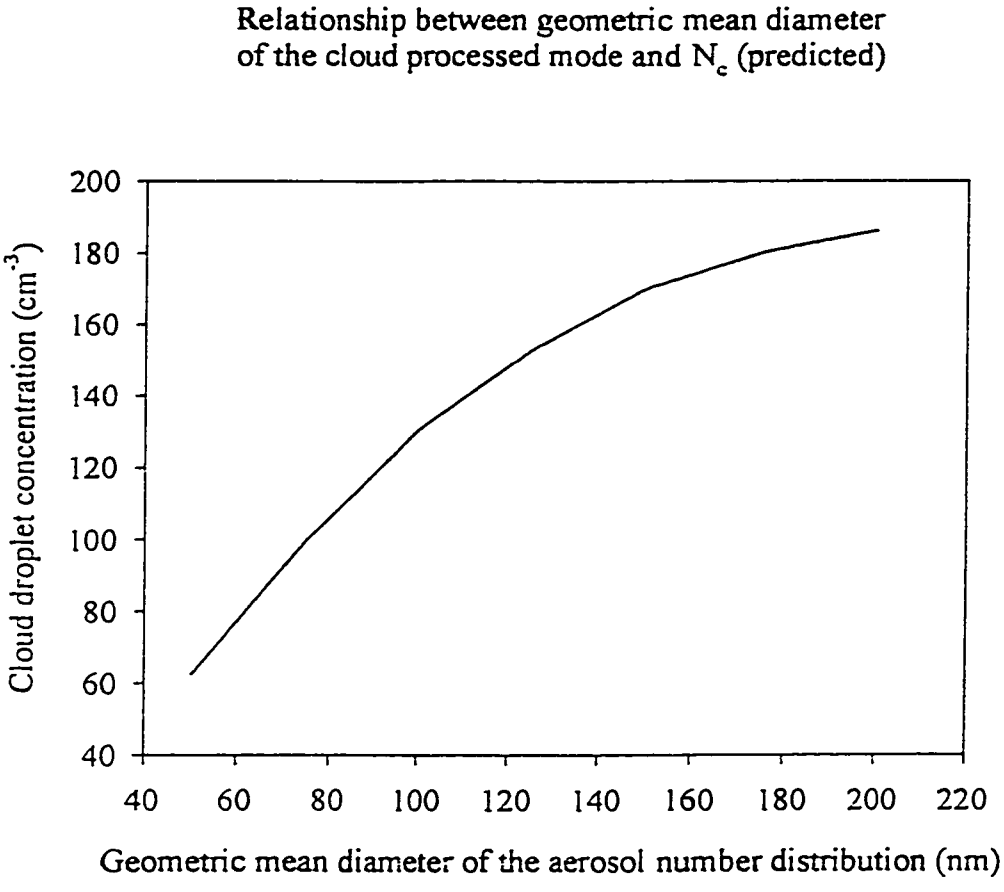

Figure 6.12 Relationship between the geometric mean diameter of the aerosol number distribution and the cloud droplet concentration predicted by Equations 2 and 3. More aerosol particles become cloud droplets as the mean size of the particles increases. The updraft velocity used is 30 cm s^{-1} and the number concentration is 200 cm^{-3}.

Relationship between geometric mean diameter of the cloud processed mode and N_c (measured at Cheeka Peak and Homer)

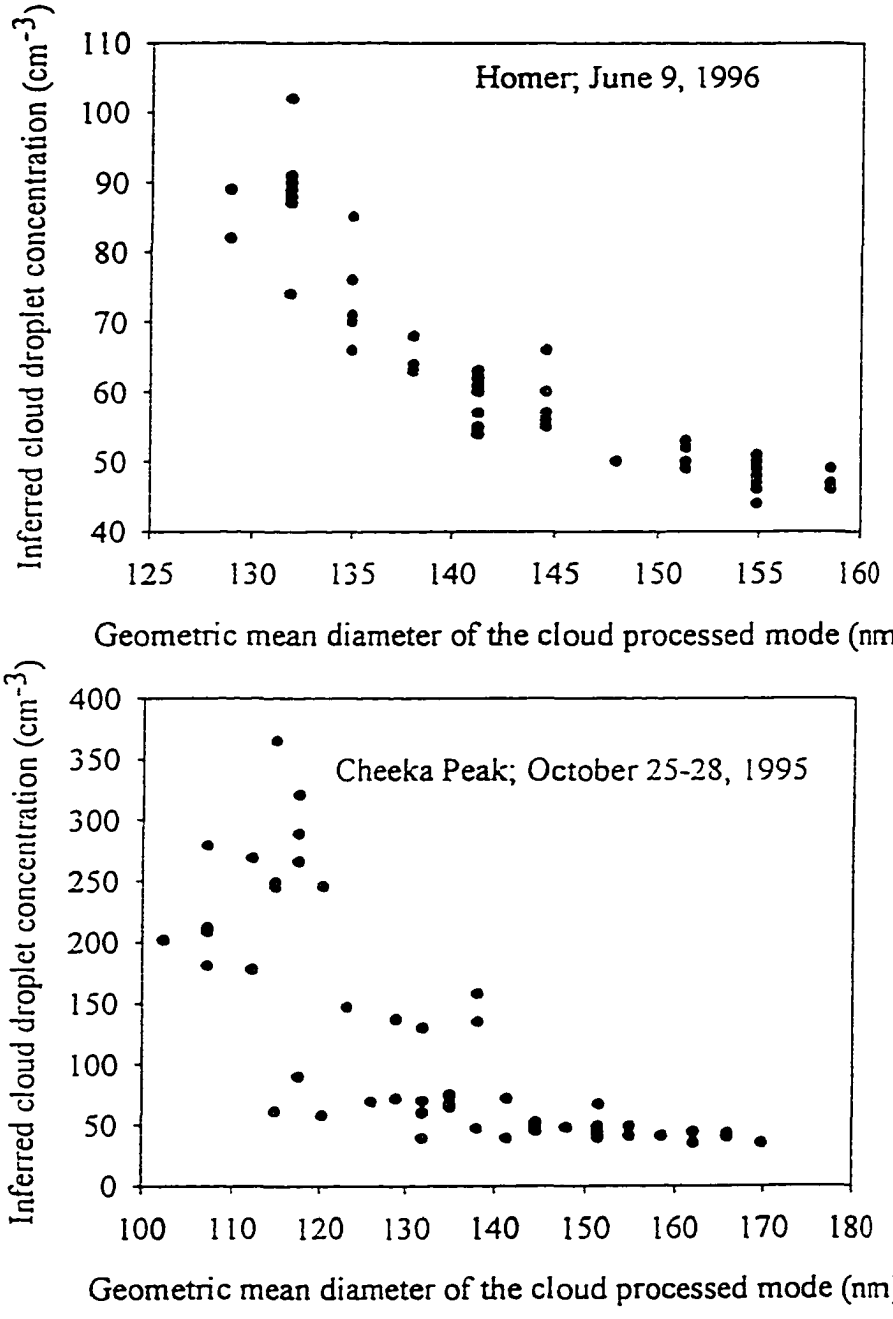

Figure 6.13 Relationship between geometric mean diameter of the cloud processed mode and Nc, found in selected episodes in the data set. The two are inversely correlated, indicating that some process other than cloud activation is operating. Conversion of sulfur gases to sulfate in cloud would most likely produce a trend like that shown here.

Average properties at the five sampling sites

Station	**Number in sample**	**Supersaturation (%) ; σ**	**Droplet number (cm^{-3}) ; σ**	**Diameter of cloud mode (nm) ; σ**
Cheeka Peak	406	0.29 ; 0.06	100 ; 60	130 ; 20
Poker Flat	958	0.27 ; 0.07	100 ; 30	130 ; 20
Hawaii	296	0.4 ; 0.1	120 ; 40	140 ; 10
Wallops Island	138	0.12 ; 0.02	1700 ; 1300	220 ; 40
Homer	87	0.30 ; 0.07	70 ; 30	150 ; 20

Table 6.1 The number of samples in each data set, and the average across the data set for maximum supersaturation, droplet concentration, and geometric mean diameter of the cloud processed mode inferred from bimodal aerosol number distributions. The standard deviation, σ, is shown after each of the averages. The properties are remarkably constant between the widely separated stations, with the exception of Wallops Island, which was heavily influenced by anthropogenic sources.

Chapter 7

Conclusions

"I won't read a thesis over 100 pages." -Glenn Shaw

Summary

Using a new instrument, developed and refined at the Geophysical Institute over the last five years, we can establish a relationship between the aerosol number distribution and the CCN supersaturation spectrum. The instrument accurately characterizes the CCN spectrum from 0.13% to 1% supersaturation, and in most operating conditions, the errors in supersaturation and CCN concentration are ±10% or less.

With our unique ability to relate the CCN spectrum to the aerosol number distribution, we were able to establish that the aerosol number distribution can only be reliably converted to CCN supersaturation spectrum if the aerosol soluble fraction is known. The CCN spectrum calculated from the aerosol number distribution assuming a composition of ammonium sulfate would overpredict the actual CCN spectrum by 30 to 40%. By incorporating the measured aerosol soluble fraction, the overall agreement between the modeled and measured CCN spectra was within instrumental errors. The agreement in individual cases was better when the concentrations of organic species were low.

During a cruise from Goa, India to Port Luis, Mauritius, we established a significant latitudinal variation in the concentration of CCN. This variation corresponds to a similar variation in aerosol mass. The polluted, Northern Hemisphere air mass exhibited a significant discrepancy between measured CCN spectra and spectra calculated from the aerosol number distribution, up to a factor of two in the most

extreme examples. We were not able to compare the measured spectra with modeled spectra using a measured aerosol soluble fraction in this case.

Anthropogenic activity is altering the aerosol burden in the atmosphere, and changing the properties of the aerosol properties. Through a series of volatility experiments, we have shown that aerosol particles in an Arctic air mass could be coated, presumably with sulfuric acid. These changes in aerosol properties could affect their ability to act as CCN by changing the surface properties, which is the first part of the aerosol particle to respond to changes in water vapor concentration.

In some instances, the aerosol number distribution can be used to infer cloud microphysical properties because the clouds through which the aerosol particles cycle leave a signature. Bimodal aerosol number distributions frequently indicate that the aerosol have been cloud processed, and the position of the minimum between the two modes can be used as a proxy for the maximum supersaturation in the cloud. The number of aerosol particles in the larger mode can be taken as the number concentration of cloud droplets in the most vigorous cloud cycle. In an analysis of over 1700 bimodal distributions, we showed that maximum supersaturation, cloud droplet concentration, and geometric mean diameter of the cloud processed mode are remarkably constant over a wide variety of geographic regions and seasons. Polluted air masses have strikingly different characteristics from those not strongly influenced by anthropogenic sources.

Where to go from here?

One of the most frustrating, yet at the same time invigorating, aspects of science is that almost every answer implies another question. In Chapters 3 and 4 of this thesis, we show that the relationship between the aerosol number distribution and the CCN supersaturation spectrum can be quite complex, especially in polluted air masses. Over the Indian Ocean, it appears that the aerosol soluble fraction may be quite low. However, it is not clear whether this is due to an actual deficit in soluble species or the result of

some other component which may be preventing the soluble species from taking up water. Further measurements with the CCN Remover, coupled with corollary measurements such as the hygroscopic growth factors and detailed single particle chemistry, should be used to address this question. The hygroscopic growth factor was measured during the second Aerosol Characterization Experiment, so we were able to compare the measured CCN spectra with the CCN spectra calculated from the aerosol number distribution. The overall agreement was within the errors of the two instruments, but the agreement was worst during time periods when a substantial fraction of the aerosol mass was organic. The role that organics play in the activation of cloud condensation nuclei should be explored in a laboratory setting. If organic species are preventing aerosol particles from activating, then it should be identified and quantified in the laboratory. The CCNR has the unique capability of directly relating aerosol particles to CCN. This is exactly the sort of information needed to clarify the role that organic species might play in enhancing or suppressing the activation of CCN.

Though we have pointed out some important implications of our results in Chapters 3 and 4, there are still other avenues remaining to be explored. Though we can speculate as to how our results might affect cloud properties, data such as we have collected during ACE 2 and INDOEX need to be incorporated into modeling studies to adequately explore how the cloud microphysical properties might be changed by the anthropogenic influences we have documented. The cloud microphysical properties derived from bimodal aerosol number distributions which we presented in Chapter 6 are a potentially powerful tool for model validation on a regional or global scale. The technique is straightforward and relatively inexpensive. It provides an excellent complement to the global databases of cloud properties derived from satellite observations.

Technical Manuals

Cloud Condensation Nucleus Counter, Model M1, DH Associates, 1993.

References

Abdul-Razzak, H., S.J. Ghan, and C. Rivera-Carpio, A parameterization of aerosol activation 1. Single aerosol type. *J. Geophys. Res.*, **103**, 6123-6131, 1998.

Aitken, J., On dust, fogs, and clouds. *Proc. Roy. Sco. Edinb.*, **9**, 14-18, 1880.

Albrecht, B.A., Aerosols, cloud microphysics, and fractional cloudiness. *Science*, **245**, 1227-1230, 1989.

Alofs, D.J., D.E. Hagen, and M.B. Trueblood, Measured spectra of the hygroscopic fraction of atmospheric aerosol particles. *J. Appl. Met.*, **28**, 126-136, 1989.

Andrews, E. And S. Larson, Effect of surfactant layers on the size changes of aerosol particles as a function of relative humidity. *Environ. Sci. Technol.*, **27**, 857-865, 1993.

Barrie, L.A. and M.J. Barrie, Chemical components of lower tropospheric aerosols in the high Arctic: Six years of observations, *J. Atmos. Chem.*, **11**, 211-226, 1990.

Barrie, L.A., and R.M. Hoff, The oxidation rate and residence time of sulphur dioxide in the Arctic atmosphere, *Atmos. Environ.*, **18**, 2711-2722, 1984.

Berg. O. H., E. Swietlicki, and R. Krejci, Hygroscopic growth of aerosol particles in the

marine boundary layer over the Pacific and Southern Oceans during the First Aerosol Characterization Experiment (ACE 1). *J. Geophys. Res.*, **103**, 16,535-16,545, 1998.

Bigg, E.K., Discrepancy between observation and prediction of concentrations of cloud condensation nuclei. *Atmos. Res.*, **20**, 82-86, 1986.

Bigg, E.K., Comparison of aerosol at four baseline atmospheric monitoring stations, *J. Appl. Meteor.*, **19**, 521-533, 1980.

Bigg, E.K., J.L. Gras, and D.J.C. Mossop, Wind-produced submicron particles in the marine atmosphere. *Atmos. Res.*, **36**, 55-68, 1995.

Bodhaine, B.A., Aerosol absorption measurements at Barrow, Mauna Loa, and the south pole, *J. Geophys. Res.*, **100**, 8967-8975, 1995.

Bodhaine, B.A., Aerosol measurements at four background sites, *J. Geophys. Res.*, **88**, 10753-10768, 1983.

Bott, A., A numerical model of the cloud-topped planetary boundary-layer: Impact of aerosol particles on the radiative forcing of stratus clouds. *Q.J. Meteorol. Soc.*, **123**, 631-656, 1997.

Boucher, O. and U. Lohmann, The sulfate-CCN-cloud albedo effect A sensitivity study with two general circulation models. *Tellus*, **47B**, 281-300, 1995.

Cantrell, W., G. Shaw, and R. Benner, Cloud properties inferred from bimodal aerosol number distributions. *J. Geophys. Res.*, submitted 1998.

Charlson, R.J., S.E. Schwartz, J.M. Hales, R.D. Cess, J.A. Coakley, Jr., J.E. Hansen, and D.J. Hofman, Climate forcing by anthropogenic aerosols. *Science*, **255**, 423-430, 1992.

Chuang, P.Y., R.J. Charlson, and J.H. Seinfeld, Kinetic limitations on droplet formation in clouds. *Nature*, **390**, 594-596, 1997.

Clarke, A., A Thermo-Optic technique for *in situ* analysis of size-resolved aerosol physicochemistry, *Atmos. Environ.*, **25A**, 635-644, 1991.

Clarke, A., In-situ measurements of the aerosol size distributions, physicochemistry and light absorption properties of Arctic Haze, *J. Atmos. Chem.*, **9**, 255-266, 1989.

Clarke, A.D., N.C. Ahlquist,, and D.S. Covert, The Pacific marine aerosol : Evidence for natural acid sulfates, *J. Geophys. Res.*, **92**, 4179-4190, 1987.

Coakley, J.A., Jr., R.L. Bernstein, and P.A. Durkee, Effect of ship-stack effluents on cloud reflectivity. *Science*, **237**, 1020-1022, 1987.

Covert, D.S. and J. Heintzenberg, Size distributions and chemical properties of aerosol at Ny Ålesund, Svalbard, *Atmos. Environ.*, **27A**, 2989-2997, 1993.

Covert, D.S., J.L. Gras, A. Wiedensohler, and F. Stratman, Comparison of directly measured CCN with CCN modeled from the number-size distribution in the marine boundary layer during ACE 1 at Cape Grim, Tasmania. *J. Geophys. Res.*, **103**, 16597-16608, 1998.

Covert, D.S., A. Wiedensohler, P. Aalto, J. Heintzenberg, P.H. McMurry, and C. Leck, Aerosol number size distributions from 3 to 500 nm diameter in the arctic marine boundary layer during summer and autumn. *Tellus*, **48B**, 197-212, 1996.

Cruz, C. and S. Pandis, The effect of organic coatings on the cloud condensation nuclei activation of inorganic atmospheric aerosol. *J. Geophys. Res.*, **103**, 13,111-13,123, 1998.

Cruz, C. and S. Pandis, A study of the ability of pure secondary organic aerosol to act as cloud condensation nuclei. *Atmos. Environ.*, **31**, 2205-2214, 1997.

Fassi-Fihri, A., K. Suhre, and R. Rosset, Internal and external mixing in atmospheric aerosols by coagulation: Impact on the optical and hygroscopic properties of the sulphate-soot system. *Atmos. Environ.*, **31**, 1393-1402, 1997.

Fitzgerald, J.W., Dependence of the supersaturation spectrum of CCN on aerosol size distribution and composition. *J. Atmos. Sci.*, **30**, 628-634, 1973.

Fitzgerald, J.W., A study of the intial phase of cloud droplet growth by condensation : Comparison between theory and observation. University of Chicago, IL, 60637, 1972.

Fitzgerald, J.W., C.F. Rogers, and J.G. Hudson, Review of isothermal haze chamber performance. *J. Rech. Atmos.*, **15**, 333-346, 1981.

Fuchs, N.A., *The mechanics of aerosols*, 408 pp., Dover, New York, NY, 1989.

Fukuta, N. and V.K. Saxena, The principle of a new horizontal thermal gradient cloud

condensation nucleus spectrometer. *J. Rech. Atmos.*, **13**, 169-188, 1979.

Fukuta, N. and A. Walter, Kinetics of hydrometeor growth from a water spherical model. *J. Atmos. Sci.*, **27**, 581-598, 1970.

Ghan, S.J., L.R. Leung, R.C. Easter, and H. Abdul-Razzak, Prediction of cloud droplet number in a general circulation model. *J. Geophys. Res.*, **102**, 21777-21794, 1997.

Gill, P.S., T.E. Graedel, and C.J. Weschler, Organic films on atmospheric aerosol particles, fog droplets, cloud droplets, raindrops, and snowflakes. *Rev. Geophys. Space Phys.*, **21**, 903-920, 1983.

Gillani, N.V., S.E. Schwartz, W.R. Leaitch, J.W. Strapp, and G.A. Isaac, Field observations in continental stratiform clouds: Partitioning of cloud particles between droplets and unactivated interstitial aerosols. *J. Geophys. Res.*, **100**, 18687-18706, 1995.

Gras, J.L., CN, CCN, and particle size in Southern Ocean air at Cape Grim. *Atmos. Res.*, **35**, 233-251, 1995.

Han, Q., W.B. Rossow, and A.A. Lacis, Near-global survey of effective droplet radii in liquid water clouds using ISCCP data. *J. Climate*, 7, 465-497, 1994.

Hänel, G., The role of aerosol properties during the condensational stage of cloud : A reinvestigation of numerics and microphysics. *Beitr. Phys. Atmosph.*, **60**, 321-339, 1987.

Hinds, W.C., *Aerosol Technology Properties, Behavior, and Measurement of Airborne Particles*. John Wiley & Sons, 424 pp., 1983

Hoppel, W.A., Measurement of the size distribution and CCN supersaturation spectrum of submicron aerosols over the ocean. *J. Atmos. Sci.*, **36**, 2006-2015, 1979.

Hoppel, W.A., G.M. Frick, and J.W. Fitzgerald, Deducing droplet concentration and supersaturation in marine boundary layer clouds from surface aerosol measurements. *J. Geophys. Res.*, **101**, 26553-26565, 1996.

Hoppel, W.A., G.M. Frick, and R.E. Larson, Effect of nonprecipitating clouds on the aerosol size distribution in the marine boundary layer. *Geophys. Res. Lett.*, **13**, 125-128, 1986.

Hoppel, W.A., G.M. Frick, J.W. Fitzgerald, and R.E. Larson, Marine boundary layer measurements of new particle formation and the effects non-precipitating clouds have on aerosol size distribution. *J. Geophys. Res.*, **99**, 14443-14459, 1994a.

Hoppel, W.A., G.M. Frick, J.W. Fitzgerald, and B.J. Wattle, A cloud chamber study of the effect that nonprecipitatingwater clouds have on the aerosol size distribution. *Aerosol Sci. Technol.*, **20**, 1-30, 1994b.

Hudson, J.G., Cloud condensation nuclei. *J. Appl. Meteor.*, **32**, 596-607, 1993.

Hudson, J.G., An instantaneous CCN spectrometer. *J. Atmos. Ocean. Technol.*, **6**, 1055-1065, 1989.

Hudson, J.G., and D.J. Alofs, Performance of the continuous flow diffusion chambers. *J. Rech. Atmos.*, **15**, 321-331, 1981.

Jayaraman, A., D. Lubin, S. Ramachandran, V. Ramanathan, E. Woodbridge, W.D. Collins, and K.S. Zalpuri, Direct observations of aerosol radiative forcing over the tropical Indian Ocean during the January-February 1996 pre-INDOEX cruise. *J. Geophys. Res.*, **103**, 13,827-13,836, 1998.

Ji, Q., G. Shaw, and W. Cantrell. A new instrument for measuring cloud condensation nuclei : Cloud Condensation Nucleus "Remover". *J. Geophys. Res.*, **103**, 28013-28019, 1998.

Jodwalis, C., Oceanic emissions of sulfur : Application of new techniques. University of Alaska, Fairbanks, AK 99775, 1998.

Jones, P.D., S.C.B. Raper, and T.M.L. Wigley, Southern hemisphere surface air temperature variations: 1851-1984. *J. Climate Appl. Meteor.*, **25**, 1213-1230, 1986.

Junge, C. and E. McLaren, Relationship of cloud nuclei spectra to aerosol size distribution and composition. *J. Atmos. Sci.*, **28**, 382-390, 1971.

Kerminen, V.-M., The effects of particle chemical character and atmospheric processes on particle hygroscopic properties. *J. Aerosol Sci.*, **28**, 121-132, 1997.

Köhler, H., The nucleus in and the growth of hygroscopic droplets. *Trans. Faraday Soc.*, **32**, 1152-1161, 1936.

Krishnamurti, T.N., B. Jha, J.M. Prospero, A. Jayaraman, and V. Ramanathan, Aerosol and pollutant transport over the tropical Indian Ocean during the 1996 northeast monsoon and the impact on radiative forcing. *Tellus*, submitted 1998.

Laaksonen, A., P. Korhonen, M. Kulmala, and R. Charlson, Modification of the Köhler equation to include soluble trace gases and slightly soluble substances. *J. Atmos. Sci.*, **55**, 853-862, 1998.

Laktionov, A.G., A constant temperature method of determining the concentrations of cloud condensation nuclei. *Izv., Atmos. Ocean. Phys.*, **8**, 672-677, 1972.

Langsdorf, A., Jr., A continuously sensitive cloud chamber. *Phys. Rev.*, **49**, 422, 1936.

Li, Z., A. Williams, and M.J. Rood, Influence of soluble surfactant properties on the activation of aerosol particles containing inorganic solute. *J. Atmos. Sci.*, **55**, 1859-1866, 1998.

Liu, P.S.K., W.R. Leaitch, C.M. Banic, S. -M. Li, D. Ngo, and W.J. Megaw, Aerosol observations at Chebogue Point during the 1993 North Atlantic Regional Experiment : Relationships among cloud condensation nuclei, size distribution, and chemistry. *J. Geophys. Res.*, **101**, 29971-28990, 1996.

Matsumoto, K., H. Tanaka, I. Nagao, and Y. Ishizaka, Contribution of particulate sulfate and organic carbon to cloud condensation nuclei in the marine atmosphere. *Geophys. Res. Lett.*, **24**, 655-658, 1997.

Matsumoto, K., I. Nagao, H. Tanaka, H. Miyaji, T. Iida, and Y. Ikebe, Seasonal characteristics of organic and inorganic species and their size distributions in atmospheric aerosols over the northwest Pacific Ocean., *Atmos. Environ.*, **32**, 1931-1946, 1998.

Novakov, T. And J.E. Penner, Large contribution of organic aerosols to cloud-

condensation-nuclei concentrations. *Nature*, **365**, 823-826, 1993.

O'Dowd, C.D. and M.H. Smith, Physicochemical properties of aerosols over the Northeast Atlantic : Evidence for wind-speed-related submicron sea-salt aerosol production, *J. Geophys. Res.*, **98**, 1137-1149, 1993.

O'Dowd, C.D., M.H. Smith, I.E. Consterdine, and J.A. Lowe, Marine aerosol, sea-salt, and the marine sulfur cycle : A short review. *Atmos. Environ.*, **31**, 73-80, 1997.

Ogren, J. and H. Rodhe, Measurements of the chemical composition of cloud water at a clean air site in central Scandinavia, *Tellus*, **38B**, 190-196, 1986.

Olsson, P.Q., J.Y. Harrington, G. Feingold, W.R. Cotton, and S.M. Kreidenweis, Exploratory cloud-resolving simulations of boundary-layer Arctic stratus clouds Part I : Warm-season clouds. *Atmos. Res.* **47-48**, 573-597, 1998.

Pielke Sr., R.A., J. Eastman, T.N. Chase, J. Knaff, and T.G.F. Kittel, 1973-1996 Trends in depth-averaged tropospheric temperature. *J. Geophys. Res.*, **103**, 16927-16933, 1998.

Pilinis, C., S.N. Pandis, and J.H. Seinfeld, Sensitivity of direct climate forcing by atmospheric aerosols to aerosol size and composition, *J. Geophys. Res.*, **100**, 18739-18754, 1995.

Pincus, R. And M.B. Baker, Effect of precipitation on the albedo susceptibility of clouds in the marine boundary layer, *Nature*, **372**, 350-352, 1994.

Pinnick, R.G., S.G. Jennings, and G. Fernandez. Volatility of aerosols in the arid

southwestern United States. *J. Atmos. Sci.*, **44**, 562-576, 1987.

Pitchford, M.L. and P.H. McMurry, Relationship between measured water vapor growth and chemistry of atmospheric aerosol for Grand Canyon, Arizona, in winter 1990. *Atmos. Environ.*, **28**, 827-839, 1994.

Pruppacher, H.R. and R. Jaenicke, The processing of water vapor and aerosols by atmospheric clouds, a global estimate. *Atmos. Res.*, **38**, 283-295, 1995.

Rader, D.J. and P.H. McMurry, Application of the tandem differential mobility analyzer to studies of droplet growth or evaporation. *J. Aerosol Sci.*, **17**, 771-787, 1986.

Rhoads, K.P., P. Kelley, R.R. Dickerson, T.P. Carsey, M. Farmer, D.L. Savoie, J.M. Prospero, Composition of the troposphere over the Indian Ocean during the monsoonal transition. *J. Geophys. Res.*, **102**, 18,981-18,995, 1997.

Rivera-Carpio, C.A., C.E. Corrigan, T. Novakov, J.E. Penner, C.F. Rogers, and J. Chow, Derivation of contributions of sulfate and carbonaceous aerosols to cloud condensation nuclei from mass size distributions. *J. Geophys. Res.*, **101**, 19483-19493, 1996.

Saxena, P., L.M. Hildemann, P.H. McMurry, and J.H. Seinfeld, Organics alter hygroscopic behavior of atmospheric particles, *J. Geophys. Res.*, **100**, 18755-18770, 1995.

Seidl, W., Initial cloud droplet concentrations in clean and polluted areas : Simulation by a condensation model and comparison with measurements. *Atmos. Res.*, **31**, 157-185,

1994.

Seinfeld, J. And S. Pandis, *Atmospheric Chemistry and Physics*. John Wiley & Sons, Inc., 1326 pp., 1998.

Shaw, G.E., Chemical air mass systems in Alaska. *Atmos. Environ.*, **22**, 2239-2248, 1988.

Shaw, G.E., On the aerosol particle size distribution spectrum in Alaskan air mass systems: Arctic Haze and non-haze episodes, *J. Atmos. Sci.*, **40**, 1313-1320, 1983.

Shulman, M., M.C. Jacobsen, R.J. Charlson, R.E. Synovec, and T.E. Young, Dissolution behavior and surface tension effects of organic compounds in nucleating cloud droplets, *Geophys. Res. Lett.*, **23**, 277-280, 1996.

Stolzenberg, M.R. and P.H. McMurry, TDMAFIT user's manual, *Publ. 653*, Part. Technol. Lab., Univ. of Minn., St. Paul, 1988.

Svenningsson, B., H.-C. Hansson, A. Wiedensohler, K. Noone, J. Ogren, A. Hallberg, and R. Colvile, Hygroscopic growth of aerosol particles and its influence on nucleation scavenging in cloud : Experimental results from Kleiner Feldberg. *J. Atmos. Chem.*, **19**, 129-152, 1994.

Szumowski, M.J., R.M. Rauber, H.T. Ochs III, and L.J. Miller, The microphysical structure and evolution of Hawaiin rainband clouds. Pt. I: Radar observations of rainbands containing high reflectivity cores. *J. Atmos. Sci.*, **54**, 369-385, 1997.

Tang, I.N., Chemical and size effects of hygroscopic properties on light scattering coefficients. *J. Geophys. Res.*, **101**, 19,245-19,250, 1996.

Tang, I.N. and H.R. Munkelwitz, Water activities, densities, and refractive indices of aqueous sulfates and sodium nitrate droplets of atmospheric importance, *J. Geophys. Res.*, **99**, 18,801-18,808, 1994.

Twomey, S., Aerosols, clouds and radiation. *Atmos. Environ.*, **11**, 2435-2442, 1991.

Twomey, S., *Atmospheric Aerosols*, 302 pp., Elsevier Scientific, New York, NY, 1977.

Twomey, S., On the composition of cloud nuclei in the northeastern United States, *J. de Rech. Atmos.*, **3**, 281-285, 1968.

Twomey, S., Measurements of natural cloud nuclei. *J. Rech. Atmos.*, **1**, 101-105, 1963.

Twomey, S.A., M. Piepgrass, and T.L. Wolfe, An assessment of the impact of pollution on global cloud albedo. *Tellus*, **36B**, 356-366, 1984.

Wieland, W., Die Wasserdampfkondensation an natürlichem Aerosol bei geringen Übersättigungen. *Z. Angew. Math. Phys.*, 7, 428-459, 1956.

Yuan, S.W., *Foundations of Fluid Mechanics*. Prentice-Hall, Inc. 608pp, 1967.